TWO-DIMENSIONAL HYDRODYNAMIC SIMULATION OF BASIN IRRIGATION: ANALYSIS OF FIELD SHAPE EFFECTS ON IRRIGATION PERFORMANCE

by

Enrique Playán Jubillar

A dissertation submitted in partial fulfillment
of the requirements for the degree

of

DOCTOR OF PHILOSOPHY

in

Agricultural and Irrigation Engineering

Approved:

Major Professor	Committee Member
Committee Member	Committee Member
Committee Member	Dean of Graduate Studies

UTAH STATE UNIVERSITY
Logan, Utah

1992

To José and Maria.

ACKNOWLEDGEMENTS

I am deeply indebted to my major professor, Dr. Wynn R. Walker, and to my committee member, Dr. Gary P. Merkley, for the motivation and guidance they gave me and their confidence in my success.

I also want to thank the other members of my graduate committee, Dr. Lyman S. Willardson, Dr. Christopher M. U. Neale, and Dr. Ronald W. Jeppson, for their support and valuable contributions.

My gratitude to Dr. José Faci and Dr. Ramón Aragües of the Servicio de Investigación Agraria de la Diputación General de Aragón, Zaragoza, Spain, for their support of my graduate program and continuous guidance in my career.

I also want to express my gratitude to La Caixa International Programs of Barcelona, Spain, and the Dirección General de Investigación Científica y Técnica del Ministerio de Educación y Ciencia of the Government of Spain for their financial support.

Enrique Playán Jubillar

TABLE OF CONTENTS

LIST OF TABLES

LIST OF FIGURES

LIST OF SYMBOLS AND NOTATION

Symbol	Definition	Units
a	Kostiakov empirical exponent	
A	Cross-sectional flow area	m^2
[A]	Coefficient matrix for the two-dimensional shallow water equations	
[B]	Coefficient matrix for the two-dimensional shallow water equations	
c	Celerity of a small gravity wave	m/s
D_l	Energy term for seepage outflow	
D_{lx}	Energy term for seepage outflow (x direction)	m^2/s^2
D_{ly}	Energy term for seepage outflow (y direction)	m^2/s^2
[D]	Coefficient matrix for the shallow water equations	
DPR	Deep percolation ratio	%
E_1, E_2, E_3	Error induced in a point in each of the governing equations by estimated values of the dependent variables	
E_a	Application efficiency	%
E_r	Water requirement efficiency	%
f	Generic variable	
f_1, f_2, f_3	Elements of an error vector	
f_0	Kostiakov empirical coefficient	$m^3/min/m$
F	Error vector	
g	Acceleration of gravity	m/s^2
h	Flow depth	m
i	Infiltration rate	m^2/s

I	Number of inflows	
j	Iteration number in a Newton-Raphson procedure	
$O(\Delta t^3)$	Third-order element of a Taylor expansion	
p	Unit discharge (x direction)	m^2/s
q	Unit discharge (y direction)	m^2/s
Q	Discharge	m^3/s
k	Kostiakov empirical coefficient	$m^3/min^a/m$
l	Number of nodes affected by a line inflow boundary condition	
ΔL	Length of a cord through the centroid of an element along the resultant flow direction	m
m	Number of nodes in the computational domain	
$\min()$	Minimum value	
n	Manning's roughness coefficient	
N	Bilinear shape function	
R_e	Reynolds number	
n_x	Number of cells in the x direction (deformable control volume approach)	
n_y	Number of cells in the y direction (deformable control volume approach)	
S_0	Field slope	
S_{0x}	Field slope (x direction)	
S_{0y}	Field slope (y direction)	
S_f	Friction slope	
S_{fx}	Friction slope (x direction)	
S_{fy}	Friction slope (y direction)	
t	Time	s

t_i	Turn-out time of an inflow	s
t_o	Cut-off time of an inflow	s
T	Top width of flow	m
^{T}	Matrix transposition (superscript)	
u	Flow velocity (x direction)	m/s
U	Vector of unknowns for the two-dimensional shallow water equations	
$\hat{U}$	Estimate for the vector of unknowns for the two-dimensional shallow water equations	
v	Flow velocity (y direction)	m/s
V_h	Overland volume	m^3
V_z	Infiltrated volume	m^3
w	Weighing factor for the Gauss-Legendre quadrature rule	
W	Set of weighing functions	
x	Space coordinate	m
y	Space coordinate	m
z	Infiltrated depth	m
z_0	Bed elevation from an arbitrary datum	m
α	Summation index	
β	Adaptative grid node distribution parameter	
Δ	Finite increment	
∂	Partial derivative	
ε_x	Dissipation parameter (x direction)	
ε_y	Dissipation parameter (y direction)	
ε	Coefficient of turbulent viscosity	m^2/s
η	Natural coordinate for a linear quadrilateral finite element	

ξ	Natural coordinate for a linear quadrilateral finite element	
ν	Kinematic viscosity	m^2/s
τ	Opportunity time	min
Ω	Domain of a surface integral	
θ	Parameter of a theta differencing procedure	

ABSTRACT

Two-Dimensional Hydrodynamic Simulation of Basin Irrigation: Analysis of Field Shape Effects on Irrigation Performance

by

Enrique Playán Jubillar, Doctor of Philosophy

Utah State University, 1992

Major Professor: Dr. Wynn R. Walker
Department: Biological and Irrigation Engineering

Overland flow of water over a porous bed in two spatial dimensions is governed by three partial differential equations accounting for continuity of momentum in the x and y directions and continuity of mass.

After consideration of several numerical procedures, an explicit finite difference leapfrog numerical procedure was applied to the solution of this system of equations for the initial and boundary conditions that characterize level basin irrigation. The numerical procedure has proven to be stable and robust for many different applications. A design model was developed for use in PC compatible computers. The model implements a user friendly interface and uses three-dimensional graphics to facilitate data analysis. The model is an innovative tool for the design of level basin irrigation systems. Better irrigation system designs at the

farm level will improve water management and optimize the use of farm production resources.

The level basin irrigation design model can deal with three different inflow configurations: line, corner, and fan, which simulate inflow from an overflowing canal on a field boundary and at point sources from a corner or in the middle of a straight boundary, respectively. The results of the model have been validated with field data from basin irrigation field evaluations, and the agreement has been satisfactory.

The model was used to study the effects of field shape on irrigation performance. The results show that one-dimensional models accurately predict the recession time and efficiency terms of rectangular basins irrigated from a corner, but they underestimate the time of advance by up to 20%, especially if the field width is larger than 40% of the field length. (159 pages)

CHAPTER I

INTRODUCTION

Statement of the Problem

Surface irrigation is the oldest and most extensively used irrigation method with the distinguishing characteristic that water is distributed over the field by gravity. Walker and Skogerboe (1987) listed some of the inherent advantages of surface irrigation: minimum capital investment, low maintenance costs, and low energy requirement. Yet, in spite of these and other advantages, the efficiency of surface irrigation systems is typically low. Strelkoff and Katopodes (1977) estimated that only about one half of the water applied to the field in surface irrigation systems is utilized by the plants. They attributed this poor performance to imperfect design and/or unsuitable operation.

The level basin system is one of the most popular types of on-farm surface irrigation. In this system, water is delivered to a large leveled area which is diked to prevent runoff. Clemmens et al. (1981) reported an increase in the popularity of level basin irrigation due to high uniformity of application, elimination of runoff, and low labor requirements.

One of the main priorities in irrigation practice today is to develop designs that increase efficiency in the use of water and energy (Schmitz and Seus, 1989). Mathematical

modeling provides an important tool for the achievement of this objective (Clemmens, 1979).

Surface irrigation systems have commonly been modeled using a one-dimensional analysis in which the flow of water over and under the soil surface is supposed to be repeated across the width of the field. This assumption has produced good results in cases such as furrow irrigation (where flow can be considered to be linear). However, in some basin irrigation configurations, the one-dimensional hypothesis cannot be easily justified, especially if the field geometry is irregular or if water does not enter the field continuously along one of its sides.

A two-dimensional model of basin irrigation is fully justified by its capability to deal with two additional variables for design and operation: irregular field shape and a point or linear water inlets. The use of efficient computational procedures and state of the art computers can produce a two-dimensional model fast and inexpensive enough to be applied interactively as a design and diagnosis tool in surface irrigation engineering.

Objectives

The objectives of this research are:

1. To develop a full hydrodynamic, two-dimensional simulation model able to predict the advance, storage, depletion, and recession phases of an irrigation event in an

irregularly shaped level basin having point or linear water inlets;

2. To implement this model in a microcomputer environment which is user friendly and can be operated by individuals who are not particularly familiar with the underlying theory;

3. To use this model to analyze the effect of irregular field boundaries on basin irrigation efficiency, and to analyze the error introduced by the one-dimensional hypothesis; and

4. To test the model with field data and evaluate its predictive capability.

Scope of Study

1. The study will be limited to level fields. However, the model could be extended to handle nonlevel conditions with little additional theoretical complication. Field work will only involve level basins; and

2. The model will be designed to simulate actual field conditions but not to optimize them, although it might ultimately be used for optimizing design and operation if run iteratively.

CHAPTER II

LITERATURE REVIEW

Surface Irrigation Modeling

The overland flow of water in surface irrigation is manifested by nonuniform, unsteady, gradually varied flow. The hydrodynamic equations describing this kind of flow are the Saint Venant equations, attributed to A. J. C. Barré de Saint-Venant (Chow, 1959). Several authors have proposed different forms of these equations (Chow, 1959; Kruger and Basset, 1965; Strelkoff, 1969; Bassett, 1972; Kincaid et al., 1972), but the most generalized form is that which uses flow depth and velocity as dependent variables:

$$\frac{\partial A}{\partial t} + \frac{\partial Q}{\partial x} + i = 0 \tag{1}$$

$$\frac{1}{g}\frac{\partial v}{\partial t} + \frac{v}{g}\frac{\partial v}{\partial x} + \frac{\partial h}{\partial x} - (S_0 - S_f) - D_1 = 0 \tag{2}$$

where v is the flow velocity (m/s); h is the flow depth (m); A is the cross-sectional flow area (m^2); Q is the discharge across the area A (m^3/s); t is the independent variable time (s); x is the independent variable space (m); i is the infiltration rate (m^2/s); g is the acceleration of gravity (m/s^2); S_0 is the field slope; S_f is the friction slope; and D_1 accounts for the momentum transfer associated with seepage outflow.

The friction slope term is computed using Manning's formula:

$$S_f = \frac{v^2 n^2}{h^{\frac{4}{3}}} \tag{3}$$

where n is the Manning roughness coefficient. This formula is adapted to the particular characteristics of basin irrigation: unit width and unit wetted perimeter. The infiltration rate i can be computed using the Kostiakov-Lewis equation:

$$i = k a t^{a-1} + f_0 \tag{4}$$

where τ is the opportunity time (min); k is an empirical coefficient ($m^3/min^a/m$); a is an empirical exponent; and f_0 is an empirical coefficient ($m^3/min/m$).

The time integrated form of Eq. 4 gives the expression for the infiltrated depth:

$$z = k\tau^a + f_0\tau \tag{5}$$

where z is the infiltrated depth (m).

The following approximation is introduced for D_1:

$$D_1 = \frac{vi}{2Ag} \tag{6}$$

Equation 1 is the continuity equation, which expresses the conservation of mass, while Eq. 2 is the equation of motion, denoting conservation of momentum.

The Saint Venant equations can be applied to surface irrigation flow provided the following assumptions are satisfied (Bassett, 1972; Kincaid et al., 1972):

1. The field slope is small;
2. Vertical accelerations are negligible;
3. Pressure distribution is hydrostatic;
4. Velocity of the infiltrated flow is negligible; and
5. Energy dissipation in nonuniform flow is equal to the dissipation in a uniform flow having the same hydraulic characteristics.

Equations 1 and 2 are the basis for the construction of sophisticated surface irrigation models. According to Katopodes and Strelkoff (1977a), accurate models should be:

1. Theoretically sound and free of empiricism;
2. Numerically consistent, stable, and accurate;
3. Physically complete, i.e., covering all phases of an irrigation event; and
4. Simple to program and inexpensive to operate.

The same authors (Strelkoff and Katopodes, 1977) defined the input and output requirements of such models as applied to border irrigation:

Input: Topography, slope, length, roughness, infiltration characteristics, and inflow hydrograph.

Output: Areal distribution of water infiltrated and amount of runoff (if any).

Equations 1 and 2 constitute a set of first-order, nonlinear, hyperbolic partial differential equations with no

closed solution. Strelkoff (1970) reported that graphical solutions had been attempted since the beginning of this century, while analytical solutions have been obtained only for simplified cases.

Kruger and Bassett (1965) presented the first application of the Saint Venant equations to surface irrigation modeling. The finite difference method was used to solve the equations of continuity and motion over a fixed rectangular grid in the (x, t) plane for the advance phase of a border.

The first hydrodynamic solution of the recession problem is attributed to Schreiber and Bassett (1967), who also used a finite difference scheme to solve the flow equations.

Surface irrigation modeling has followed the recent evolution of computers and programming languages. Different levels of simplification have been applied to the Saint Venant equations in order to produce easy-to-use, fast, and inexpensive codes. This process has created four different types of surface irrigation models: volume balance, kinematic wave, zero inertia, and hydrodynamic.

The hydrodynamic model, considered in this study, is the most theoretically correct and is characterized by a numerical solution of the complete Saint Venant equations. Examples of this type of approach can be found for the advance phase in Kruger and Bassett (1965), Kincaid et al. (1972), Bassett (1972), and Sakkas and Strelkoff (1974). Complete models have been presented by Bassett and

Fitzsimmons (1976), Katopodes and Strelkoff (1977a), and Souza (1981).

The Irrigation Software Engineering Division at Utah State University (1989) developed the SIRMOD software. In this model, the hydrodynamic, zero inertia, and kinematic wave approaches are used to simulate irrigation events for level basins, borders, and furrows. Hydrodynamic models obtain the highest level of accuracy in the solutions and therefore can be used as a standard for evaluation and calibration of simpler methods (Katopodes and Strelkoff, 1977a).

Every approach to the solution of the Saint Venant equations must deal with a set of partial differential equations. Typically a numerical procedure is used to solve the system, although analytical solutions have been found for some highly simplified cases, like the one reported by Schmitz and Seus (1989) for zero-inertia conditions.

Dimensional analysis techniques have often been used to reduce the number of independent variables and to ease the study of the system's response to changes in the operational parameters (Walker and Skogerboe, 1987). Katopodes and Strelkoff (1977b) nondimensionalized the full hydrodynamic equations using the governing equations scheme. The process implies normalization of all variables dividing them by characteristic values. These normalized variables are then substituted into the governing equations and the initial and boundary conditions. The results depend on the

characteristic values, and different approaches can be found in Clemmens and Strelkoff (1979), Clemmens et al. (1981), Elliott et al. (1983), and Shatanawi and Strelkoff (1984).

Bassett and Fitzsimmons (1976) described six types of boundary conditions that can be found in surface irrigation events. The left, upstream boundary can be located at the left end (during advance or depletion) or can be a moving boundary (during recession). The right, downstream boundary will be located at the right end during storage, depletion, and probably recession, and otherwise will be a moving boundary.

The initial condition in a hydrodynamic approach can be provided by the following assumptions (Walker and Skogerboe, 1987):

1. Velocity is constant during the first time increment;
2. The inlet depth is set to critical depth; and
3. The bed slope (if any) can be neglected due to the high value of the friction slope.

Under these conditions, the equation of motion reduces to a differential equation which can be solved for depth and volume storage. A volume balance is then used to locate the advancing tip.

Katopodes and Strelkoff (1977a) pointed out that if the numerical scheme used in the solution procedure is unconditionally stable, the solution will converge to the same flow conditions independent of the initial condition.

A more sophisticated initial condition scheme was developed by Strelkoff and Katopodes (1977) for their zero inertia approach. Simplifications related to the shape of the flow profile were applied to the two governing equations, and the resulting pair of nonlinear, simultaneous algebraic equations were solved using a Newton-Raphson procedure.

Strelkoff (1970) reviewed the numerical methods available to solve the Saint Venant equations. He found that four procedures had already been used. After 20 years of modeling, only two of them have been extensively utilized: the characteristic approach and the deformable control volume approach.

In the network of characteristics method, a change in the independent variables is introduced to transform the system of partial differential equations into a single, ordinary differential equation that must be solved along a forward and a backward characteristic simultaneously. A numerical method such as the Newton-Raphson procedure is applied to solve the system of nonlinear algebraic equations which approximate the ordinary differential equations. This method was successfully applied by Kincaid et al. (1972), Bassett (1972), Sakkas and Strelkoff (1974), Bassett and Fitzsimmons (1976), and Katopodes and Strelkoff (1977a).

Bassett and Fitzsimmons (1976) reported potential instability problems of the characteristic approach. Walker and Humpherys (1983) recognized the superiority of the deformable control volume method over the characteristic

approach on the basis of its adaptability to surged and continuous flows, low sensitivity to the size of the time step, and better numerical stability. Finally, Walker and Skogerboe (1987) stated that the method of characteristics will usually need a long computational time (because the stability condition requires a short time interval), and that it also has a fundamental mathematical problem at the advancing tip, where instability can appear even for very small time steps.

Elliott (1981) used the deformable control volume approach in his model. In this method, the (x, t) plane is divided into a finite number of cells, and the equations of continuity and motion are expressed in an integrated form using a finite difference approximation to a desired level of approximation.

The Lagrangian and Eulerian theory of fluid dynamics produces two deformable control volume approaches (Walker and Skogerboe, 1987). In the Lagrangian scheme, the main cell deformation will occur at the field inlet, and the cells will have a forward velocity (moving grid system), while in an Eulerian analysis, cells will be stationary, and the main deformation will occur at the end tip of the flow (fixed grid system). Both the Eulerian and Lagrangian approaches have been successfully applied to different types of surface irrigation systems and to different levels of simplification of the Saint Venant equations.

Lagrangian integration has been used in hydrodynamic (Souza, 1981) and zero inertia models (Elliott, 1981; Strelkoff and Katopodes, 1977) to increase the stability of the numerical solution. The downstream movement of the cells produces an oblique cell structure that gives good initial estimates of the values of the desired variables at the next time step (Elliott, 1981). On the other hand, the Eulerian approach has accurately simulated the complex hydraulics of surge irrigation in the Kinematic-Wave model by Walker and Humpherys (1983).

The solution of a deformable control volume problem follows an implicit scheme. For a new time step the values of depth and discharge at all nodes will be known simultaneously. Two equations at each cell plus the two boundary conditions provide an equal number of equations and unknowns. The integrated flow equations are locally linearized by means of a Taylor Series expansion, and a solving algorithm such as the double sweep is used to compute the new values of discharge and depth at the new time step. Elliott (1981) introduced the matrix form of the linearized set of equations, which reveals the banded nature of the coefficient matrix.

A review of the literature denotes that a great variety of models has been created following different approximations to the problem. Models have traditionally been validated using field data. Strelkoff (1977) pointed out that the results of the model can only be as good as the input data,

referring to the difficulty of getting reasonable estimates of parameters such as infiltration characteristics and hydraulic roughness. Katopodes and Strelkoff (1977a) also warned that the comparison of model results with field measurements can be meaningless, given the difficulty in field observation of the advance and recession phenomena.

Under these circumstances, it is difficult to evaluate the applicability of the different approaches to the problem. A common practice has been to use the full hydrodynamic models as a standard for comparisons.

Two-Dimensional Modeling of Overland Flow

No reference has been found in the literature regarding two-dimensional modeling of surface irrigation, although several approaches to two-dimensional overland flow have been developed in the last few decades dealing with the dam-break problem or with estuary modeling.

The transition from one-dimensional to two-dimensional schemes drastically increases the volume of necessary computations (Katopodes and Strelkoff, 1978). According to Cunge et al. (1980), the main difficulty associated with two-dimensional problems is that while in one-dimensional problems, flow direction is well-defined and channel points are aligned forming branches; in two-dimensional problems, the flow direction is undetermined. Furthermore, the whole concept of channel disappears. This situation produces complicated networks of interconnected cells.

The equations of flow also change in accommodation to the two-dimensional spatial layout. The main difference with the one-dimensional set of equations is that a third equation is needed to account for momentum conservation in the new spatial coordinate. Several authors have used different equations adapted to their specific problems. The equations included in this review follow the description by Akanbi and Katopodes (1988):

$$\frac{\partial h}{\partial t} + \frac{\partial}{\partial x}(uh) + \frac{\partial}{\partial y}(vh) + i = 0 \tag{7}$$

$$\frac{\partial}{\partial t}(uh) + \frac{\partial}{\partial x}(u^2h) + \frac{\partial}{\partial y}(uvh) + g\frac{\partial}{\partial x}(\frac{h^2}{2}) - gh(S_{0x} - S_{fx}) - D_{1x} = 0 \tag{8}$$

$$\frac{\partial}{\partial t}(vh) + \frac{\partial}{\partial y}(v^2h) + \frac{\partial}{\partial x}(uvh) + g\frac{\partial}{\partial y}(\frac{h^2}{2}) - gh(S_{0y} - S_{fy}) - D_{1y} = 0 \tag{9}$$

where u and v are the x and y components of fluid velocity (m/s); S_{fx} and S_{fy} are the friction slope terms in the x and y directions; S_{0x} and S_{0y} are the bed slope terms in the x and y directions; and D_{1x} and D_{1y} account for the momentum transfer associated to seepage outflow in the x and y directions (m^2/s^2).

The following approximations are introduced:

$$D_{1x} = \frac{ui}{2} \tag{10}$$

$$D_{1y} = \frac{vi}{2} \tag{11}$$

A two-dimensional version of Manning's formula is used for the friction slope:

$$S_{fx} = \frac{n^2 u (u^2+v^2)^{\frac{1}{2}}}{h^{\frac{4}{3}}} \tag{12}$$

$$S_{fy} = \frac{n^2 v (u^2+v^2)^{\frac{1}{2}}}{h^{\frac{4}{3}}} \tag{13}$$

The following expressions are used for bed slope:

$$S_{0x} = - \frac{\partial z_0}{\partial x} \tag{14}$$

$$S_{0y} = - \frac{\partial z_0}{\partial y} \tag{15}$$

where z_0 is the bed elevation from an arbitrary datum (m).

After all these substitutions, the flow equations can be written in the following way:

$$\frac{\partial h}{\partial t} + \frac{\partial p}{\partial x} + \frac{\partial q}{\partial y} + i = 0 \tag{16}$$

$$\frac{\partial p}{\partial t} + \frac{\partial}{\partial x}\left(\frac{p^2}{h}+\frac{gh^2}{2}\right) + \frac{\partial}{\partial y}\left(\frac{pq}{h}\right) + gh\frac{\partial z_0}{\partial x}$$

$$+ gn^2 \frac{p(p^2+q^2)^{\frac{1}{2}}}{h^{\frac{7}{3}}} - \frac{p}{h}\left(\frac{i}{2}\right) = 0 \tag{17}$$

$$\frac{\partial q}{\partial t} + \frac{\partial}{\partial y}\left(\frac{q^2}{h}+\frac{gh^2}{2}\right) + \frac{\partial}{\partial x}\left(\frac{pq}{h}\right) + gh\frac{\partial z_0}{\partial y}$$

$$+ gn^2\frac{q(p^2+q^2)^{\frac{1}{2}}}{h^{\frac{7}{3}}} - \frac{q}{h}\left(\frac{i}{2}\right) = 0 \qquad (18)$$

where p is the unit discharge in the x direction (m^2/s), and q is the unit discharge in the y direction (m^2/s). Equations 16, 17, and 18 are known as the p-q set of equations.

Katopodes and Strelkoff (1978) introduced a matrix form of the two-dimensional shallow water equations:

$$\frac{\partial U}{\partial t} + [A]\frac{\partial U}{\partial x} + [B]\frac{\partial U}{\partial y} + [D] = 0 \qquad (19)$$

where:

$$U = \begin{bmatrix} h \\ p \\ q \end{bmatrix} \qquad (20)$$

$$[D] = \begin{bmatrix} gh\dfrac{\partial z_0}{\partial x} + gn^2\dfrac{p(p^2+q^2)^{1/2}}{h^{7/3}} - \dfrac{p}{h}\dfrac{i}{2} \\ gh\dfrac{\partial z_0}{\partial y} + gn^2\dfrac{q(p^2+q^2)^{1/2}}{h^{7/3}} - \dfrac{q}{h}\dfrac{i}{2} \end{bmatrix} \qquad (21)$$

$$[A] = \begin{bmatrix} 0 & 1 & 0 \\ -\frac{p^2}{h^2} + gh & \frac{2p}{h} & 0 \\ -\frac{pq}{h^2} & \frac{q}{h} & \frac{p}{h} \end{bmatrix} \tag{22}$$

$$[B] = \begin{bmatrix} 0 & 0 & 1 \\ -\frac{pq}{h^2} & \frac{q}{h} & \frac{p}{h} \\ -\frac{q^2}{h^2} + gh & 0 & \frac{2q}{h} \end{bmatrix} \tag{23}$$

The variables p and q relate to flow depth and velocity in the following way:

$$p = uh \tag{24}$$

$$q = vh \tag{25}$$

The p-q form of the shallow water equations has some inherent advantages for basin irrigation simulation because the boundary conditions are expressed in terms of discharge, and not in terms of velocity. However, this set of equations has a more complicated expression because the fact that the depth of flow figures in the denominator of several fractions

will make it more sensitive to singularities produced by a zero depth of flow.

The first reference of a two-dimensional scheme for the shallow water equations is the model for storm surges by Reid and Bodine (1968). They used finite differences to simulate the water profile in a bay. The model tracks a moving boundary by turning some cells on and off and preserving the mass conservation principle.

Xanthopoulos and Koutitas (1976) developed a model for the dam-break problem that shows a high degree of similarity with the objectives of this dissertation. A finite difference scheme is used to simulate water advance over a dry plain area after the instantaneous breakage of a dam. The model used a fixed rectangular grid and accounted for some topography effects.

Katopodes and Strelkoff (1978) also simulated the dam-break problem, but used a very different approach. They discretized the domain using a moving rectangular grid and used the method of characteristics to solve for the dependent variables. They successfully simulated the flooding of a channel by an advancing front.

Walters and Cheng (1979) used a finite element approach to simulate a tidal estuary. Their model considered curve-sided elements to fit the shoreline boundaries. The discretization grid was manually established for each estuary. The use of six node triangular elements provided an accurate fit to the shape of the domain.

Akanbi and Katopodes (1988) also used finite elements for the dam-break problem. They introduced a deforming moving grid system based on a coordinate transformation. The plain bed was supposed to be porous and initially dry, and infiltration was characterized by a Kostiakov formula. They used field data from border irrigation to validate the advance phase of their model in a one-dimensional application.

Katopodes (1980) used the same approach in a two-dimensional model for open channels. He successfully simulated a supercritical flood wave over a square dry domain using a deforming moving grid.

Mader (1988) developed an estuary model adapted to the study of tsunamis (tidal waves). A finite difference approach simulates advance over a fixed rectangular grid.

Casulli (1990) also used finite differences over a fixed rectangular grid to solve the shallow water equations and applied his model to the solution of tidal circulation problems.

All the previously discussed models follow the same steps:

1. Gridding of the physical domain;
2. Determination of the initial and boundary conditions; and
3. Discretization of the governing equations and numerical solution.

Grid Selection

Fixed and moving grids have been used in two-dimensional overland flow modeling. Fixed grids arise from the Eulerian point of view of fluid dynamics, while moving grids are best suited for Lagrangian analysis.

Lynch and Gray (1980) reported that most modeling developments for transient field problems had been made over fixed grids. They also discussed the advantages and disadvantages of fixed and moving grids.

To preserve an acceptable level of accuracy, high spatial resolution is needed in a zone surrounding a moving boundary. Lynch and Gray (1980) pointed out that, in the presence of a fixed grid, this high resolution will have to be maintained during the whole simulation in all areas where the moving boundary can be located, thus unnecessarily increasing the computational effort.

Moving grid systems are designed to minimize the truncation error or to track the movement of a boundary (Arney and Flaherty, 1986). In this way, finer meshes are only used where needed, therefore reducing the dispersive errors and providing for more efficient computer codes. As a consequence of this node displacement, moving grids are usually irregular grids too. Moving grids have been proven to reduce the numerical oscillations behind a propagating wave (Arney and Flaherty, 1986).

Application of moving grids requires modification of the governing equations to accommodate the description of flow

velocity and discharge from nodes that have their own velocity. Examples of these modifications can be found in Katopodes (1980) and Akanbi and Katopodes (1988).

Most applications of moving grids have been carried out for finite element schemes (Akanbi and Katopodes, 1988; Katopodes, 1980), taking advantage of their capability to deal with irregular cell boundaries. Finite difference schemes have also been applied to deforming moving grids using coordinate transformations to map curvilinear grid systems into Cartesian spaces (Steger, 1978; Bellos et al., 1988). This approach produces more complicated forms of the governing equations but leads to easier discretization and moving boundary analysis (Steger, 1978).

Thacker (1977) described an interesting approach to the use of finite difference schemes in irregular grids. His method is based on establishing a triangular mesh and estimating the spatial partial derivative of a variable in a node as the weighted average of the slopes of this variable in each of the neighboring triangular elements. This clears the way for the application of any traditional finite difference solver, but the stability of his method relies heavily on the geometry of the mesh, requiring complicated computations to determine the optimal location of interior nodes. This complicates the application of such a model to a moving grid, where the nodal coordinates must be recomputed every time step.

Local mesh refinement has recently been introduced as a new adaptative grid technique. It has been used in combination with finite difference schemes to generate nonuniform grids (Luchini, 1987). An algorithm is used to obtain estimates of the truncation error at each grid node, and a clustering procedure is then used to define areas where mesh refinement will be performed.

Mesh refinement shows some advantages over moving grids. For example, more spatial resolution is automatically introduced where needed and within some user-defined limits (Gelinas et al., 1981; Arney and Flaherty, 1986).

Two mesh refinement schemes seem to be especially promising. Berger and Oliger (1984) developed a system for finite difference approximations to sets of hyperbolic partial differential equations. A base square grid is established over the physical domain, and every several time steps, the local truncation error is estimated to determine potential areas for mesh refinement. At these areas, a primary square cell is divided into four second-order cells. The procedure is repeated until the error estimate falls within a safe limit. One of the most interesting features of this system is that mesh refinement is also applied to the time coordinate, thus ensuring stability in refined areas and saving computational time by using large time steps when allowed by the cell size.

The approach by Luchini (1987) splits a square cell into triangles and squares alternatively, also providing an

accurate system to fit irregular boundaries. Although this approach was initially developed for steady-state problems, its application to time-dependent situations is straight forward.

The introduction of nonuniform grid techniques must be justified by the existence of large errors introduced by domains with curved solid boundaries or by high gradients in the dependent variables occurring in small regions (Luchini, 1987). Even in these cases, the benefits introduced by a nonuniform grid must overcome the cost of resource allocation for grid regeneration.

Initial and Boundary Conditions

Most of the reviewed literature utilized the Ritter solution for one-dimensional frictionless flow as an initial condition for the breached dam problem (Reid and Bodine, 1968; Katopodes and Strelkoff, 1978; Bellos and Sakkas, 1987).

Moving grid schemes require complicated initial conditions for inflows, since all the nodes fall within the advancing front, and a good estimate of the dependent variables must be supplied for each node. Fixed grids usually require much simpler initial conditions, since only the nodes where the inflow boundary conditions are located need special initial values.

Conditions at solid boundaries of the physical domain are reproduced by setting the value of the velocity normal to

the boundary to zero. In other cases, free-fall or continuative conditions should be introduced.

The downstream boundary condition for the breached dam problem is characterized by zero depth of flow. Akanbi and Katopodes (1988) used the velocity of the downstream edge to predict the advance in their moving grid, assuming that the boundary moves in the direction of the local normal vector. Bellos et al. (1988) applied the flow conditions to all the computational domain (even if the depth at nodes beyond the advancing front is zero) and accepted that the advance had reached a new node when its computed depth exceeded 1% of the normal depth. Otherwise the depth was set to zero. This last criterion is generally used for the trailing edge during a recession event.

Discretization Technique and Numerical Solution

Despite some applications of the characteristic approach to the solution of the two-dimensional shallow water equations (Katopodes and Strelkoff, 1978; Katopodes and Schamber, 1983), most of the modeling effort has used some kind of discretization technique. Akanbi and Katopodes (1988) reported the high degree of accuracy that the method of characteristics can obtain, but recognized that it cannot deal with complicated topography or geometry. They reported difficulties at the advancing edge of the fluid domain.

Cunge et al. (1980) described discretization as "the process of expressing general flow laws, written for a

continuous medium, in terms of discrete values at a finite number of points in the flow field " (p. 53). Two discretization techniques have been widely used in two-dimensional modeling of overland flow: finite differences and finite elements.

The first discretization scheme to be applied to the two-dimensional shallow water equations was the finite differences method. A great deal of experience had already been collected in one-dimensional applications where, as reported by Katopodes (1984a), no other numerical technique has proved to be more convenient.

Finite element models can deal with very flexible grids, and therefore can accurately fit irregular boundaries (Katopodes, 1984a; Katopodes, 1984b; Segerlind, 1984). Gray (1980), in his extensive review of finite element models applied to surface flow, concluded that many of them had resorted to excessive numerical damping or had other numerical pitfalls that limit their potential to accurately simulate flow profiles.

Both finite differences and finite elements can be developed in implicit or explicit ways, and this leads to four different approaches:

1. Implicit finite differences;
2. Explicit finite differences;
3. Implicit finite elements; and
4. Explicit finite elements.

Implicit Finite Differences

Implicit finite difference methods can be appropriate when solutions are desired at larger time intervals than those permitted by an explicit scheme. Steger (1978) pointed out that this can occur when the dependent variables change more rapidly in space than in time or when a boundary condition acting as a forcing function takes control of the time accuracy.

The method introduced by Preissman (Cunge et al., 1980) has been widely used to simulate two-dimensional open channel flow. This method is first-order accurate and requires an iterative Newton-Raphson procedure to solve the resulting matrix for each time step. Weare (1976) used a Crank-Nicholson implicit approach and found that the matrix solution considerably increased the computational time. The introduction of the alternating direction method tri-diagonalized the matrices, thus decreasing the number of required computations, but this approach still could not match the computational speed of an explicit method. The required computational time is much larger for implicit than for explicit methods due to the matrix handling requirement, even for one-dimensional formulations (Fennema and Chaudhry, 1986).

Serious problems arise in the application of implicit methods to an advancing phase over a rectangular grid, since nodes with zero depth and discharge will abort the numerical computation during the iterative procedure.

Explicit Finite Differences

Reports on explicit finite difference models can be found in Reid and Bodine (1968), Xanthopoulos and Koutitas (1976), and Bellos et al. (1988). The advantage of this approach is that no complicated matrix handling or iterative procedure is required.

Among the several methods described in the literature, two of them have been particularly successful: the leapfrog and the MacCormack approaches. Both of them are second-order accurate in space and time.

The leapfrog method was probably the earliest ever used in the solution of the one-dimensional wave equations (Cunge et al., 1980). The procedure is easily extended to two spatial dimensions. Different authors have used it for computational purposes or for comparison with other approaches. Successful applications of the method have been reported by Thacker (1977), Foreman (1984), and Akanbi (1986).

The particularities of the leapfrog approach stem from the fact that the depth and discharge components are staggered in time by a half time step, thus providing stability to the scheme. The method is not dissipative and, when a front steepens, short wave components of the solution may appear. Under these circumstances, the profile of the solution might become uncontrollable (Cunge at al., 1980). In these cases, artificial viscosity can be introduced in the formulae to smear these discontinuities.

When the leapfrog method is used to solve the p-q set of equations, the two equations of motion turn out to be coupled and need to be solved implicitly for the new values of p and q at each node.

The MacCormack explicit method has proved to produce consistent, conservative solutions (Arney and Flaherty, 1986) and has shown satisfactory behavior in the presence of flow discontinuities (Bellos et al., 1988). This is a two-step, predictive-corrective method belonging to the general class of Lax-Wendroff explicit schemes that shows a strong shock-capturing capability and a dissipative behavior (Bellos and Sakkas, 1987).

Abarbanel and Murman (1982) reviewed the stability of some explicit and implicit finite difference schemes for two-dimensional hyperbolic initial boundary value problems and found that the MacCormack approach shows the best stability properties under different boundary conditions as compared with other well-known methods. Garcia and Kahawita (1986) reported that the method's main advantage is its capability to deal with slowly varying flows as well as rapidly varying flows containing shocks or discontinuities.

The length of the time step in explicit schemes is determined by the Courant-Friedrichs-Lewy condition, that, according to Bellos et al. (1988), can be expressed as:

$$\Delta t < \min\left(\frac{\Delta x}{u+c}\ ,\ \frac{\Delta y}{v+c}\right) \qquad (26)$$

where Δx is the x coordinate increment between nodes (m); Δy is the y coordinate increment between nodes (m); Δt is the time increment (s); and c is the celerity of a small flow disturbance (m/s). This condition imposes a limitation on the time step that can unnecessarily increase the number of computations when high resolution in time is not desired.

Casulli (1990) presented a semi-implicit finite difference method which introduces a minimal degree of implicitness to make stability independent of the Courant-Friedrichs-Lewy condition without introducing all the computational work characteristic of implicit schemes.

Implicit Finite Elements

The earliest attempts to use the finite element method appeared in the 1970's. The method holds some properties that make it especially promising. Among them are 1) its ability to use cells of variable, irregular shape, thus accurately fitting the shape of the physical domain (Foreman, 1984), and 2) its simplicity to handle the zero depth condition at the wave front (Akanbi and Katopodes, 1988).

The finite element method allows definition of elements of variable number of sides. Each side can be defined by two or more nodes. In this last case, the side can be curved. These features permit a precise coverage of the domain with a low number of nodes.

The first finite element approaches used the Galerkin approximation. Katopodes (1984a) pointed out that its

nondissipative character makes the method inappropriate for use in flow domains containing discontinuities or steep fronts because spurious waves can completely mask the correct solution of the problem. He developed the Petrov-Galerkin approach, a dissipative scheme based on the Galerkin method and on the Lax-Wendroff finite difference method that coupled some of the advantages of finite differences and finite elements. The approach was successfully used by Katopodes (1984a and 1984b), Akanbi (1986), and Akanbi and Katopodes (1988).

This method was originally developed to deal with two-dimensional dam break and open channel problems, but it includes all the features needed for a correct simulation of basin irrigation events; its numerical scheme has proven to be stable and accurate. The following description summarizes the works by Katopodes (1984a and 1984b), Akanbi (1986), and Akanbi and Katopodes (1988).

Two problems associated with the computation of two-dimensional flood waves seem to have motivated the development of the model.

The first is the specification of the zero depth and zero discharge condition at the advancing edge. The authors recognize that this difficulty has been avoided in the past by terminating the computations shortly behind the front and then extending the solution by means of a volume balance or a power law, or by assuming a small, nonzero depth at the advancing front.

The second problem relates to the management of the expanding domain induced by the downstream moving boundary. The usual practice is to discretize the entire domain and carry out computations for all nodes, even if they have not been reached by the flood wave. A more adequate grid management would allow computations to be limited to the area reached by the flood at any time step. At the same time, the location of the advancing front has to be part of the solution, since no extra equations can be supplied to define its movements. The only clue to the displacement of the boundary is the velocity of the last node with nonzero depth.

The finite element method holds unequaled properties to deal with these problems. The numerical integration used to compute the weighted residual only uses computations in sample points within the elements, thus avoiding computation in the nodes where the zero depth and zero discharge conditions are located. Also, finite elements can reproduce the shape of the domain and change it every time step using a moving grid. All nodes are regenerated at each time step to maintain the geometry of the grid. The movement of the advancing front is approximated from the velocity of the nodes just behind the front, assuming that velocity is locally uniform.

The nondissipative character of the traditional Galerkin scheme has introduced some additional difficulties in the application of the method to the shallow water equations, since numerical oscillations can appear that compromise the

accuracy and stability of the solutions. To circumvent this problem, the authors propose a dissipative interface based on the choice of a set of weighing functions different from the shape functions.

Numerical integration in time is accomplished using a second-order finite difference scheme, and the resulting set of implicit algebraic equations is solved using a Newton-Raphson procedure on a 3m x 3m matrix, where m is the number of nodes in the domain.

One of the major drawbacks of the scheme is that it is conditionally stable, being subject to the Courant-Friedrichs-Lewy condition. This is especially inconvenient since the method is fully implicit and requires time-consuming matrix computations for every time step.

Explicit Finite Elements

Wu (1985) and Katopodes and Wu (1986), concerned by the limitations of the traditional Galerkin method and by the high computer resource consumption of the dissipative Galerkin scheme (Katopodes, 1984a), developed an explicit finite element model using a variation of the Lax-Wendroff approach that matched the accuracy of the best implicit models while drastically reducing computer costs.

The method was used to solve a simplified version of the u-v set of equations for the one- and two-dimensional shallow water flow in an innovative way. The authors call it Taylor-Galerkin because it mixes both approaches. A Taylor series

expansion is applied to each of the dependent variables in the next time step. For the depth of flow, the expansion takes the form:

$$h^{t+\Delta t} = h^{t} + \Delta t\left(\frac{\partial h}{\partial t}\right)^{t} + \frac{1}{2}\Delta t^{2}\left(\frac{\partial^{2} h}{\partial t^{2}}\right)^{t} + O(\Delta t^{3}) \qquad (27)$$

where $O(\Delta t^3)$ represents a third-order term that is truncated in this approach. The first and second temporal derivatives are computed by direct application of the Galerkin finite element method to the governing equations or transformations of them that provide expressions for the second temporal derivatives.

Computation of each of the terms in Eq. 27 proceeds implicitly, therefore requiring the solution of six m x m matrices, two for each dependent variable. Once the time derivatives are computed, the values of the dependent variables are updated using the Taylor expansion formula. The method can use any type of element, thus adapting to any shape of the computational domain. The model was reported to be four times faster and to use 30% of the memory that comparable implicit models use, but again, its stability depends on the size of the time step.

Discussion of the Different Methods

As a conclusion of his extensive discussion about discretization methods for the two-dimensional shallow water equations, Weare (1976) stated that finite elements are

economically inefficient when faced with their finite difference counterparts. Also, Gray (1980), after reviewing a number of finite element models for surface flow, arrived at the same conclusion based on the cost associated with band algorithms used to solve implicit finite element problems.

Recent developments in semi-implicit finite differences and explicit finite elements introduce new arguments to the reviews by Weare (1976) and Gray (1980); now the decision about implicit or explicit approaches seems to be as important as the decision about finite differences or finite elements, considering computational costs. Katopodes and Wu (1986) pointed out that the extension of an implicit problem to two dimensions drastically increases the computational cost, although for an explicit problem the cost increase is marginal.

Despite the decision about whether to use an implicit or explicit solution procedure, the programming effort will still be considerably higher for finite elements than for finite differences.

CHAPTER III

THEORETICAL AND DEVELOPMENT

Selection of Models

The first approach to the problem was to apply the deformable control volume method to the two-dimensional shallow water equations. This method has been particularly successful in one-dimensional surface irrigation simulation, and its application to the two-dimensional equations seemed to be straightforward. It soon became evident that the method produced an unbalanced system of nonlinear algebraic equations, where the number of unknowns is usually larger than the number of equations.

The application of the method to a hypothetical rectangular grid of $n_x + 1$ nodes in the x direction and $n_y + 1$ nodes in the y direction can be described in the following manner: The nodes are numbered from 0 to n_x and n_y, respectively. Under these circumstances, the total number of nodes is $(n_x + 1)(n_y + 1)$, the total number of cells is $(n_x n_y)$, and, because all three governing equations are written for each cell, the total number of equations is $(3\ n_x\ n_y)$.

The number of unknowns can be computed considering the location of each node in the grid: In a corner inflow configuration, there is one inflow node with one unknown (flow depth). The remaining three corner nodes also have one unknown each. There are $2(n_x - 1) + 2(n_y - 1)$ straight boundary nodes with two unknowns each (flow depth and one of

the components of discharge) and $(n_x - 1)(n_y - 1)$ interior nodes with all three unknowns each. The total number of unknowns is $3\ n_x\ n_y + n_x + n_y - 1$.

The number of equations and the number of unknowns are then different, and the unbalance (equations - unknowns) follows the expression $1 - n_x - n_y$. Different domain geometries would yield different expressions of this unbalance, and irregular configurations with a large perimeter and a small area could actually have more equations than unknowns.

The inherent problem of the deformable control volume method is that the flow equations are written for each cell. In one-dimensional configurations, the system is balanced, but in two-dimensional problems, the set of resulting algebraic equations will be unbalanced because the method does not allow writing the equations for each node. The deformable control volume method was then discarded, and attention was paid to other methods that had been successfully used in the literature.

Among all the models described in the literature, two were selected for detailed study: the Petrov-Galerkin implicit finite elements model and the leapfrog explicit finite differences scheme. The other approaches were discarded in the early stages of the research for different reasons, as outlined below.

Implicit finite difference methods are not suited to the problem since the zero depth and discharge conditions would

produce singularities that could cause the numerical procedure to diverge.

The MacCormack approach is an interesting method for two-dimensional surface flow computations, and it proved to be accurate and stable for applications dealing with wave propagation in open channels, but problems were found when it was applied to flood wave computations on a dry bed. The computation systematically aborted due to the numerical singularities introduced at the advancing edge.

Finally, explicit finite elements have some advantages over the implicit method, but they still require a large amount of matrix handling that translates into computational time. On the other hand, additional research effort should be committed to develop a moving grid formulation of the equations for the p-q set of equations.

Petrov-Galerkin Finite Element Formulation

The computational time requirements of the Petrov-Galerkin method were soon found to be too large to provide a fast, inexpensive solution to the problem, which was one of the objectives of this research. However, the model was reproduced to provide a basis of comparison for the leapfrog scheme, since the Petrov-Galerkin approach is the only method reported in the literature that has come close to solving the two-dimensional basin irrigation simulation problem. The following is an outline of the method that reports its procedure and its main strengths and weaknesses.

Numerical Scheme

The Petrov-Galerkin method was described in detail by Katopodes (1984a and 1984b), Akanbi (1986), and Akanbi and Katopodes (1988). A brief summary of its features as applied to basin irrigation simulation follows.

Two modifications must be introduced to the governing equations due to the nature of the model: first, the slope of the field (represented by S_{0x} and S_{0y}) is zero, and second, the coordinate system must undergo a transformation to a moving coordinate system.

Let (ξ, η, t) be a moving coordinate system respect to the original set of coordinates (x, y, t). The new set of equations is defined by:

$$x = x(\xi, \eta, t) \tag{28}$$

$$y = y(\xi, \eta, t) \tag{29}$$

The coordinate transformation yields the following expression of the governing equations in matrix form:

$$\frac{\partial U}{\partial t} - \frac{\partial x}{\partial t}\frac{\partial U}{\partial x} - \frac{\partial y}{\partial t}\frac{\partial U}{\partial y} + A\frac{\partial U}{\partial x} + B\frac{\partial U}{\partial y} + D = 0 \tag{30}$$

where the terms $\partial x/\partial t$ and $\partial y/\partial t$ are the elemental velocities, W_x and W_y, respectively (both in m/s), computed by interpolation of the nodal velocities. If these velocities are set to zero, the grid becomes stationary.

The finite element expression of the governing equations can be easily formulated if the transformed coordinates are identified with the natural coordinate system for a linear quadrilateral element, both ranging from -1 to 1 within the element. The moving coordinates can be related to the (x, Y, t) system by the formulae:

$$x(\xi,\eta,t) = \sum_{\alpha=1}^{4} X_\alpha(t) N_\alpha(\xi,\eta) \tag{31}$$

$$y(\xi,\eta,t) = \sum_{\alpha=1}^{4} Y_\alpha(t) N_\alpha(\xi,\eta) \tag{32}$$

where the summation is extended to the four nodes that determine the element, and X_α and Y_α are the nodal values of the spatial coordinates (m), and N_α is the bilinear shape function, defined as:

$$N_\alpha = \frac{1}{4}(1+\xi_\alpha\xi)(1+\eta_\alpha\eta) \tag{33}$$

The finite element approximation for the solution vector U can be given by:

$$\hat{U} = \sum_{\alpha=1}^{4} N_\alpha U_\alpha \tag{34}$$

The weighted residual finite element formulation can be expressed as:

$$\int_{\Omega} W^T \left(\frac{\partial \dot{U}}{\partial t} - \frac{\partial x}{\partial t}\frac{\partial \dot{U}}{\partial x} - \frac{\partial y}{\partial t}\frac{\partial \dot{U}}{\partial y} + [A]\frac{\partial \dot{U}}{\partial x} + [B]\frac{\partial \dot{U}}{\partial y} + [D] \right) d\Omega = 0 \tag{35}$$

where W is a suitable set of spatial weighing functions; Ω represents the area of the element; and the superscript T implies matrix transposition. In the Galerkin scheme, these functions are taken equal to the shape functions. Katopodes (1984a) pointed out the nondissipative character of the Galerkin scheme and proposed a different set of weighing functions to introduce a dissipative effect that dumps out the high frequency parasitic waves that characterize the solutions provided by the Galerkin method.

The Petrov-Galerkin weighing functions follow the expression:

$$W_\alpha = N_\alpha + \varepsilon_x [A]^T \frac{\partial N_\alpha}{\partial x} + \varepsilon_y [B]^T \frac{\partial N_\alpha}{\partial y} \tag{36}$$

where ε_x and ε_y are the dissipation parameters in the x and y directions, respectively, that, according to Katopodes (1984a), must be computed in the following way for the solution to be accurate to the fifth order with respect to the mesh size:

$$\varepsilon_x = \varepsilon_y = \frac{\Delta L}{\left[\sqrt{\left(\frac{p}{h}\right)^2 + \left(\frac{q}{h}\right)^2} + c \right] \sqrt{15}} \tag{37}$$

where h, p, and q are the values of the dependent variables at the centroid of the element, and ΔL is the length of a cord through the centroid of the element along the resultant flow direction.

The numerical procedure assumes that an error vector F is equaled to Eq. 35. The equations will reach a solution when the values of the dependent variables set all terms in F to values smaller than a given threshold. The F vector is decomposed into three vectors, f1, f2, and f3, corresponding to each of the governing equations. Each of them has four components representing the error induced in each of the four nodes of the element by the estimates of the dependent variables. The expressions for the error vector are:

$$f_1 = \int_\Omega (N^T E_1 + \varepsilon_x \frac{\partial N^T}{\partial x} E_2 + \varepsilon_y \frac{\partial N^T}{\partial y} E_3)\, d\Omega \tag{38}$$

$$f_2 = \int_\Omega \{N^T E_2 + \varepsilon_x \frac{\partial N^T}{\partial x} [(gh - \frac{p^2}{h^2}) E_1 + (\frac{2p}{h}) E_2] + \varepsilon_y \frac{\partial N^T}{\partial y} [-(\frac{pq}{h^2}) E_1 + (\frac{q}{h}) E_2 + (\frac{p}{h}) E3]\}\, d\Omega \tag{39}$$

$$f_3 = \int_\Omega \{N^T E_3 + \varepsilon_x \frac{\partial N^T}{\partial x} [-(\frac{pq}{h^2}) E_1 + (\frac{q}{h}) E_2 + (\frac{p}{h}) E_3] + \varepsilon_y \frac{\partial N^T}{\partial y} [(gh - \frac{q^2}{h^2}) E_1 + (\frac{2q}{h}) E_3]\}\, d\Omega \tag{40}$$

where:

$$E_1 = \frac{\partial h}{\partial t} - W_x\frac{\partial h}{\partial x} + \frac{\partial p}{\partial x} - W_y\frac{\partial h}{\partial y} + i \tag{41}$$

$$E_2 = \frac{\partial p}{\partial t} + (gh-\frac{p^2}{h^2})\frac{\partial h}{\partial x} + (\frac{2p}{h}-W_x)\frac{\partial p}{\partial x} - (\frac{pq}{h^2})\frac{\partial h}{\partial y} + (\frac{q}{h}-W_y)\frac{\partial p}{\partial y} + (\frac{p}{h})\frac{\partial q}{\partial y} + gn^2\frac{p(p^2+q^2)^{\frac{1}{2}}}{h^{\frac{7}{3}}} - \frac{pi}{2h} \tag{42}$$

$$E_3 = \frac{\partial q}{\partial t} + (gh-\frac{q^2}{h^2})\frac{\partial h}{\partial y} + (\frac{2q}{h}-W_y)\frac{\partial q}{\partial y} - (\frac{pq}{h^2})\frac{\partial h}{\partial x} + (\frac{p}{h}-W_x)\frac{\partial q}{\partial x} + (\frac{q}{h})\frac{\partial p}{\partial x} + gn^2\frac{q(p^2+q^2)^{\frac{1}{2}}}{h^{\frac{7}{3}}} - \frac{qi}{2h} \tag{43}$$

The integrals are evaluated numerically using the Gauss-Legendre quadrature rule. Four sampling points are defined inside each element, and the integral is substituted by the following expression:

$$\int_\Omega f(\xi,\eta)\,d\Omega = \int_{-1}^{1}\int_{-1}^{1} f(\xi,\eta)\,d\eta\,d\xi = \sum_{\alpha=1}^{4} w_\alpha f(\xi_\alpha,\eta_\alpha) \tag{44}$$

where w is the value of the weighing factor for the Gauss-Legendre quadrature.

The time derivatives are approximated using a second-order accurate finite difference that follows the expression:

$$\frac{\dot{U}^{t+\Delta t}-\dot{U}^{t}}{\Delta t} = \frac{1}{2}(\frac{\partial \dot{U}}{\partial t})^{t+\Delta t} + \frac{1}{2}(\frac{\partial \dot{U}}{\partial t})^{t} \tag{45}$$

which is reformulated as:

$$\left(\frac{\partial \dot{U}}{\partial t}\right)^{t+\Delta t} = \frac{\dot{U}^{t+\Delta t} - \dot{U}^{t}}{\frac{1}{2}\Delta t} - \left(\frac{\partial \dot{U}}{\partial t}\right)^{t} \tag{46}$$

and applied to the finite element equations, resulting in a set of 12 implicit algebraic equations per element.

Computations are then carried out for all the elements in the domain and all the equations assembled into a unique vector of dimension 3m, where m is the number of nodes in the domain. Since the equations are implicit, a Newton-Raphson method has to be applied to the solution of the system, and therefore the equations must be differentiated with respect to all the unknown variables and the derivatives assembled into a 3m x 3m matrix. The resulting matrix must be solved iteratively to obtain the values of p, q, and h for all the nodes that set the values of the residuals to a value close enough to zero.

This iterative process follows the equation:

$$\dot{U}^{j+1} = \dot{U}^{j} - \Delta \dot{U}^{j} \tag{47}$$

where the superscript j indicates the iteration number, and $\Delta \dot{U}^{j}$ is the solution to the linear system of equations:

$$\left(\frac{\partial F^{j}}{\partial \dot{U}^{j}}\right) \Delta \dot{U}^{j} = - F^{j} \tag{48}$$

where F is the global error vector, resulting from assembling f1, f2, and f3 over the elements.

In the first iteration of each time step, the value of the dependent variables at the previous time step is supplied to the numerical procedure as a guess for the unknown variables. Dirichlet boundary conditions are also set to their corresponding values.

In each iteration, the value of the unknowns is replaced with the output from the solution of the equations, except for the boundary conditions which are not updated.

Advancing Front

Because integration in Eq. 35 is substituted by a numerical procedure that uses a linear combination of the value of the residual in four points inside the element, the depth of flow in these sampling points will be different from zero even if some of the nodes are located at the advancing front. This means that the model will not have to deal with points containing singularities, thus ensuring good behavior at the advancing front.

The location of the advancing edge is computed at the beginning of each time step by assuming that the value of velocity at the node just behind the front is a good estimate of the velocity of the front itself. Edge nodes are then advanced in the direction of the flow, and the whole grid is regenerated.

Grid Management

A locally refined moving grid was implemented to improve the stability of the method. The distribution of the nodes attempts to follow the gradients of depth so that the nodes are set closer where the profile gets steeper. Straight lines are drawn from the inflow location to the advancing edge, and the nodes are allocated along these lines following a symmetrical pattern that tends to concentrate the nodes in the extremes, where the inflow and the advancing edge are located. This pattern associates each node with a percentage of the actual distance between the inflow and the advance nodes so that when the last node is advanced to a new position, the total distance is computed, and the whole net is regenerated.

After regeneration of the grid, nodal velocities can be computed as a ratio of the x and y displacement of the nodes over the length of the time interval. Because the velocity of the front is estimated from the conditions at the penultimate node, it is important that this node is as close as possible to the last one so that a good estimate of front velocity is obtained.

Time Interval

Although the procedure is fully implicit, a time restriction characteristic of explicit schemes has been found. The Courant-Friedrichs-Lewy condition restricts the length of the time step according to an expression that makes

it directly proportional to the node spacing and inversely proportional to the local velocity plus the celerity of a small flow disturbance (Eq. 26).

This condition turns out to be especially restrictive since the number of computations required to advance the solution by one time step is very high, and the limitation on the time step will produce many more time intervals than required by the nature of the problem. In particular, the maximum time step length will shorten if nodes are disposed closely, even if it only happens locally, thus requiring a delicate trade-off between accuracy and computational time.

Computational Time and Number of Nodes

Another important factor influencing the total computational time is the number of nodes, as the size of the matrix to be solved iteratively is proportional to it. The matrix is banded, and a large percentage of the elements is zero. In order to save memory allocation, the matrix was stored in a compressed way, namely, in an array of 27 x 3m elements instead of the original 3m x 3m.

A sparse matrix-solving routine was installed in the model to save computational time and to relax its dependence on the size of the matrix.

Leapfrog Explicit Finite Difference Formulation

The following pages report on the adaptation of the leapfrog scheme to solve the advance, storage, depletion, and

recession phases of a basin irrigation event and to deal with the possibility of irregular field shapes and several simultaneous inflow points.

Discretization of the Domain

As previously mentioned, this model has the capability of dealing with irregular field shapes. Figure 1 illustrates the process of discretization of the physical domain. The first step is to define a grid where the actual field shape can be fit. Grid spacing in the x and y directions will be denoted as Δx and Δy, respectively. Next, some of the cells in the original grid are discarded to better represent the domain. The last step is to assign a code to each of the nodes in the grid to determine its type. The different cases are as follows.

Points out of the domain. No computations have to be carried out on them, since these points are not part of the problem.

Interior points. These have no boundary conditions. There are three unknowns in each of them: flow depth and unit discharge in the x and y directions.

Corners. There are four kinds: upper right, upper left, lower right, and lower left. Only one variable, flow depth, is unknown in them, because the discharge components are zero at these points.

Vertical boundaries. These are left and right of the domain. The parallel flow condition imposes that the

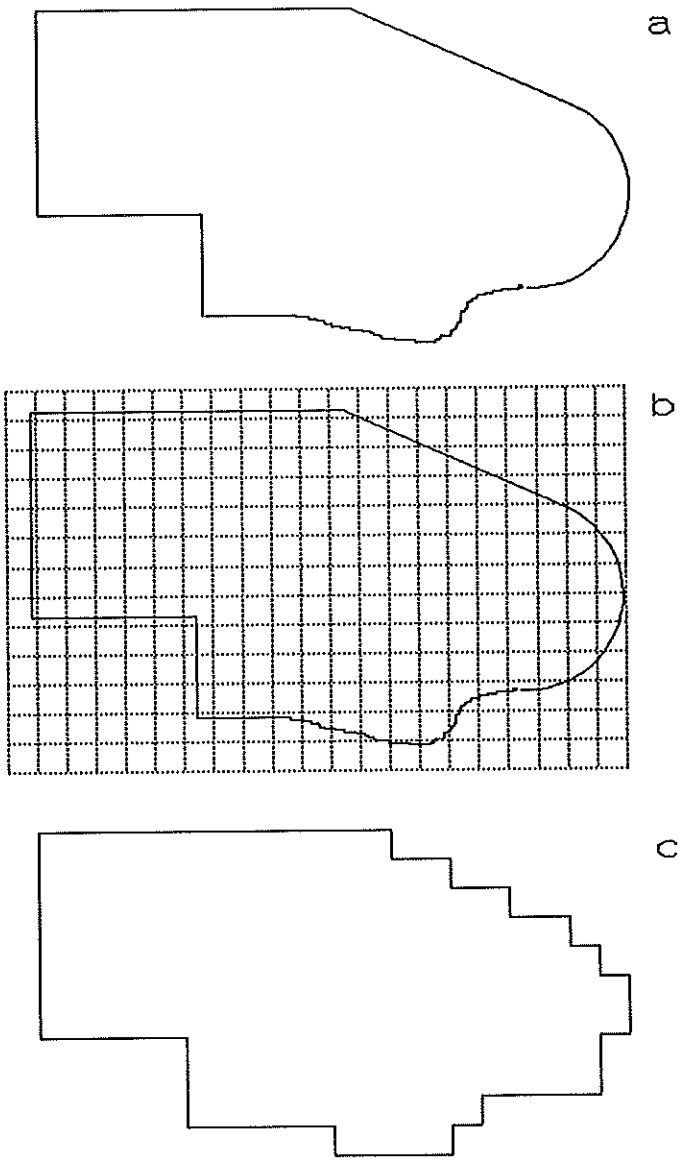

FIGURE 1. Domain Discretization Process. a. Original Field Shape; b. A Grid is superimposed; c. Final Discretized Domain.

discharge component normal to the boundary is zero at these points, since no outflow is allowed. The unknowns are then the vertical discharge component and the depth of flow.

Horizontal boundaries. These are located on the top or bottom of the domain. The unknown variables are the depth of flow and the horizontal unit discharge.

Diagonal points. These follow the condition that although they are on the boundary of the domain, none of their four neighbors falls out of it. Both components of discharge are zero, and the only unknown is flow depth.

Figure 2 provides examples of the different node types on a hypothetical domain. Each different node type will require a different finite differencing technique and will need different solution procedures.

The x coordinate runs from left to right and the y coordinate from the bottom to the top of the domain. The p and q components of unit discharge are considered positive when they flow towards the right and to the top of the domain, respectively.

Inflow Boundary Conditions

Three types of inflow boundary conditions were implemented in the model, which correspond to three characteristic field conditions. A description of each boundary with the expressions used to compute the nodal values follows. The setup of the boundary conditions was

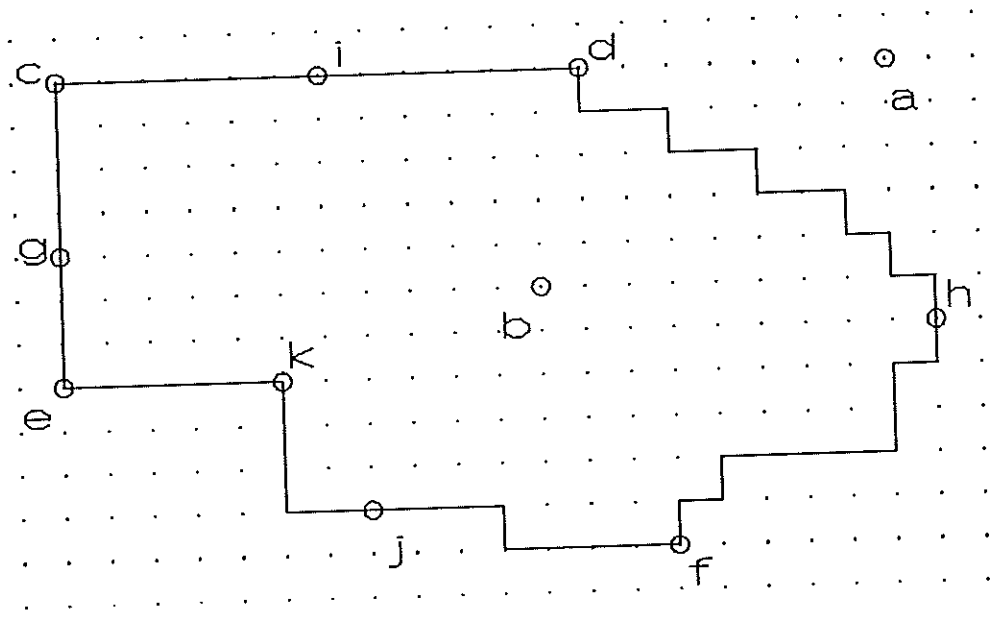

FIGURE 2. Different Node Types. a. Node Out of the Domain; b. Interior Node; c. Upper Left Corner; d. Upper Right Corner; e. Lower Left Corner; f. Lower Right Corner; g. Left Vertical boundary; h. Right Vertical Boundary; i. Upper Horizontal Boundary; j. Lower Horizontal Boundary; and k. Diagonal Node.

designed to ensure stability and mass conservation at the inflow nodes.

Corner inflow. This inflow type simulates flooding of the domain from a point source located in one of its corners. The boundary condition involves three nodes, as sketched in Fig. 3. Nodal values of p and q are imposed in the corner node and its two neighbors. On the corner node, the values for p and q are:

$$p = \pm \frac{Q}{2\Delta y} \tag{49}$$

$$q = \pm \frac{Q}{2\Delta x} \tag{50}$$

where Q is the total discharge assigned to the inflow boundary condition (m^3/s). The appropriate sign has to be selected according to the orientation of the corner. On the horizontal neighboring node, the value of p has to be computed, and the value of q is set to:

$$q = \pm \frac{Q}{4\Delta x} \tag{51}$$

On the vertical neighboring node, the value of q has to be computed, and the value of p is set to:

$$p = \pm \frac{Q}{4\Delta y} \tag{52}$$

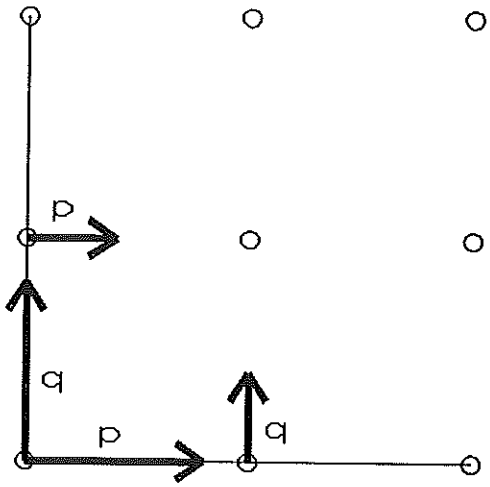

FIGURE 3. Representation of a Lower Left Corner Inflow Boundary Condition.

Line inflow. This boundary simulates a line source along a straight boundary of the domain. This represents an overflowing ditch or several point sources located close to each other along the side of a basin. The nodal values of discharge in the affected nodes will vary according to the boundary condition at the extreme nodes of the line inflow. The boundary configuration is illustrated in Fig. 4.

If the inflow is laid out over a vertical boundary, the vertical component of discharge q will always be set to zero. If both extreme nodes have a vertical line boundary condition, the expression for the horizontal unit discharge p at all the affected nodes is as follows:

$$p = \pm \frac{Q}{l\Delta y} \tag{53}$$

where l is the number of nodes affected by the boundary.

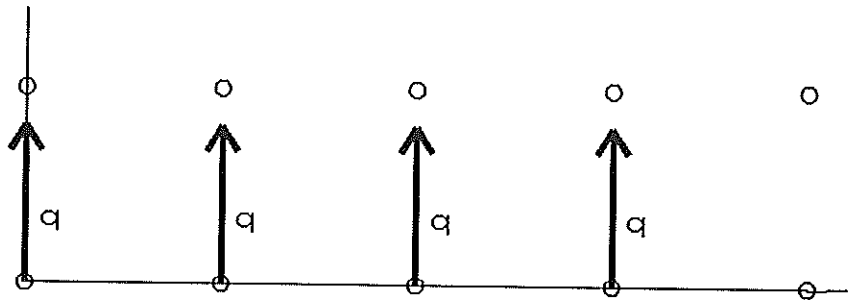

FIGURE 4. Representation of a Lower Horizontal Line Inflow Boundary Condition.

If one of the extremes has a corner boundary condition, the nodal value of p follows the expression:

$$p = \pm \frac{Q}{(1-\frac{1}{2})\Delta y} \tag{54}$$

Finally, if both extremes have corner boundary conditions, the expression for p is:

$$p = \pm \frac{Q}{(1-1)\Delta y} \tag{55}$$

If the line inflow boundary condition sits on a horizontal boundary, the value of p is set to zero in all the affected nodes. If both extremes have line boundary conditions, the nodal value of q is computed as follows:

$$q = \pm \frac{Q}{1\Delta x} \tag{56}$$

If one of them has a corner boundary condition, q follows the expression:

$$q = \pm \frac{Q}{(1-\frac{1}{2})\,\Delta x} \tag{57}$$

If both extremes are corners, the expression for q is:

$$q = \pm \frac{Q}{(1-1)\,\Delta x} \tag{58}$$

Fan Inflow. This boundary condition simulates a point source located on a straight boundary. Figure 5 illustrates its layout. The definition of a fan inflow boundary always affects two nodes. In the case of a vertical fan boundary, the expressions for p and q in the upper node are:

$$p = \pm \frac{Q}{2\,\Delta y} \tag{59}$$

$$q = \frac{Q}{2\,\Delta y} \tag{60}$$

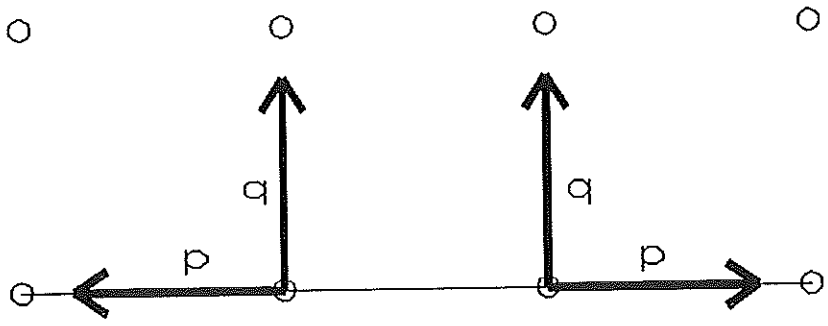

FIGURE 5. Representation of a Lower Horizontal Fan Inflow Boundary Condition.

In the lower node, p and q are computed as:

$$p = \pm \frac{Q}{2\Delta y} \tag{61}$$

$$q = - \frac{Q}{2\Delta y} \tag{62}$$

Similarly, for a horizontal fan boundary, the expressions for p and q in the right node are:

$$p = \pm \frac{Q}{2\Delta x} \tag{63}$$

$$q = \frac{Q}{2\Delta x} \tag{64}$$

In the left node, p and q are computed as:

$$q = \pm \frac{Q}{2\Delta x} \tag{65}$$

$$p = - \frac{Q}{2\Delta x} \tag{66}$$

The initial depth associated with each of the boundary nodes involved in an inflow is computed following the expression

$$h = 1.05 \left(\frac{p^2+q^2}{g}\right)^{\frac{1}{3}} \tag{67}$$

that corresponds to the critical depth increased by 5% to ensure subcritical flow conditions at the inlet. If an inflow started after the node had been flooded, the depth at

the node would be computed as the maximum between the actual depth and the one supplied by Eq. 67.

An interesting characteristic of this inflow boundary condition setup is that no inflow conditions have to be specified in interior nodes, as would be the case with moving grid schemes.

The definition of an inflow boundary condition is completed by the specification of its turn-out time and its cut-off time. The turn-out time does not have to be zero, except for one of the inflows so that there is some flow at the beginning of the simulation.

Artificial Viscosity

The nondissipative nature of the leapfrog scheme recommends the introduction of artificial viscosity as a mechanism to effectively dampen small frequency waves from the solution (Cunge et al., 1980). Two terms in second partial derivatives are added to each equation of motion, namely:

$$\varepsilon \left(\frac{\partial^2 p}{\partial x^2} + \frac{\partial^2 p}{\partial y^2} \right) \tag{68}$$

for the first equation, and

$$\varepsilon \left(\frac{\partial^2 q}{\partial x^2} + \frac{\partial^2 q}{\partial y^2} \right) \tag{69}$$

for the second equation, where ε is the coefficient of turbulent viscosity (m^2/s), or eddy coefficient, whose value

is determined empirically for each problem. The implementation of artificial viscosity in the model should be regarded as a tool for particular applications, and is not intended to be used in every problem. Experience with the model dictates that values of ε up to 5.0 may be useful in smoothing the flow profile. Grid refinement can sometimes yield the same results at the cost of some additional computational effort.

Numerical Procedure

The distinctive feature of the leapfrog scheme is that the net is staggered in time, meaning that not all the variables are computed at all time intervals. Second-order finite difference approximations are introduced for space and time derivatives, following the expressions:

$$\frac{\partial f}{\partial x} \approx \frac{f^{t}_{x+\Delta x,y} - f^{t}_{x-\Delta x,y}}{2\Delta x} \tag{70}$$

$$\frac{\partial f}{\partial y} \approx \frac{f^{t}_{x,y+\Delta y} - f^{t}_{x,y-\Delta y}}{2\Delta y} \tag{71}$$

$$\frac{\partial f}{\partial t} \approx \frac{f_{x,y}^{t+\frac{\Delta t}{2}} - f_{x,y}^{t-\frac{\Delta t}{2}}}{\Delta t} \tag{72}$$

It has to be noted that computations proceed in half time intervals. At half time steps, p and q are computed for all nodes, while at whole time steps, h is computed. This means that an entire time step separates two computations of

the same variable at the same node, thus satisfying the Courant-Friedrichs-Lewy condition.

The expressions for the spatial derivatives take different forms at the boundaries where some of the nodes required for the second-order approximation may fall out of the domain. Forward and backward first-order approximations are used in these cases.

The second partial derivatives needed for the viscosity terms are computed as the derivatives of the first derivatives instead of using the corresponding finite difference approximations. This economizes the code and reduces the number of elemental computations.

At whole time steps, the equation of continuity has to be solved for the value of h at all the nodes. The equation is discretized as follows:

$$\frac{h^{t+\Delta t}-h^{t}}{\Delta t} + \frac{\partial p}{\partial x} + \frac{\partial q}{\partial y} + i = 0 \qquad (73)$$

where the spatial partial derivatives and the infiltration term are evaluated at time $t+\Delta t/2$. It allows the solution for $h^{t+\Delta t}$ explicitly:

$$h^{t+\Delta t} = h^{t} - \Delta t\left(\frac{\partial p}{\partial x} + \frac{\partial q}{\partial y} + i\right) \qquad (74)$$

At half time steps, the two equations of motion are solved for p and q. Finite differencing yields the following expressions of the equations:

$$\frac{p^{t+\frac{\Delta t}{2}}-p^{t-\frac{\Delta t}{2}}}{\Delta t} + (gh-\frac{p^2}{h^2})\frac{\partial h}{\partial x} + \frac{2p}{h}\frac{\partial p}{\partial x}$$

$$- \frac{pq}{h^2}\frac{\partial h}{\partial y} + \frac{q}{h}\frac{\partial p}{\partial y} + \frac{p}{h}\frac{\partial q}{\partial y} + gn^2p\frac{(p^2+q^2)^{\frac{1}{2}}}{h^{\frac{7}{3}}}$$

$$- \frac{pi}{2h} + \varepsilon(\frac{\partial^2 p}{\partial x^2}+\frac{\partial^2 p}{\partial y^2}) = 0 \qquad (75)$$

for motion in the x direction, and

$$\frac{q^{t+\frac{\Delta t}{2}}-q^{t-\frac{\Delta t}{2}}}{\Delta t} + (gh-\frac{q^2}{h^2})\frac{\partial h}{\partial y} + \frac{2q}{h}\frac{\partial q}{\partial y}$$

$$- \frac{pq}{h^2}\frac{\partial h}{\partial x} + \frac{p}{h}\frac{\partial q}{\partial x} + \frac{q}{h}\frac{\partial p}{\partial x} + gn^2q\frac{(p^2+q^2)^{\frac{1}{2}}}{h^{\frac{7}{3}}}$$

$$- \frac{qi}{2h} + \varepsilon(\frac{\partial^2 q}{\partial x^2}+\frac{\partial^2 q}{\partial y^2}) = 0 \qquad (76)$$

for motion in the y direction where the spatial derivatives and the infiltration rate are evaluated at time t.

Estimates of the dependent variables p and q are obtained using the formulae:

$$p = \theta p^{t-\frac{\Delta t}{2}} + (1-\theta)p^{t+\frac{\Delta t}{2}} \qquad (77)$$

$$q = \theta q^{t-\frac{\Delta t}{2}} + (1-\theta)q^{t+\frac{\Delta t}{2}} \qquad (78)$$

where θ is a parameter between 0 and 1 that usually takes the value of 0.5.

Equations 75 and 76 constitute a set of coupled implicit equations on $p^{t+\Delta t/2}$ and $q^{t+\Delta t/2}$. Their solution is accomplished by means of an iterative Newton-Raphson method. Suppose that f_1 is defined as the result of Eq. 75 and f_2 as the result of Eq. 76. The derivative terms needed for the solution of the equations are:

$$\frac{\partial f_1}{\partial p^{t+\frac{\Delta t}{2}}} = \frac{1}{\Delta t} + \left(-\frac{2p}{h^2}\frac{\partial h}{\partial x} + \frac{2}{h}\frac{\partial p}{\partial x} - \frac{q}{h^2}\frac{\partial h}{\partial y} + \frac{1}{h}\frac{\partial q}{\partial y}\right.$$

$$\left. + gn^2 \frac{(p^2+q^2)^{\frac{1}{2}} + \frac{p^2}{(p^2+q^2)^{\frac{1}{2}}}}{h^{\frac{7}{3}}} - \frac{i}{2h}\right)(1-\theta) \qquad (79)$$

$$\frac{\partial f_1}{\partial q^{t+\frac{\Delta t}{2}}} = \left(\frac{p}{h^2}\frac{\partial h}{\partial y} + \frac{1}{h}\frac{\partial p}{\partial y} + gn^2 \frac{pq}{(p^2+q^2)^{\frac{1}{2}}}\right)(1-\theta) \qquad (80)$$

$$\frac{\partial f_2}{\partial p^{t+\frac{\Delta t}{2}}} = \left(\frac{q}{h^2}\frac{\partial h}{\partial x} + \frac{1}{h}\frac{\partial q}{\partial x} + gn^2 \frac{pq}{(p^2+q^2)^{\frac{1}{2}}}\right)(1-\theta) \qquad (81)$$

$$\frac{\partial f_2}{\partial q^{t+\frac{\Delta t}{2}}} = \frac{1}{\Delta t} + \left(-\frac{2q}{h^2}\frac{\partial h}{\partial y} + \frac{2}{h}\frac{\partial q}{\partial y} - \frac{p}{h^2}\frac{\partial h}{\partial x} + \frac{1}{h}\frac{\partial p}{\partial x}\right.$$

$$\left. + gn^2 \frac{(p^2+q^2)^{\frac{1}{2}} + \frac{q^2}{(p^2+q^2)^{\frac{1}{2}}}}{h^{\frac{7}{3}}} - \frac{i}{2h}\right)(1-\theta) \qquad (82)$$

The solution of the two simultaneous equations is only necessary for interior points. Vertical and horizontal boundary nodes require the solution of one of the implicit equations, since one of the components of discharge is known to be zero. Finally, corners and diagonal points do not require the solution of the motion equations, since both discharge components are zero.

Initial Conditions

The numerical procedure requires all depths to be greater than zero for stability reasons. This means that a nonzero depth must be assigned to points that have not been reached by an advancing front, implying that in fact the whole domain is ponded with water at the beginning of the advance phase. A small, positive value of 10^{-10} m is initially assigned to the depth of flow at all computational nodes in the domain. The same value is used to initialize p and q.

Conservative Properties

The quality of the simulation is often evaluated in the literature by means of a mass conservation study. This is an indication of how the model respects the equation of mass continuity (Eq. 16). The principle of continuity as applied to the whole domain states that the overland plus infiltrated volume has to be equal to the summation of the product of discharge times application time for each inflow boundary condition. This principle can be expressed as:

$$V_h + V_z = \sum_{j=1}^{I} Q_j \, (t_i - t_o)_j \tag{83}$$

where V_h is the overland volume (m^3), V_z is the infiltrated volume (m^3), t_i is the turn-out time of an inflow (s) and t_o is the cut-off time of an inflow (s). Violations of Eq. 83 create an error whose expression is:

$$e = 100 \, \frac{V_h + V_z - \sum_{j=1}^{I} Q_j \, (t_i - t_o)_j}{\sum_{j=1}^{I} Q_j \, (t_i - t_o)_j} \tag{84}$$

where e is the mass balance error, expressed as a percentage.

The mass balance error is typically high at the beginning of the simulation due to the approximation introduced by the initial condition and has a tendency to decrease as the computation proceeds, asymptotically approaching a value of zero.

Advance and Infiltration

Special attention must be devoted in this case to the definition of the advance phenomenon because the numerical procedure considers a nonzero depth in all nodes, thus denying the existence of an advancing front. Also, the opportunity time should start counting in all nodes since the first time step.

This is far from what really happens in the field. A procedure was introduced to ignore all flow depths smaller than a certain user-defined threshold, the minimum depth

needed for the model to consider this point as part of the advancing front and allow infiltration from it. This minimum depth must be greater than 10^{-10}. Values in the order of 10^{-3} m produced satisfactory results.

Every time the depth of flow is computed for a node, the model checks for the validity and significance of the new value. If this value is smaller than 10^{-10}, it is reset to 10^{-10} to protect the numerical procedure from singularities introduced by zero or negative flow depths.

If the computed depth is greater than the minimum depth, the opportunity time for this node starts counting, and the node is ready to start infiltrating in the next time step. A common problem found in the following time steps is that the volume that needs to be infiltrated is larger than the volume supplied to the node by overland flow. This will produce a negative depth as a result of the solution of the continuity equation. When this negative value is reset to 10^{-10}, a mass balance error is introduced because the continuity equation is violated.

To minimize this error, the infiltrated depth in the node is diminished by the amount of mass balance violation, and a Newton-Raphson method is used to solve the Kostiakov-Lewis equation for the opportunity time corresponding to the new value of the infiltrated depth.

The end of the advance phase occurs when flow depth at all nodes in the domain is greater than the minimum depth. The value of time at this point is the advance time.

End of the Simulation

For the simulation to come to an end, all defined inflows must have been cut off, and one of the following two conditions must happen:

1. End of advance.

2. Discharge all over the domain is negligible (a threshold value of 10^{-4} m^2/s for p and q is set in the model).

At this point there may be a considerable overland volume in the field, but because the domain is considered to be flat, the assumption is made that the flow profile also becomes flat at this time and remains flat until all the water is infiltrated.

This assumption will not limit the validity of the model since, in the first case, the overland volume is usually large enough as to expect the profile to flatten before any node runs dry. In the second case, which is an incomplete advance, the flow profile will be sensibly flat and the overland volume will be fairly small.

Once this condition is reached, the numerical procedure is abandoned, and the Kostiakov-Lewis infiltration equation takes full control of the simulation, increasing the infiltrated depth at each node until the overland volume is consumed. The value of time at this point is the depletion time, and thus the simulation has ended.

Computational Time
and Number of Nodes

The leapfrog scheme is also constrained by the Courant-Friedrichs-Lewy condition, but the time step will usually be longer than the one required for the Petrov-Galerkin scheme because node spacing is constant and usually larger (no adaptative grid is used).

On the other hand, the computational effort per time step is much smaller. No global matrices are required, and only in some nodes is a second-order Newton-Raphson method necessary.

CHAPTER IV

DESCRIPTION OF THE B2D SOFTWARE

The B2D Software

The leapfrog numerical procedure was implemented into a software application called B2D, which stands for "Basin, Two Dimensions." The motivation in writing this software was to provide an easy-to-use, inexpensive tool for two-dimensional design of irrigated basins that could be used by individuals who are not particularly familiar with the underlying theory. Most of the current standards in user interfacing were adopted in B2D to minimize the learning time for new users. Also, an on-line help system provides the user with specialized assistance.

The model was developed for IBM PC and compatible microcomputers using the C++ programming language. The Irrigation Software Division of the Biological and Irrigation Engineering Department at Utah State University (1992) fully described the model in their User's Manual. A brief report of its features follows.

User Interface

B2D has four different screens that are used in different parts of the simulation process. These four screens are the problem edit screen, the field shape edit screen, the run-time screen, and the file view screen.

Problem Edit Screen

B2D's edit screen is divided into three parts that serve different purposes.

The upper part is a pull-down menu line that guides the user through the different features of the model and allows the editing, saving, and loading of application files. Items in a menu can be selected by scrolling a highlighted bar or by hitting a hot key. The variables that define the problem are input in dialogue windows that always offer default values and that check the input value for feasibility. A file utilities section is provided to ease file loading and saving, file directories, environmental settings, and temporary operating system shelling.

The middle part displays the value of characteristic variables and informs the user about the state of the problem being defined.

The lower part of the screen is a status line that informs the user about hot keys, displays a real-time clock and calendar, and pops up error messages when appropriate.

Field Shape Edit Screen

The shape editor allows the user to define the field shape and inflow points in an interactive way. A user-defined rectangular grid is mapped on the screen, and the user is allowed to clip off parts of the net to accommodate it to the actual shape of the field. B2D informs the user about distances within the grid and the area of the selected

domain. Both exterior and interior regions may be clipped from the grid.

The user can define up to six different inflow boundary conditions in each field. These inflows can have corner, line, or fan configurations to best simulate the field conditions.

Run-Time Screen

A run-time screen is displayed to supply information about the problem as it is being solved. The software has the capability to record the results of a simulation in a file that can reproduce the run-time graphs without going through the numerical solution procedure. This option is intended to be a tool to review the results of problems whose simulation takes a long time.

The text part of the run-time screen informs the user about the current time and total discharge, displays a mass balance, and supplies information about the possible actions the user can take. The graphical part of the run-time screen displays contour line or three-dimensional plots of overland flow depth or infiltration depth. Three different scales are available to make the most of the computer screen. B2D is ready to display graphics on CGA, EGA, VGA, or more advanced monitors.

File View Screen

An ASCII file viewer is provided as part of the B2D software to check the contents of the output files without

leaving the program. It implements utilities to navigate through large files with minimum wait time.

Input and Output Files

Problem definition files have a B2D extension. These are the only input files. There are two different output file types. The first type has an OUT extension and contains a customized, comprehensive output from the model. The second type has a DAT extension and is used by B2D to reproduce the run-time graphics. DAT files are also written in a format easily read by spreadsheets and three-dimensional plotting packages. Appendix A contains selective printouts from typical B2D input and output files.

The OUT file echoes the problem definition, reports on the nodal values of h, z, p, q, u, and v at selected time steps, and contains a final report with the values of the advance and recession times, final opportunity times, and infiltrated depths. It also contains an efficiency report that provides values of the application efficiency (E_a), deep percolation ratio (DPR), and water requirement efficiency (E_r) for different values of the required irrigation depth.

CHAPTER V

ANALYSIS OF RESULTS

Petrov-Galerkin and Leapfrog Schemes

A series of computational experiments was performed to compare the Petrov-Galerkin finite element and the leapfrog finite difference schemes in terms of predictive capability and CPU time requirement. One-dimensional applications of the two-dimensional models were used in the experiments to permit the use of a reliable one-dimensional model as a source for comparison. SIRMOD was chosen for this purpose.

All three models were used to simulate the following case study 1: A rectangular level basin is irrigated from its west side, and the models must predict the overland and infiltrated profiles during the first 30 min of advance. The characteristics of the field are given in Table 1.

The Petrov-Galerkin finite element scheme (PGFE) was configured in the following way: The domain was covered with parallel arrays of seven nodes each, running from the inflow side to the advancing tip. These nodes constitute a moving grid that characterizes the approach. Four different node configurations were used, each represented by a different value of a parameter ß. Figure 6 illustrates the node disposition for values of ß of 25, 50, 75, and 100. A ß value of 100 places the nodes equally between the inflow and the advancing front, while decreasing values of ß gradually push nodes toward the extremes. This adaptative grid scheme

TABLE 1. Characteristics of Case Study 1.

Columns: Variable	x Spacing (m): Variable
Rows: Variable	y Spacing (m): Variable
Area (m^2): Variable	Shape: Rectangular
Inflows: Type: Line Location: West side Unit Discharge (m^2/s): 0.01 Time in (min): 0.0 Time out (min): 30.0	
Infiltration: Family 0.5 of the SCS system k ($m^3/min^a/m$): 0.00320 a: 0.504 f_0 ($m^3/min/m$): 0.000117	
Min. Depth (m): 0.001	Courant Number: 0.8
ε (m^2/s): 0.0	Manning's n: 0.04

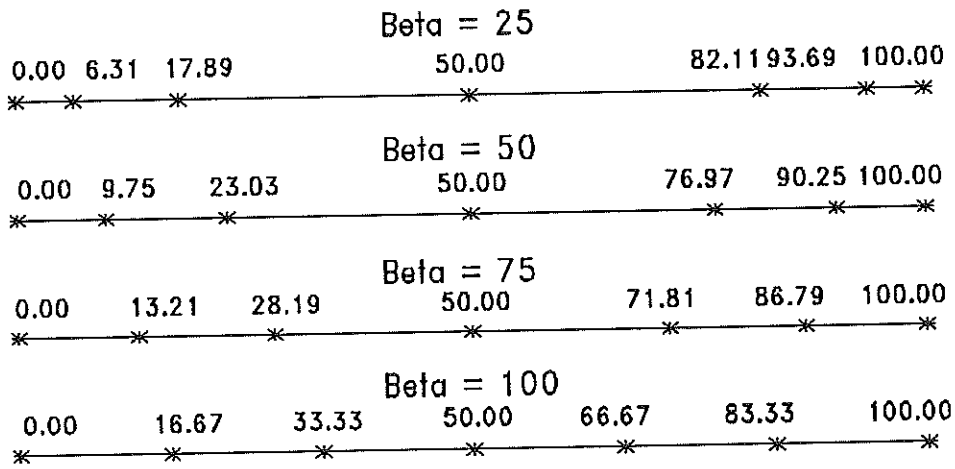

FIGURE 6. Node Layouts Corresponding to Different Values of ß for the Petrov-Galerkin Finite Element Models.

intends to locate computational nodes where gradients of the dependent variables tend to be higher. The values shown in Fig. 6 are percentages of the distance between the inflow point and the advancing tip. The grid is regenerated every time step to maintain these percentages as the wetting front advances.

The four grids shown in Fig. 6 produce four different models: PGFE100, PGFE75, PGFE50, and PGFE25. The advantage of this adaptative grid system is that better profiles can be obtained with a small number of nodes if the nodes are located where they are most needed. The disadvantage is that since the PGFE method is constrained by the Courant-Friedrichs-Lewy condition, shorter time steps will be required for low values of ß, and the computation will be slowed substantially due to the closer spacing of nodes.

The leapfrog scheme will be referred to as B2D, which is also the name given to the final software developed and used in this research. The grid is composed of 63 nodes in three horizontal lines of 21 each, spaced 10 m in each direction, and with a line inflow boundary condition in the left extreme. A total discharge of 0.200 m^3/s provided the desired unit discharge when applied along the 20 m side of the domain. No artificial viscosity was used in this simulation, and the minimum depth was set to 10^{-3} m.

Figure 7 illustrates the advance phenomenon as simulated by SIRMOD, B2D, and PGFE25. At the late stages of advance, PGFE25 and B2D produced similar results, and both showed a

difference of about 5% with SIRMOD, whose advance was slightly slower.

Figure 8 displays the same advance trajectory for the four PGFE models. The differences between them are not important, but PGFE25 shows a slower advance that is closer to the results produced by SIRMOD. Because the advance is estimated in the PGFE method using the flow velocity of the penultimate node, the closer the penultimate node is to the advancing node, the better the estimate will be. This provides a more accurate advance trajectory for PGFE25. The fact that all four models show similar advance proves that flow velocity is considerably uniform in this region for this particular case study.

Figure 9 depicts the overland and infiltrated flow profiles at 10, 20, and 30 min for SIRMOD, B2D, and PGFE25. Profiles generated by B2D show some smearing at the advancing front and small numerical oscillations throughout the profile, while SIRMOD and PGFE25 show a steeper advancing front and oscillation-free profiles. Artificial viscosity could have been used in B2D to reduce the numerical oscillations (its use will be documented later in this chapter). A finer grid would also produce better behaved results.

Figure 10 shows the same profiles for the four PGFE simulations. The beneficial effect of the adaptative grid is reflected on the progressive steepening of the profile, especially at time 30 min as the value of ß decreases.

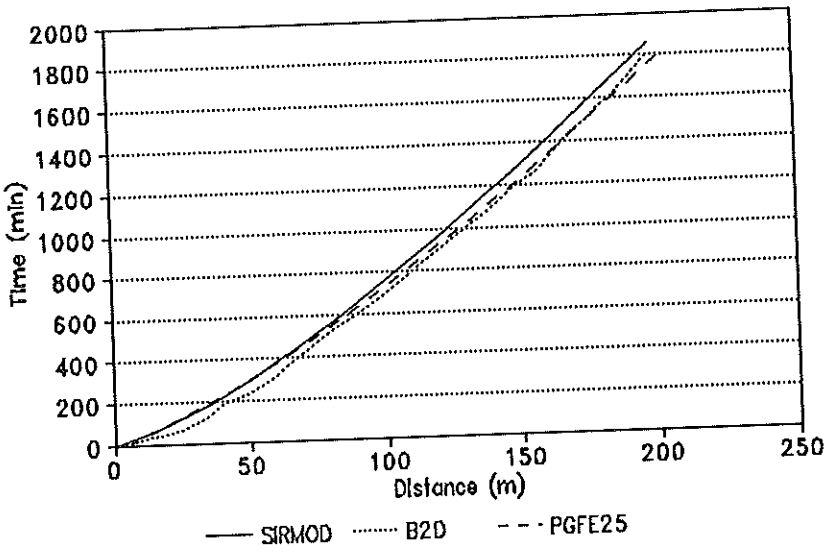

FIGURE 7. Advance Trajectory for Case Study 1 Simulated by SIRMOD, B2D, and PGFE25.

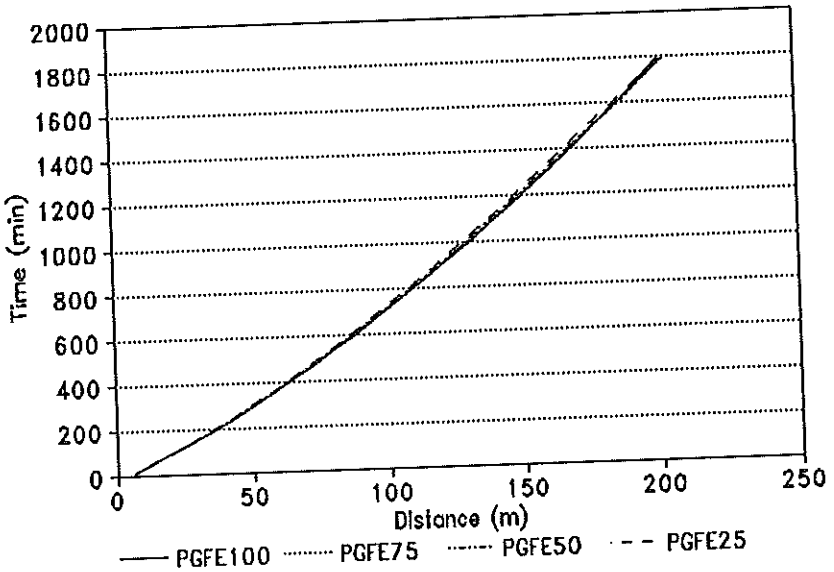

FIGURE 8. Advance Trajectory for Case Study 1 Simulated by PGFE100, PGFE75, PGFE50, and PGFE25.

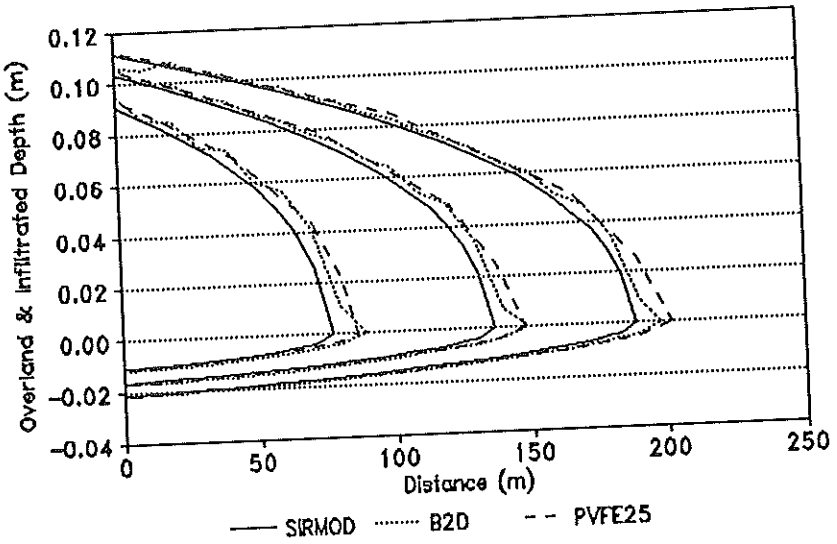

FIGURE 9. Advance Profiles for Case Study 1 at Times 10, 20 and, 30 min Simulated by SIRMOD, B2D, and PGFE25.

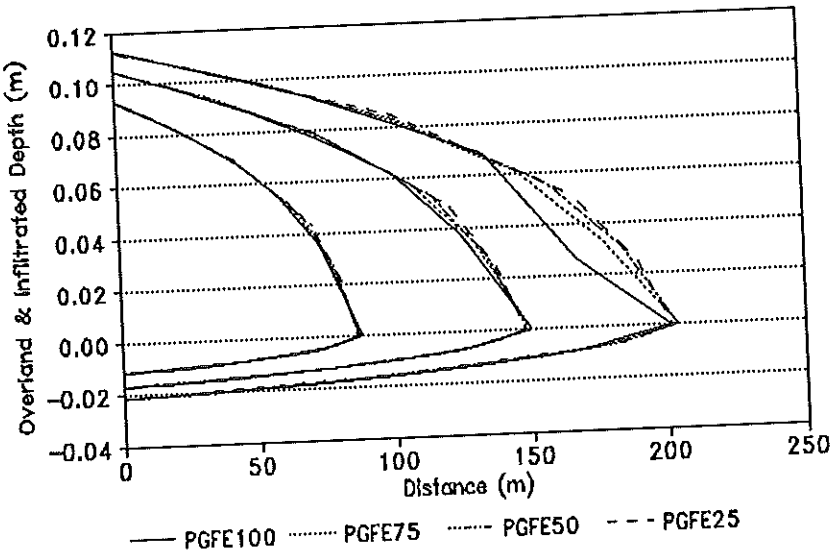

FIGURE 10. Advance Profiles for Case Study 1 at Times 10, 20, and 30 min Simulated by PGFE100, PGFE75, PGFE50, and PGFE25.

Figures 11 and 12 show the CPU time requirement by the PGFE and B2D models as a function of the number of nodes used in the analysis. All CPU times refer to a 386 SX PC compatible computer with a 387 math coprocessor. The high CPU requirements of the PGFE scheme make it impractical to run on a PC, thus a 5100 DEC workstation was used to run the bulk of the simulations. Short runs were performed on a PC to compare CPU times.

Figure 12 shows the biggest disadvantage of the PGFE method. For a 49 (7 x 7) node configuration, the CPU requirement for PGFE25 is about 3,400 times larger than for B2D. The PGFE method shows better advance profiles, but its high computer time requirements put a serious burden on one of the objectives of this research, which is implementation of the model in microcomputers with reasonable execution speed.

Figure 12 shows the differences in CPU time between the four PGFE simulations due to the different length of the time steps. For the 49-node configuration, PGFE25 requires about three times more computational time than PGFE100, but the quality of the profiles produced by PGFE25 makes it a much better solution.

The CPU requirement shown for B2D is not only much lower than the one for PGFE, but the slope of the curve is much milder too, meaning that the quality of the solution can be improved by adding nodes at a relatively low computational expense.

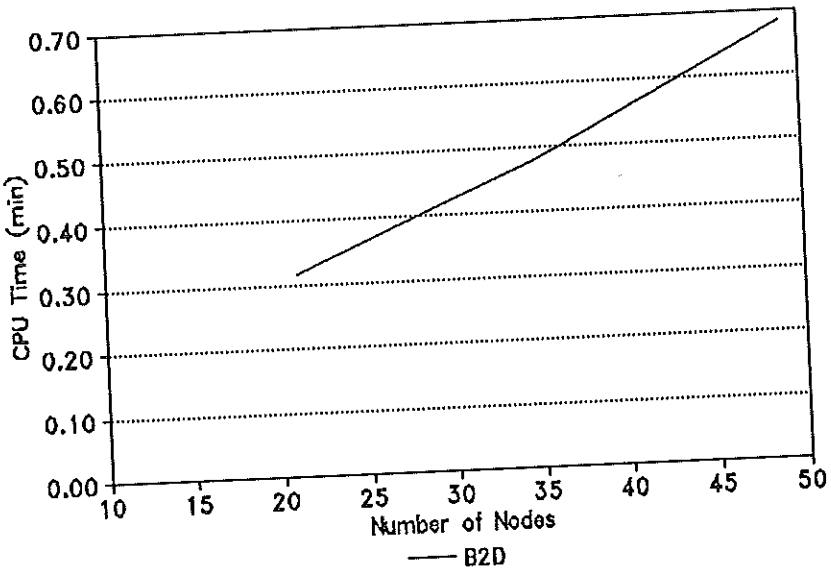

FIGURE 11. CPU Time Requirement (PC 386/387 Computer) for a B2D Simulation of Case Study 1 as a Function of the Number of Nodes.

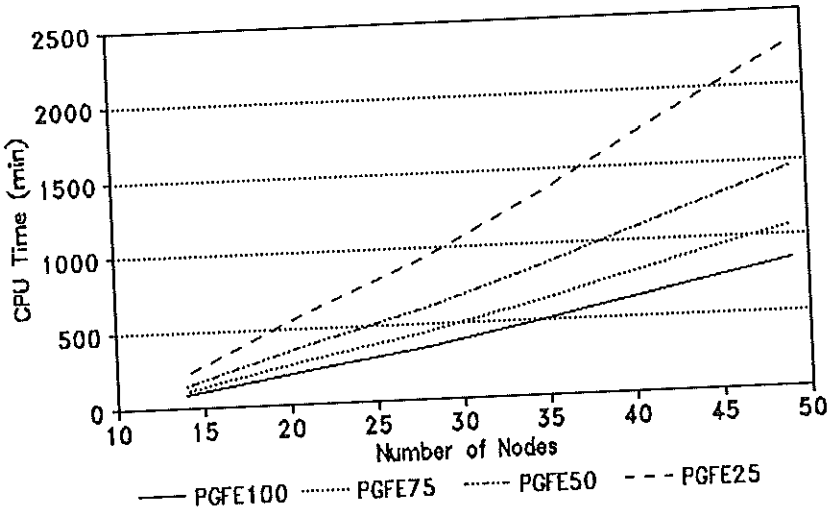

FIGURE 12. CPU Time Requirement (PC 386/387 Computer) for PGFE100, PGFE75, PGFE50, and PGFE25 Simulations of Case Study 1 as a Function of the Number of Nodes.

The use of a sparse matrix solver in PGFE greatly relaxes the dependence of computational time on the number of nodes, as shown by the fact that the curves in Fig. 12 are almost linear. In contrast, a Gaussian elimination solving technique would produce an N^3 process in which the computational time would be proportional to the third power of the number of nodes.

Consideration of the computational time favors the leapfrog scheme. The following pages will report on some features of the B2D software and examine its behavior under different circumstances.

Comparison of the B2D and SIRMOD Models

Several numerical experiments were run to compare the performance of B2D and SIRMOD in one-dimensional applications. Case study 2 was designed to make the comparison. Initial and boundary conditions are detailed in Table 2. The case consists of a line inflow that floods a rectangular field 100 m long and 1 m wide.

Infiltration was identified as a key variable in the comparison between SIRMOD and B2D. The SCS infiltration family system was used to standardize the infiltration parameters, and five different infiltration families were used to estimate advance times using both models.

Two different grids were used to study the effect of the number of nodes on the quality of the simulation. Table 3

TABLE 2. Characteristics of Case Study 2.

Columns: 11 and 21	x Spacing (m): 10.0
Rows: 5	y Spacing (m): 5.0
Area (m^2): 1,000	Shape: Rectangular
Inflows: Type: Line Location: West side Unit Discharge (m^2/s): 0.002 Time in (min): 0.0 Time out (min): 105.0	
Infiltration: Variable	
Min. Depth (m): 0.001	Courant Number: 0.8
ε (m^2/s): 0.0	Manning's n: 0.04

displays the results of the computational experiment, focusing on advance time. When the 11 x 5 nodes configuration is used in B2D, a typical 10% deviation from SIRMOD is found. When a 21 x 5 net is used, this deviation is reduced to about 5%. The deviation between B2D and SIRMOD increases as soil texture becomes coarser, especially for the 26 x 5-node configuration.

The error becomes marginal when comparisons are established between recession times, and is even smaller when efficiency terms are compared due to the buffering effect of the exponential infiltration equation. The fact that B2D always produces faster advances than SIRMOD seems to be

TABLE 3. One-Dimensional SIRMOD and B2D Advance Times (min) to 100 m.

SCS Family and Soil Texture	SIRMOD	B2D 11 x 5 nodes	B2D 21 x 5 nodes
0.10 Clay	35.9	32.2 (-10.3)	34.2 (-4.7)
0.30 Clay Loam	38.8	34.9 (-10.1)	36.8 (-5.2)
0.60 Silty Loam	43.3	39.0 (-9.9)	41.0 (-5.3)
0.90 Sandy Loam	49.4	44.4 (-10.1)	46.6 (-5.7)
2.00 Sandy	93.5	79.2 (-15.3)	86.1 (-7.9)

Note: B2D Uses Two Different Configurations of 11 x 5 and 21 x 5 Nodes. Data in Parenthesis Indicate Percentage Deviation from SIRMOD.

related to the smearing of the advancing front apparent in Fig. 9.

The predictive capability of B2D's one-dimensional applications proves to be strongly related to the fineness of the grid. Small cells reduce smearing and steepen the flow profile in the vicinity of the advancing front, thus delaying advance.

Features of the B2D Software

Three-dimensional representations of the different inflow boundary conditions implemented using B2D are shown in Fig. 13. The pictures on the left represent typical overland

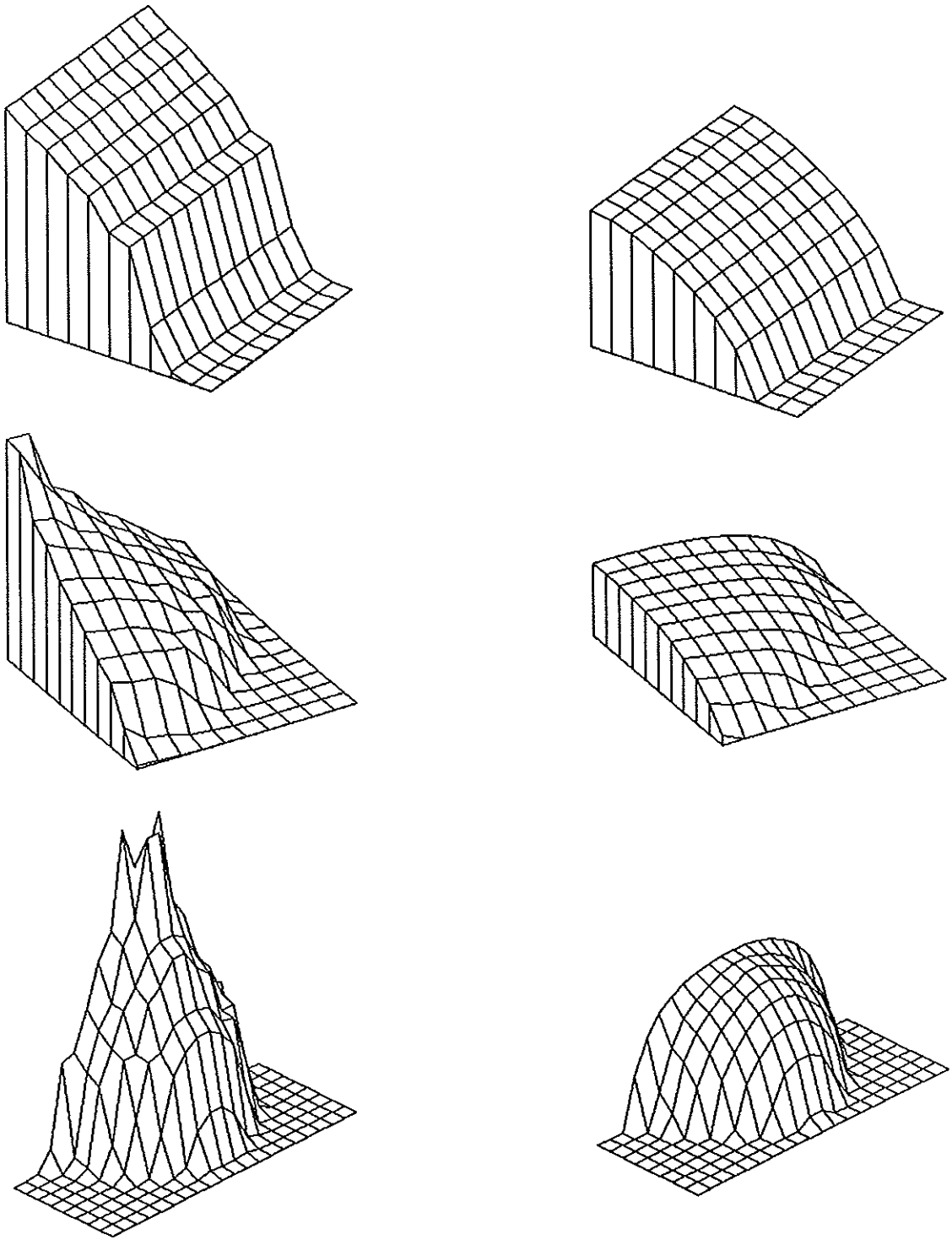

FIGURE 13. Typical Overland (Left) and Infiltrated (Right) Profiles for the Three Types of Inflow Boundary Conditions: Line (Top), Corner (Middle), and Fan (Bottom).

flow profiles. The pictures on the right represent the corresponding infiltrated profiles.

Case study 3 was developed to illustrate B2D's capability to deal with two simultaneous corner inflows into a square domain. The characteristic parameters of the problem are specified in Table 4. Figures 14, 15, 16, and 17 illustrate the results of the simulations at 5-min time steps, and from time 5 min to time 72 min, which is the time of recession. All four figures represent overland depth profiles on the left and infiltrated depth profiles on the right. The simulation shows an incomplete advance case in which the advancing front cannot reach the south edge of the domain. The 10 min delay in the northeast inflow can be noticed in all the overland and infiltrated profiles up to time 72 min.

The solution is well-behaved in all steps of the simulation, and no stability problems are induced by the introduction of a new inflow during the simulation or by the cut off of an existing one. Some numerical oscillations appear in the solution at time steps 50 and 55 min due to a poor performance of the model in conditions of mild gradients in the dependent variables. These conditions are not common in surface irrigation, except in the depletion phase. B2D circumvents this problem by dropping the leapfrog scheme once the advance has come to an end. The infiltration equations are then used to assign the overland volume to each node, assuming a horizontal water profile. If the advance

TABLE 4. Characteristics of Case Study 3.

Columns: 11	x Spacing (m): 10.0
Rows: 11	y Spacing (m): 10.0
Area (m^2): 10,000	Shape: Square
Inflows: Type: Corner Location: North West Corner Discharge (m^3/s): 0.100 Time in (min): 0.0 Time out (min): 30.0 Type: Corner Location: North East Corner Discharge (m^3/s): 0.100 Time in (min): 10.0 Time out (min): 40.0	
Infiltration: Family 0.8 of the SCS system k ($m^3/min^a/m$): 0.00324 a: 0.568 f_0 ($m^3/min/m$): 0.000174	
Min. Depth (m): 0.001	Courant Number: 0.8
ε (m^2/s): 0.0	Manning's n: 0.04

phase is not complete at the time of cut off, B2D uses the leapfrog scheme until both components of discharge at all nodes are negligible. Then the infiltration equations are used to infiltrate the remaining overland volume.

Figures 18 and 19 contain contour line maps of the Reynolds number for the third case study at times 25 and 45

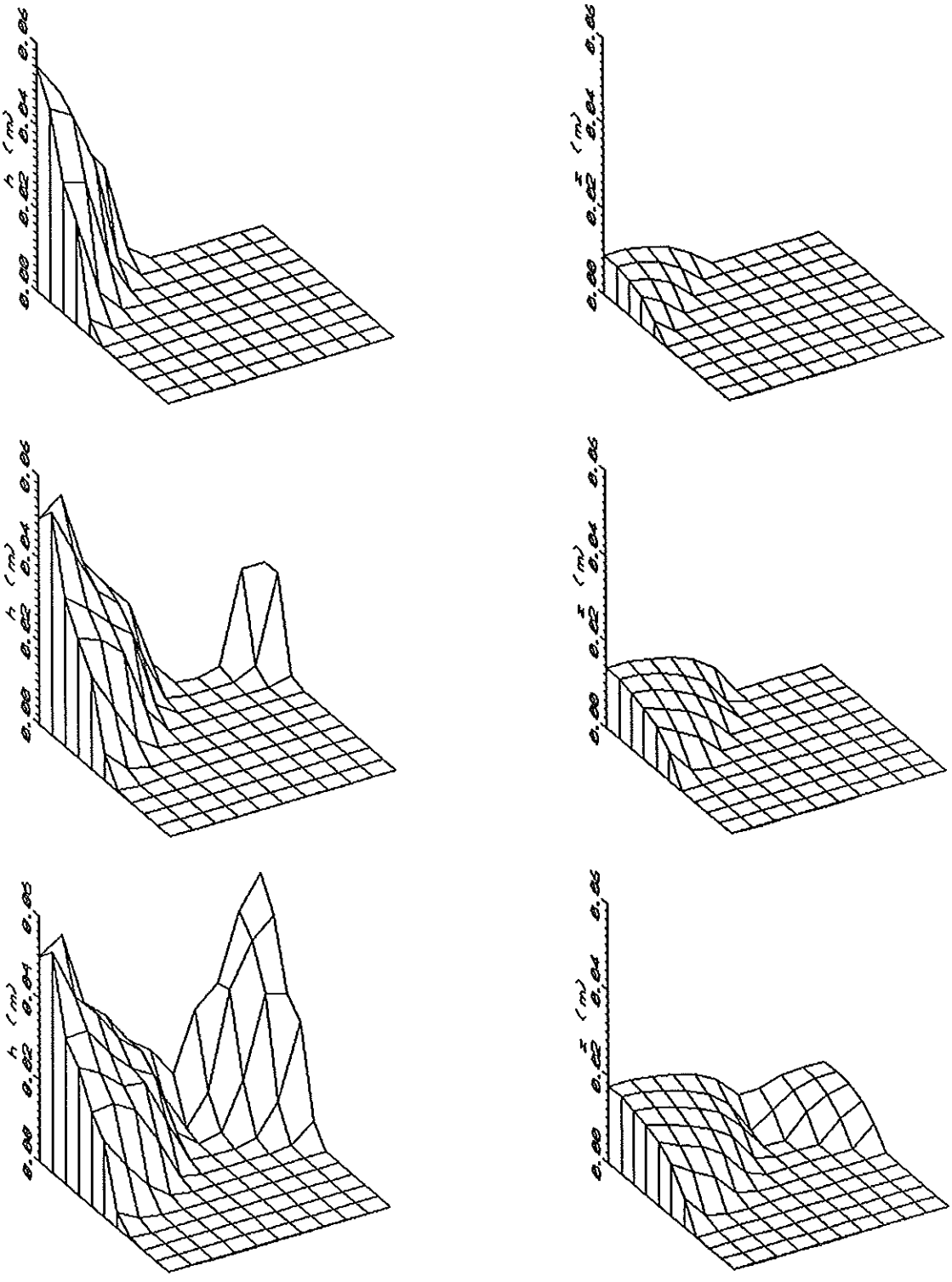

FIGURE 14. Overland (Left) and Infiltrated (Right) Profiles for Case Study 3 at Times 5, 10, and 15 min.

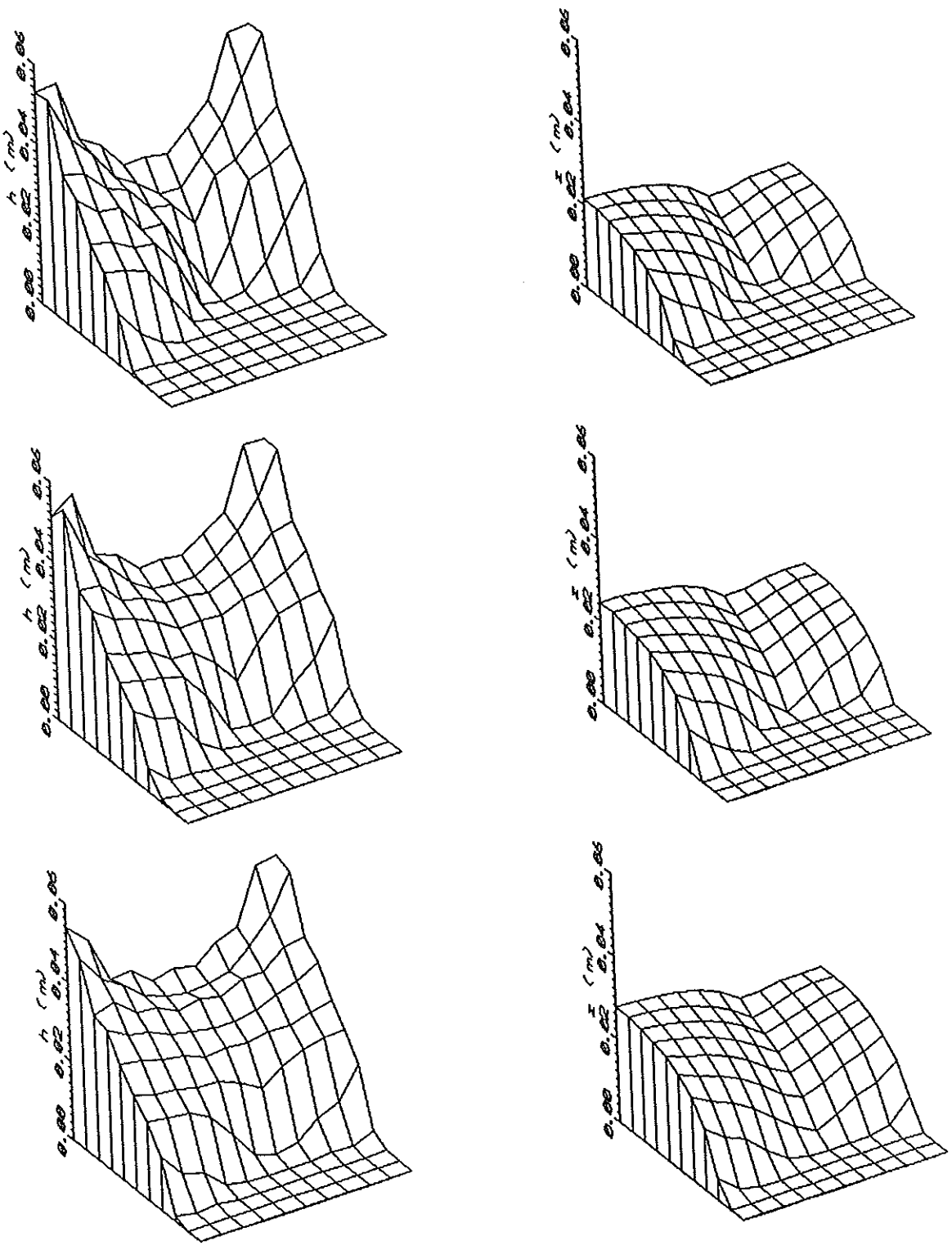

FIGURE 15. Overland (Left) and Infiltrated (Right) Profiles for Case Study 3 at Times 20, 25, and 30 min.

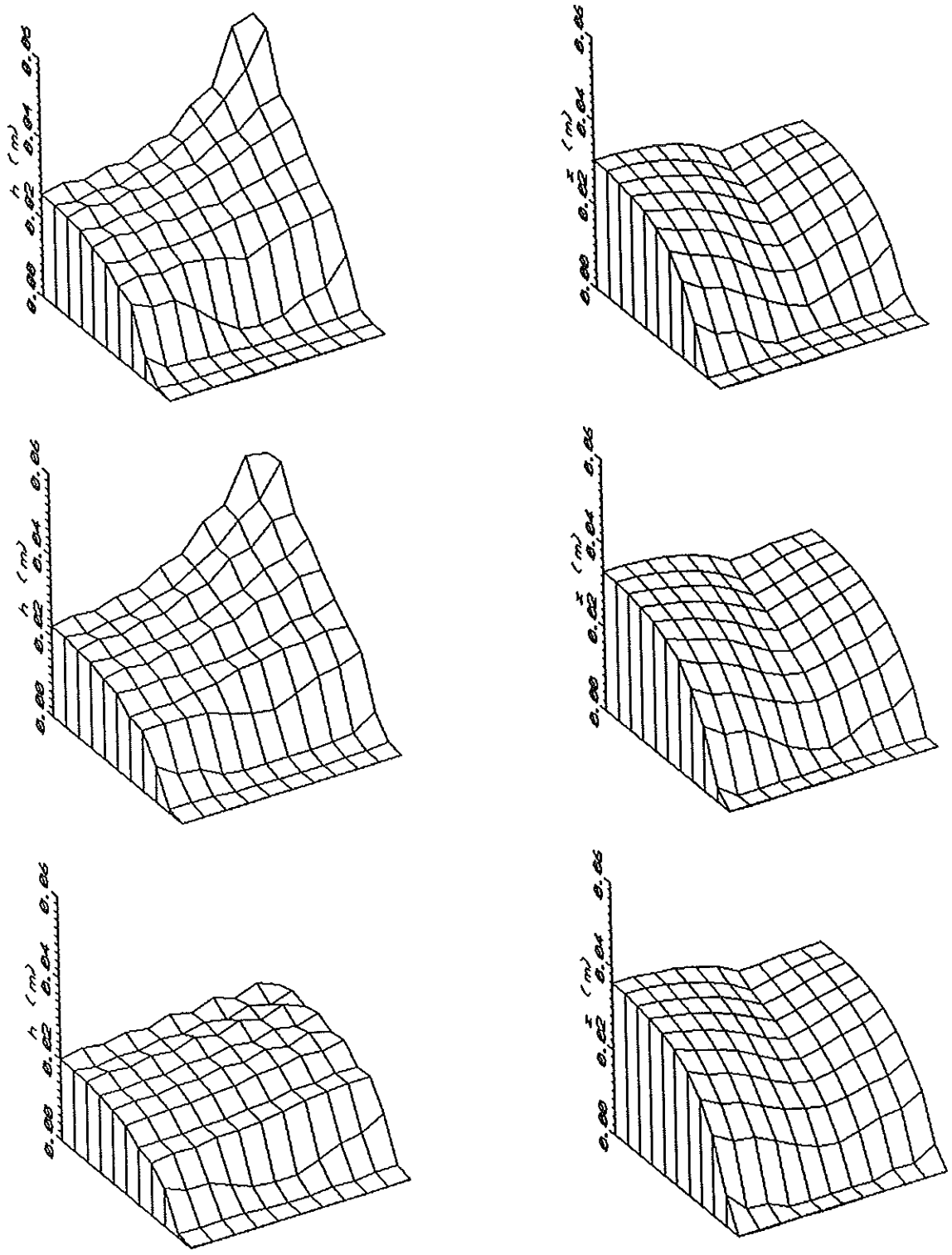

FIGURE 16. Overland (Left) and Infiltrated (Right) Profiles for Case Study 3 at Times 35, 40, and 45 min.

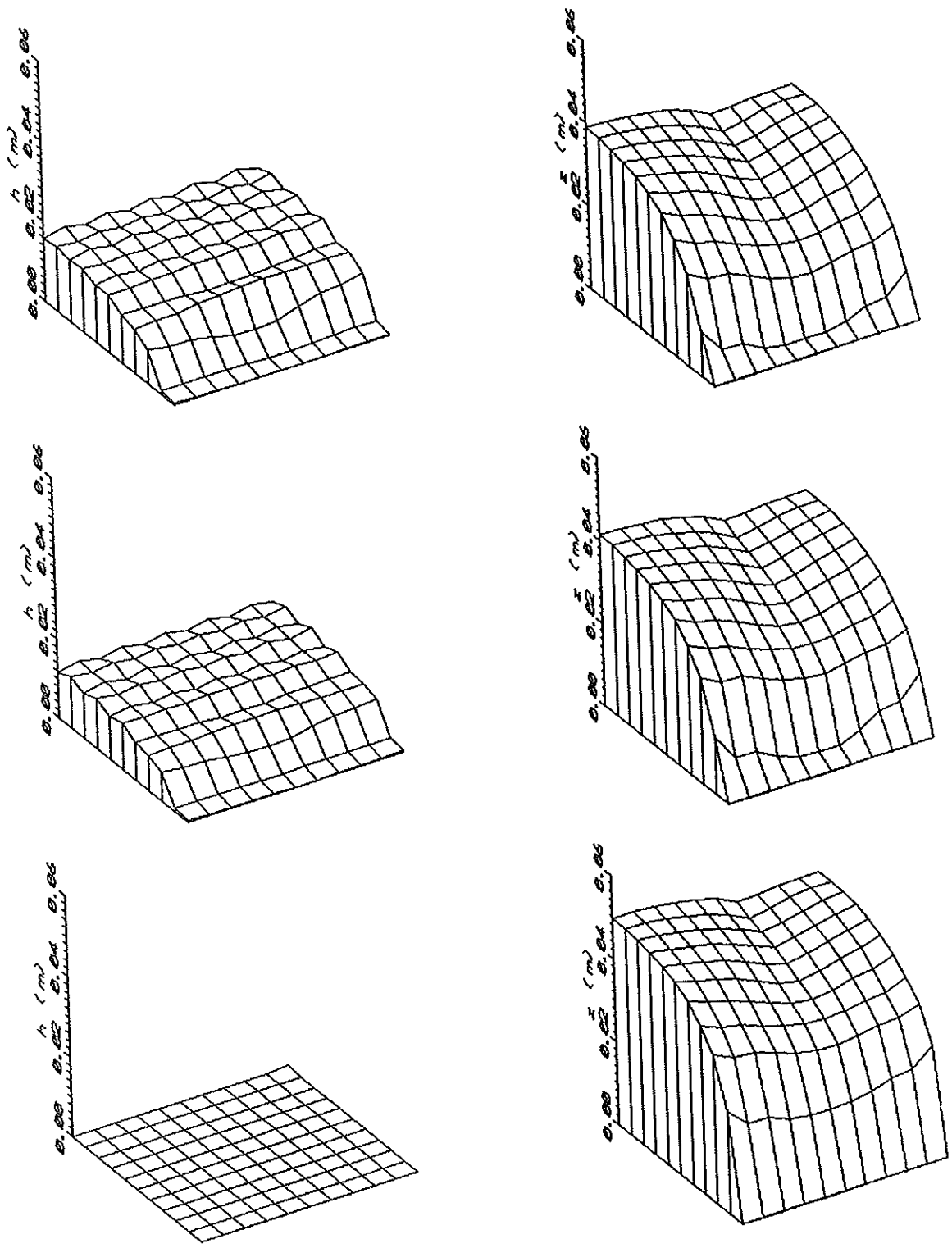

FIGURE 17. Overland (Left) and Infiltrated (Right) Profiles for Case Study 3 at Times 50, 55, and 72 min.

min, respectively. The Reynolds number was computed following the expression:

$$R_e = \frac{\sqrt{u^2+v^2}\,h}{\nu} \tag{85}$$

where R_e is the Reynolds number, and ν is the kinematic viscosity of water (m^2/s) at 15°C. The flow is considered to be laminar if R_e is lower than 500. Figure 18 shows that at time 25 min, while both inflows are still on, only a small area of the flow is laminar. At time 45 min (Fig. 19), after both inflows have been cut off, most of the flow is laminar.

The presence of large areas of laminar flow, particularly in the depletion phase of a level basin irrigation event, makes Manning's equation inadequate because this empirical formula always considers head loss as being proportional to the square of the flow velocity, while under laminar flow conditions, head loss is proportional to velocity to the first power. As a result, Manning's equation severely underestimates the friction slope of laminar flows. An effort was made to implement Chezy's equation in the model, but numerical instabilities associated with the advancing front systematically aborted the numerical procedure.

Figure 20 shows E_a, DPR, and E_r plotted as a function of the required depth (m). The application efficiency increases as the required depth increases from a value of 0% to a value of 100% at 0.05 m of required depth, since the maximum

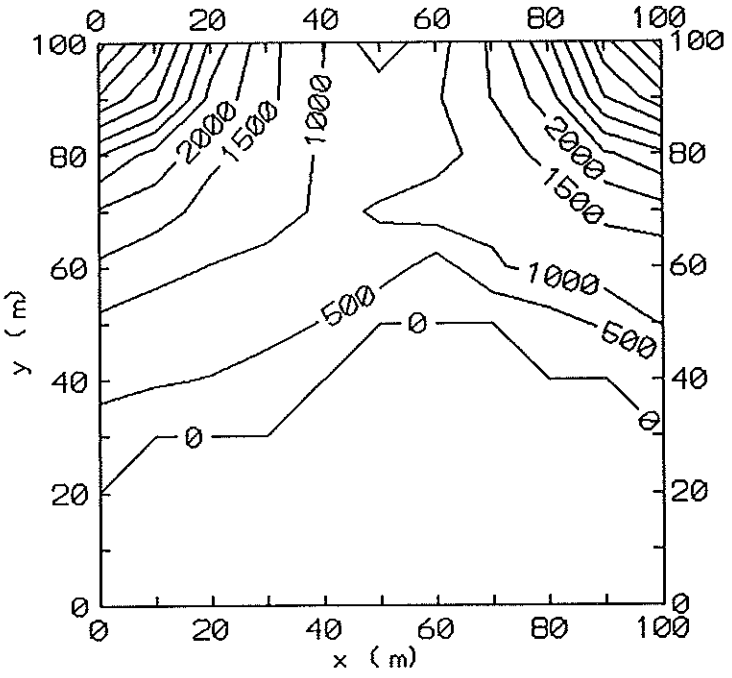

FIGURE 18. Contour Map of Reynolds Number for Case Study 3 at Time 25 min.

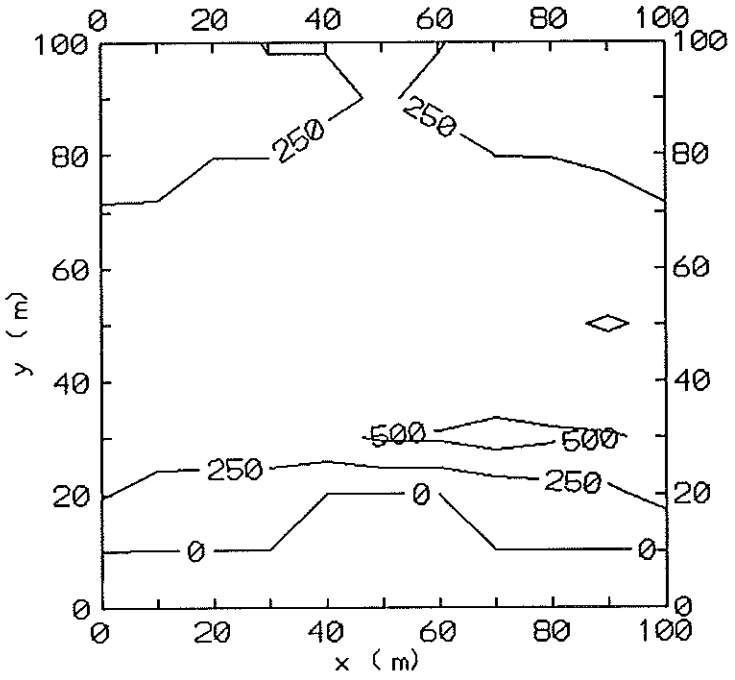

FIGURE 19. Contour Map of Reynolds Number for Case Study 3 at Time 45 min.

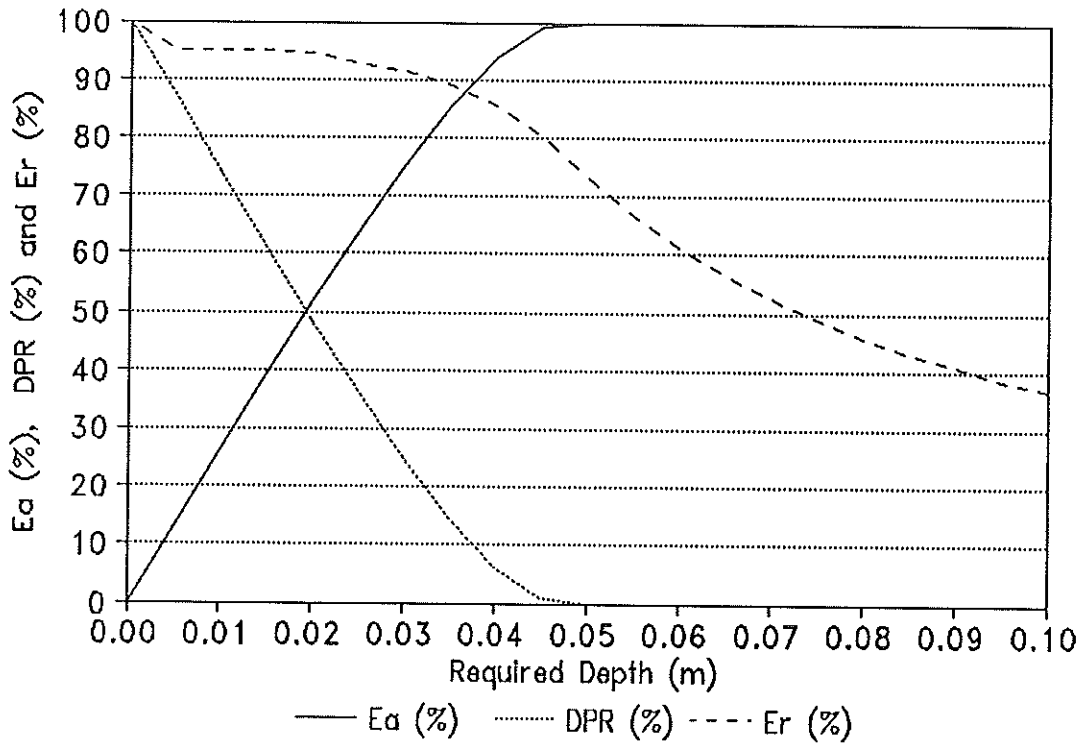

FIGURE 20. Application Efficiency, Deep Percolation Ratio, and Water Requirement Efficiency as a Function of the Required Depth for Case Study 3.

infiltrated depth happens to be 0.0497 m at the northwest corner. The water requirement efficiency starts with a value of 100%, but it decreases steadily as soon as the required depth takes nonzero values because the advance was not complete, and some nodes of the domain have an infiltrated depth of 0 m.

Case study 4 is used to illustrate two more features of the B2D model, namely, its capability to deal with irregular field shapes and high spots (islands) inside the domain. Its characteristic parameters are shown in Table 5.

TABLE 5. Characteristics of Case Study 4.

Columns: 15	x Spacing (m): 10.0
Rows: 11	y Spacing (m): 10.0
Area (m^2): 10,080	Shape: *Irregular*
Inflows: Type: Line Location: North Side Discharge (m^3/s): 0.250 Time in (min): 0.0	Time out (min): 50.0
Infiltration: Disabled	
Min. Depth (m): 0.001	Courant Number: 0.8
ε (m^2/s): 2.0	Manning's n: 0.04

An irregular domain was sketched over a rectangular grid with an initial area of 14,000 m^2. A triangular section of 1,500 m^2 in the southwest corner and an internal high spot of 1,700 m^2 were removed from the domain, resulting in a final area of 10,800 m^2.

Figure 21 displays overland flow profiles from 5 to 40 min for case study 4. The figure shows how B2D respects irregular flow boundaries and internal high spots. Overland flow circumvents the high spot and both flow branches meet on the downstream side. The complicated geometry of the domain induces numerical oscillations in the solution before completion of advance (see Fig. 21), but the overall behavior of the model is correct. B2D provides an easy way to design for irregular field shapes and to include existing internal high spots.

Artificial viscosity, a procedure used to smooth overland profiles by eliminating small frequency waves, deserves special consideration. Case study 5 is a practical application of the technique. Table 6 displays the characteristic parameters of this simulation. The same case study is run without artificial viscosity and with a coefficient of turbulent viscosity of 3.0 m^2/s. Figure 22 shows a three-dimensional plot of overland depth for the latter simulations at time 15 min.

Artificial viscosity has a clear effect on the solution. It diminishes the spikes that occur at the nodes next to the

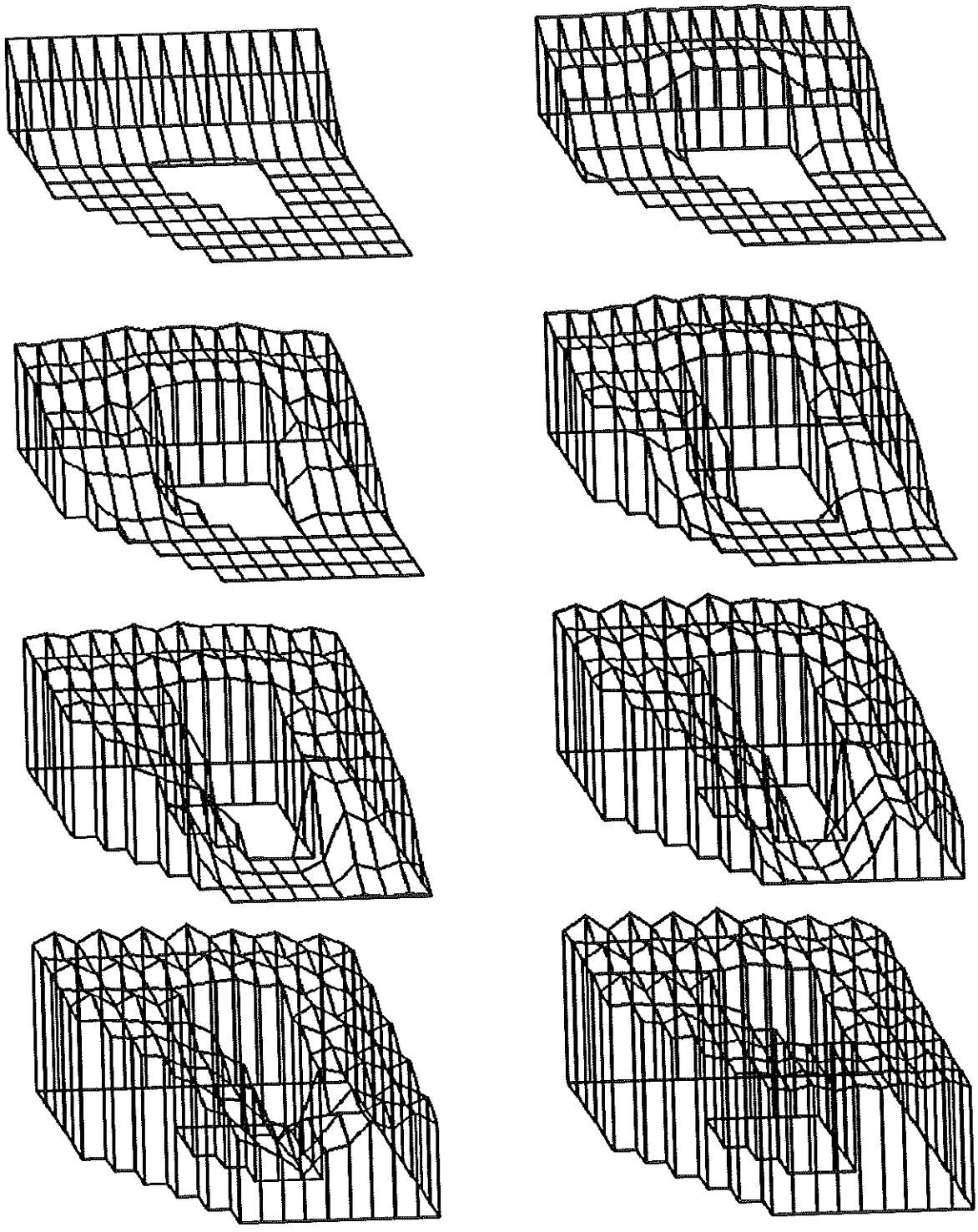

FIGURE 21. Overland Profiles for Case Study 4 at Times 5, 10, 15, 20, 25, 30, 35, and 40 min.

TABLE 6. Characteristics of Case Study 5.

Columns: 15	x Spacing (m): 10.0
Rows: 7	y Spacing (m): 10.0
Area (m^2): 8,400	Shape: Rectangular
Inflows: Type: Fan Location: North side, Nodes of coordinates (60,60) and (70,60) Discharge (m^3/s): 0.150 Time in (min): 0.0 Time out (min): 25.0	
Infiltration: Disabled	
Min. Depth (m): 0.001	Courant Number: 0.8
ε (m^2/s): 0.0 and 3.0	Manning's n: 0.04

inflow and smooths the whole profile, giving it a more realistic appearance.

Sensitivity Analysis

Two empirical parameters have been introduced in B2D that are not common to surface irrigation models: minimum depth and artificial viscosity. A series of numerical experiments was run to evaluate the effect of these parameters on the results of the model. The experiments are based on case study 6, whose characteristic parameters are displayed in Table 7. Different values of artificial

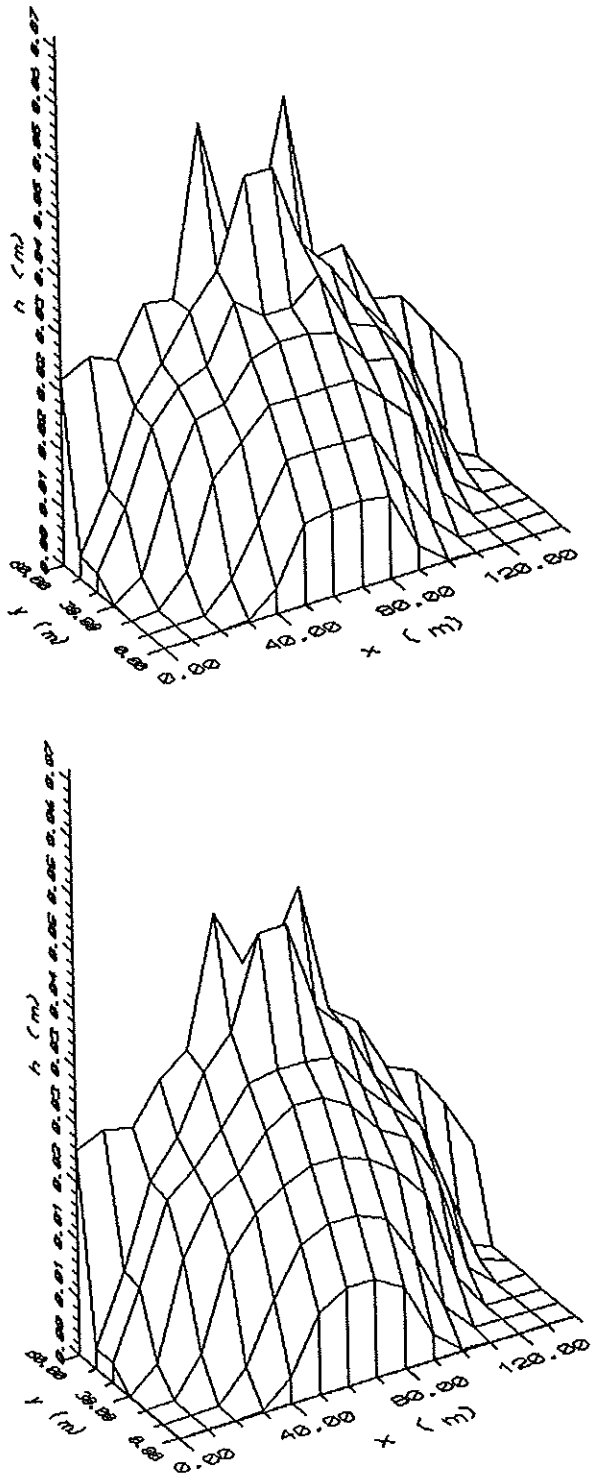

FIGURE 22. Overland Profiles for Case Study 5 without Artificial Viscosity (Top) and with a Coefficient of Turbulent Viscosity of 3.0 m^2/s (Bottom).

TABLE 7. Characteristics of Case Study 6.

Columns: 16	x Spacing (m): 6.67
Rows: 16	y Spacing (m): 6.67
Area (m^2): 10,000	Shape: Square
Inflows: Type: Corner Location: North West Corner Discharge (m^3/s): 0.200 Time in (min): 0.0 Time out (min): 60.0	
Infiltration: Family 0.5 of the SCS system k ($m^3/min^a/m$): 0.00320 a: 0.504 f_0 ($m^3/min/m$): 0.000117	
Min. Depth (m): Variable	Courant Number: 0.8
ε (m^2/s): Variable	Manning's n: 0.04

viscosity and minimum depth are used in the case study to clarify the effect of each parameter.

Minimum Depth

Five values of minimum depth were selected for comparison purposes: 0.0100 m, 0.0050 m, 0.0010 m, 0.0005 m, and 0.0001 m. Case study 6 was run without artificial viscosity for each value of the minimum depth. Figure 23 is a plot of the advance trajectory for each case. All five simulations fall within an acceptable margin of error,

although minimum depths of 0.0100 m and 0.0050 m show differences from the other three cases, indicating that these values are too high and that they slow the advance phase. The other three values of minimum depth produce similar results. It can be concluded that within these boundaries, minimum depth has no effect on the advance process and, by extension, on the whole simulation.

A minimum depth of 0.001 m or smaller is therefore recommended as a general rule, although combinations of small minimum depths and large time steps have proven to produce undesirable large mass balance errors in soils with very high infiltration rates.

Coefficient of
Turbulent Viscosity

Four values of the coefficient of turbulent viscosity, ε, were applied to case study 6: 0.0, 1.0, 2.0, and 3.0 m^2/s. The minimum depth was set to 0.0010 m for all of these simulations. Figure 24 presents the advance trajectory for all four cases. The results show a high degree of similarity, proving that artificial viscosity has a small influence on the advance process and therefore on the estimation of irrigation efficiency. Only at the end of the advance process does the simulation with a turbulent viscosity of 3.0 m^2/s show a distinctive behavior. It should be noted, however, that this simulation showed the effect of excessive dissipation, evidenced by a distorted surface flow profile. The conclusion is that values of ε that improve the

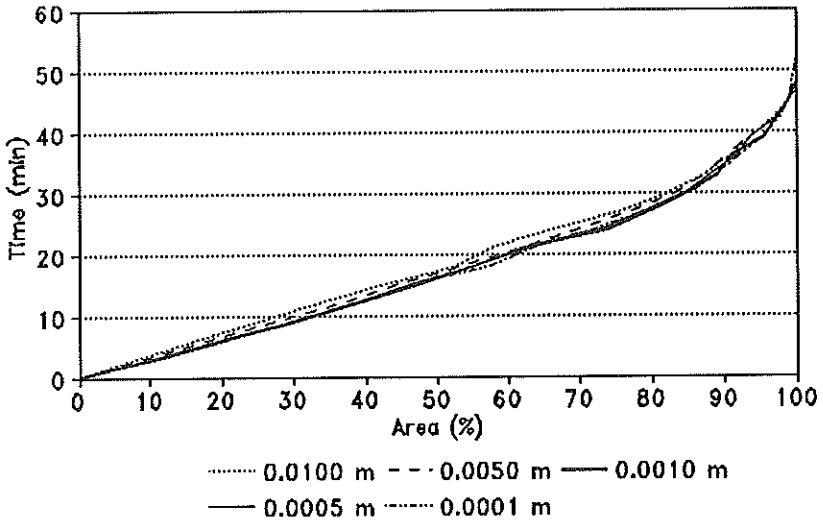

FIGURE 23. Advance Trajectory for Case Study 6 without Artificial Viscosity and with Minimum Depths of 0.0100 m, 0.0050 m, 0.0010 m, 0.0005 m, and 0.0001 m.

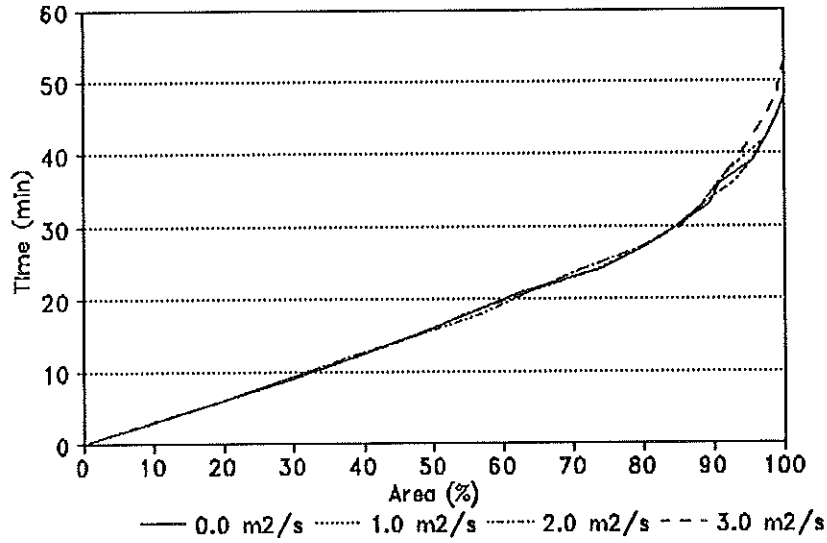

FIGURE 24. Advance Trajectory for Case Study 6 with Minimum Depth 0.0010 m, and Coefficient of Turbulent Viscosity of 0.0 m^2/s, 1.0 $m^2/2$, 2.0 m^2/s, and 3.0 m^2/s.

smoothness of the profiles do not constitute loss of accuracy in the estimation of the advance process.

A series of simulations based on case study 6 was performed to further analyze the effect of turbulent viscosity and minimum depth and to investigate possible interdependence. Tables 8 and 9 report the effects on advance and recession times, respectively, of combinations of the five minimum depths and the four levels of artificial viscosity. The tables show that minimum depth and artificial viscosity have no important effect on the overall performance of the model.

Conservative Properties

Figure 25 presents the time evolution of e, the mass balance error for case studies 1, 3, and 4. The error profile for case study 1 is typical: At the early stages of the simulation, e reaches values close to 4%, but its value decreases exponentially until the inflow is cut off at time 30 min. At this time, the error is drastically reduced to a value close to zero.

Case study 3 shows the effect of the two inflow boundary conditions. At time 10 min, e experiences a sudden rise due to the new inflow. The error then begins an exponential decrease with two sudden steps at times 30 and 40 min due to the cut off of the two inflows, and from then on, the error stabilizes on a terminal value close to zero.

TABLE 8. Advance Time (min) for Different Values of Minimum Depth and Coefficient of Turbulent Viscosity for Case Study 6.

ε m^2/s	0.0100 m	0.0050 m	0.0010 m	0.0005 m	0.0001 m
0.0	46.83	47.56	47.89	47.88	47.64
1.0	46.79	47.53	47.77	47.78	47.53
2.0	46.86	47.51	47.85	47.77	47.60
3.0	50.89	52.40	52.69	52.25	52.72

TABLE 9. Recession Time (min) for Different Values of Minimum Depth and Coefficient of Turbulent Viscosity for Case Study 6.

ε m^2/s	0.0100 m	0.0050 m	0.0010 m	0.0005 m	0.0001 m
0.0	230.17	229.50	229.18	228.84	229.18
1.0	230.20	229.54	229.20	229.17	228.87
2.0	230.52	229.86	229.17	229.20	228.83
3.0	231.19	230.17	229.84	229.49	229.49

Case study 4 shows a poorly behaved error profile due to the irregularity of the domain and the coarseness of the grid used to represent it. Oscillations in the curve can be related to sawtooth-like boundaries being reached by the advancing front. The error does not seem to reach a stable

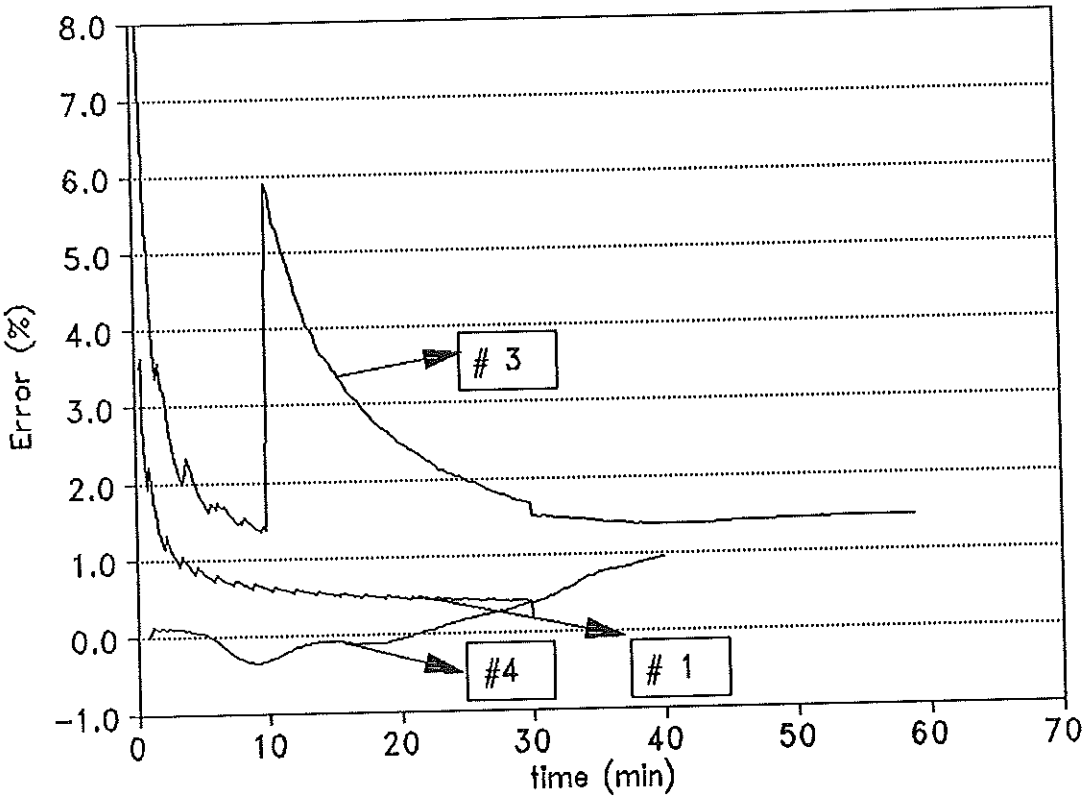

FIGURE 25. Time Evolution of the Mass Balance Error for Case Studies 1, 3, and 4.

value, but its value is small, reflecting a reasonably accurate representation of the flow profile.

Field Experiment

A field experiment was conducted in the spring of 1992 to test the predictive capability of the model. The experiment consisted of an irrigation evaluation in a rectangular, level basin field located in Delta, Utah. The dimensions of the field were 216.1 m long by 183.2 m wide with an area of 39,590 m^2. The field had recently been laser leveled, ripped and disked, and then planted with wheat.

The first irrigation of the season was monitored. The infiltration parameters were determined by means of three cylinder infiltrometer tests. The resulting parameters were:

$k = 0.0168\ m^3/min^a/m$

$a = 0.397$

$f_0 = 0.00000\ m^3/min/m$

A value of 0.10 was assigned to Manning's roughness coefficient.

The field was irrigated from its northwest corner with a constant discharge of 0.270 m^3/s, measured in the farm with a broad-crested weir. The inflow was cut off after 540 min.

The irrigation ditch was laid out in a north-south direction, and it extended 15 m into the field. This setup influenced the overall velocity of the flow, showing faster advance in the south direction than in the east direction.

The evaluation procedure consisted of surveying the advance profile at 1 h time steps and recording the advance and recession times. The advance profile at time 1 h could not be recorded due to experimental difficulties. The irrigation efficiency and deep percolation ratio were estimated from advance and infiltration data.

Field data were then compared to simulations produced by the SIRMOD and B2D models. A 21 by 21 grid was used in B2D to represent the domain; the minimum depth was set to 10^{-3} m, and no artificial viscosity was used.

Table 10 depicts characteristic times of the irrigation event for the field data and the computer simulations.

TABLE 10. Characteristic Times (min) of the Delta Field Experiment: Field Data and B2D and SIRMOD Simulations.

Time (min)	Field data	B2D	SIRMOD
Time of advance	570	525	470
Time of recession	1,020	900	863

Figures 26 to 37 illustrate the advance phenomenon and compare it to the computer simulations. Figure 26 shows that both SIRMOD and B2D profiles advance faster than those observed in the field, although B2D provides a better estimate of the time of advance.

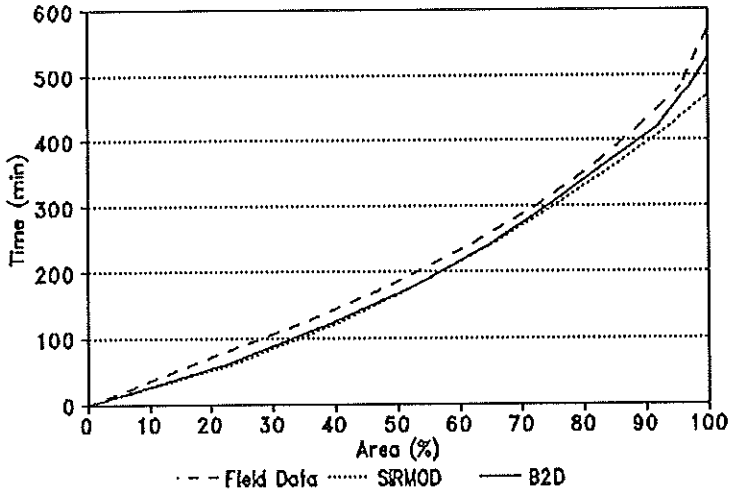

FIGURE 26. Advance Trajectory for Delta Field Experiment. Field Data in Dashed Line, SIRMOD in Dotted Line, and B2D in Continuous Line.

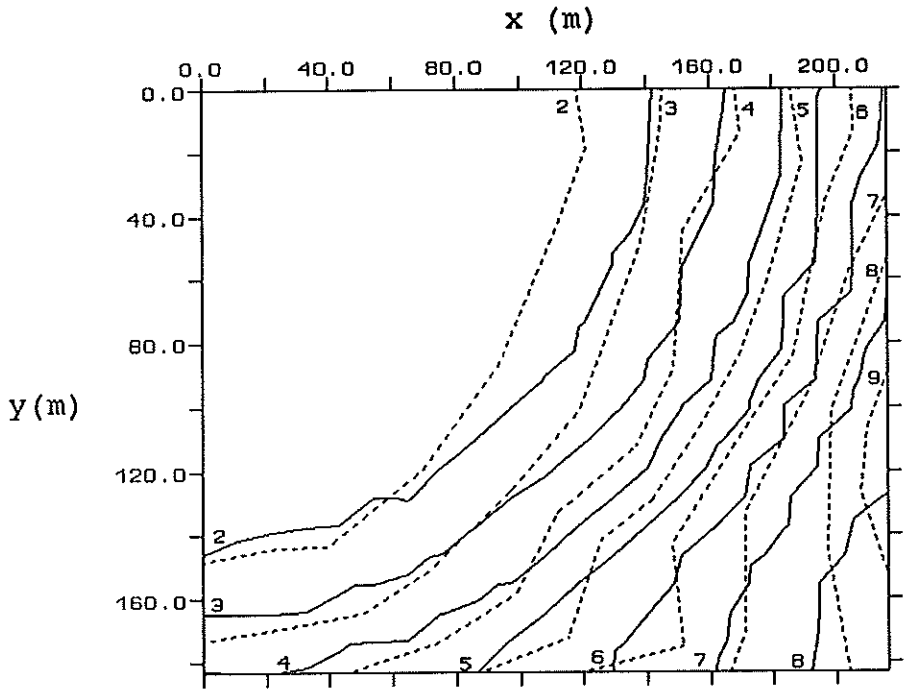

FIGURE 27. Advance Profiles for Delta Field Experiment at 1 h Intervals. Field Data in Dashed Line, Numbers in Bottom and Left Borders Indicate Time (h); B2D Simulation in Continuous Line, Numbers in Top and Right Borders Indicate Time (h).

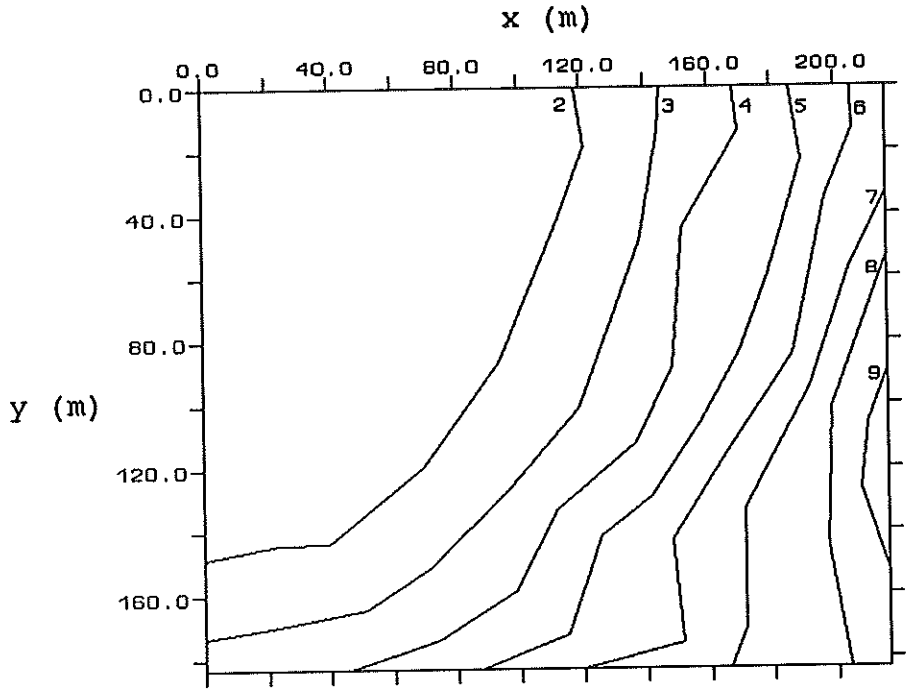

FIGURE 28. Advance Profiles Observed in the Delta Field Experiment at 1 h Intervals. Numbers Indicate Time (h).

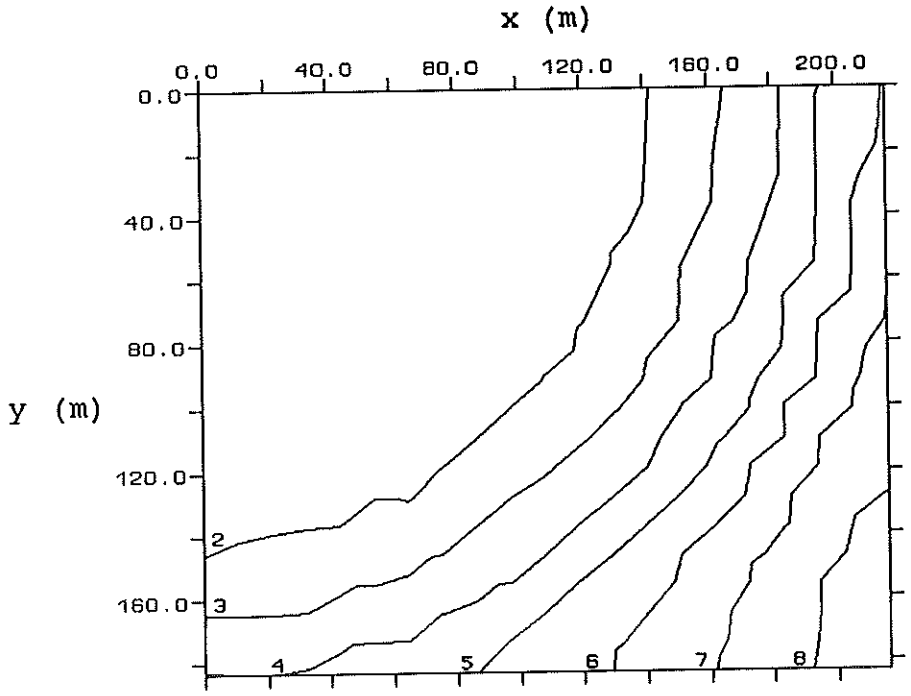

FIGURE 29. B2D Simulated Advance Profiles for Delta Field Experiment at 1 h Intervals. Numbers Indicate Time (h).

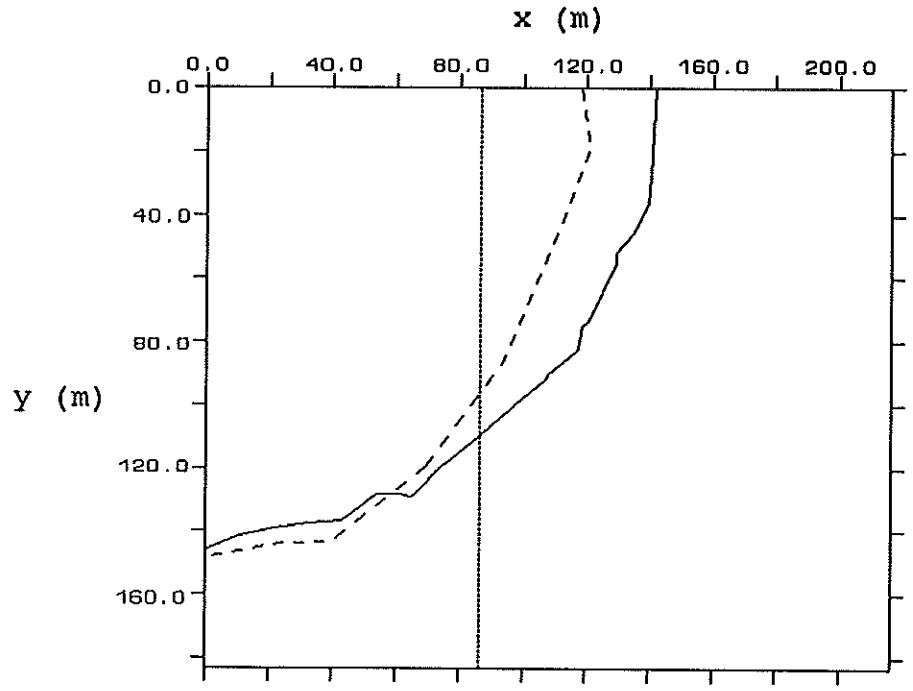

FIGURE 30. Advance Profile for Delta Field Experiment at 2 h. Field Data in Dashed Line, B2D in Continuous Line, and SIRMOD in Dotted Line.

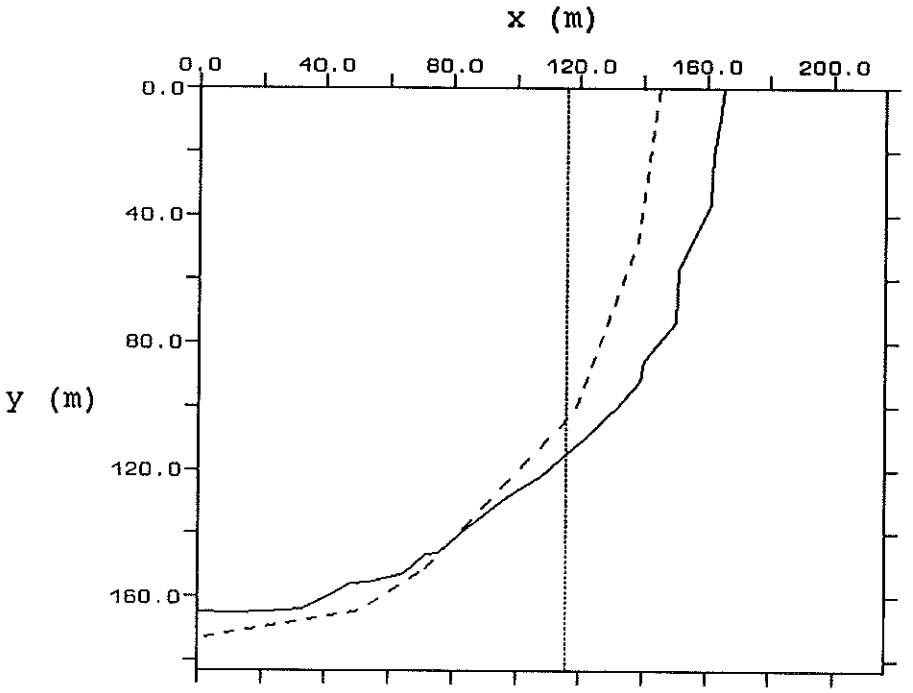

FIGURE 31. Advance Profile for Delta Field Experiment at 3 h. Field Data in Dashed Line, B2D in Continuous Line, and SIRMOD in Dotted Line.

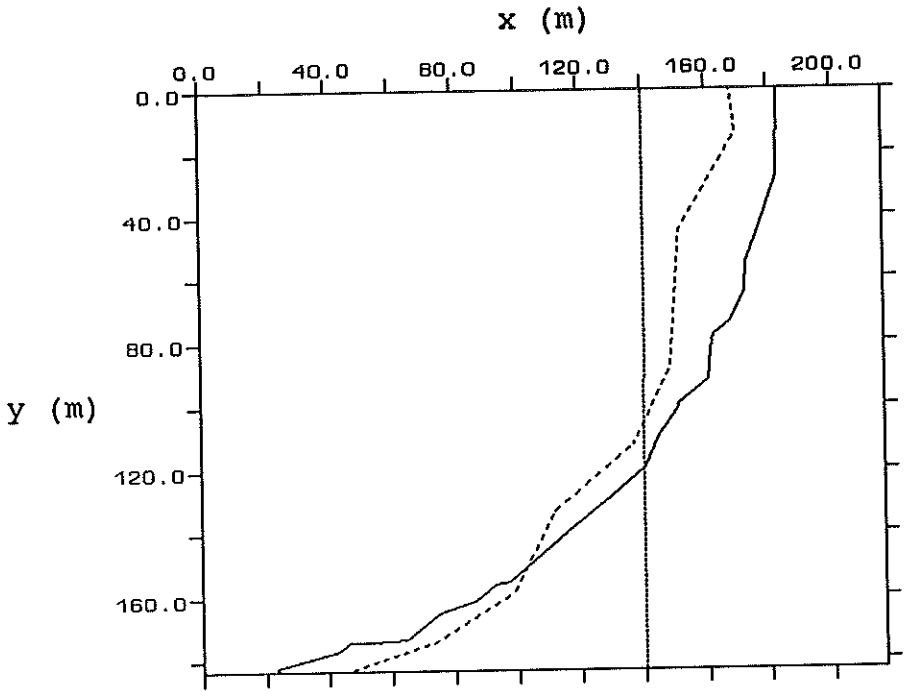

FIGURE 32. Advance Profile for Delta Field Experiment at 4 h. Field Data in Dashed Line, B2D in Continuous Line, and SIRMOD in Dotted Line.

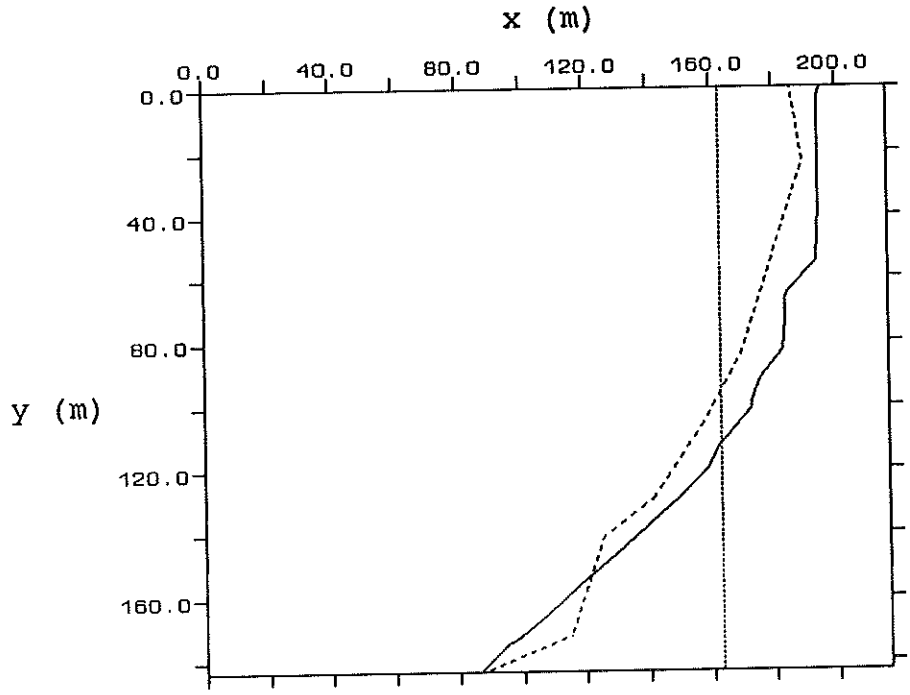

FIGURE 33. Advance Profile for Delta Field Experiment at 5 h. Field Data in Dashed Line, B2D in Continuous Line, and SIRMOD in Dotted Line.

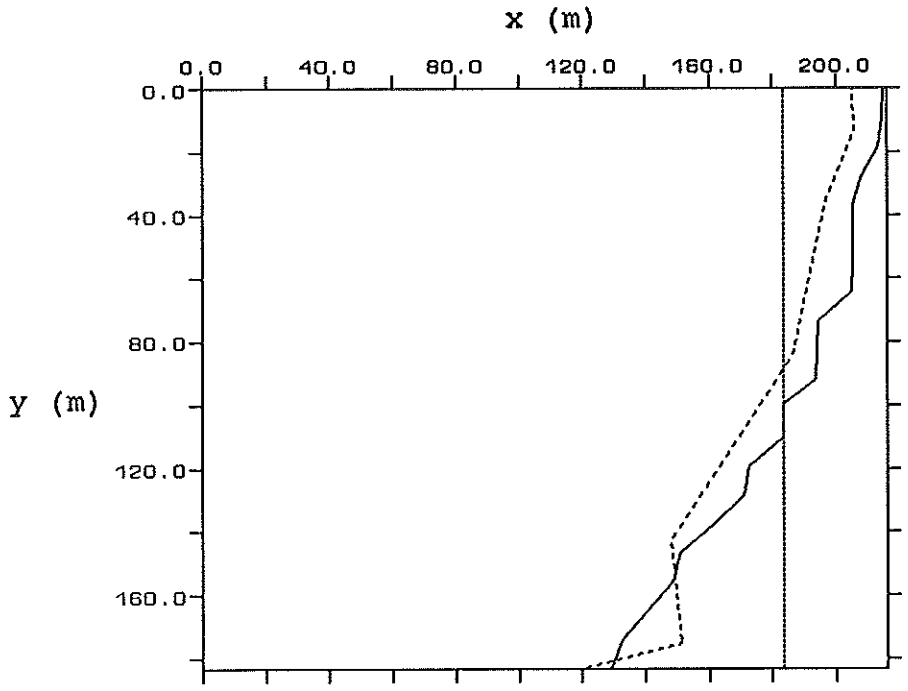

FIGURE 34. Advance Profile for Delta Field Experiment at 6 h. Field Data in Dashed Line, B2D in Continuous Line, and SIRMOD in Dotted Line.

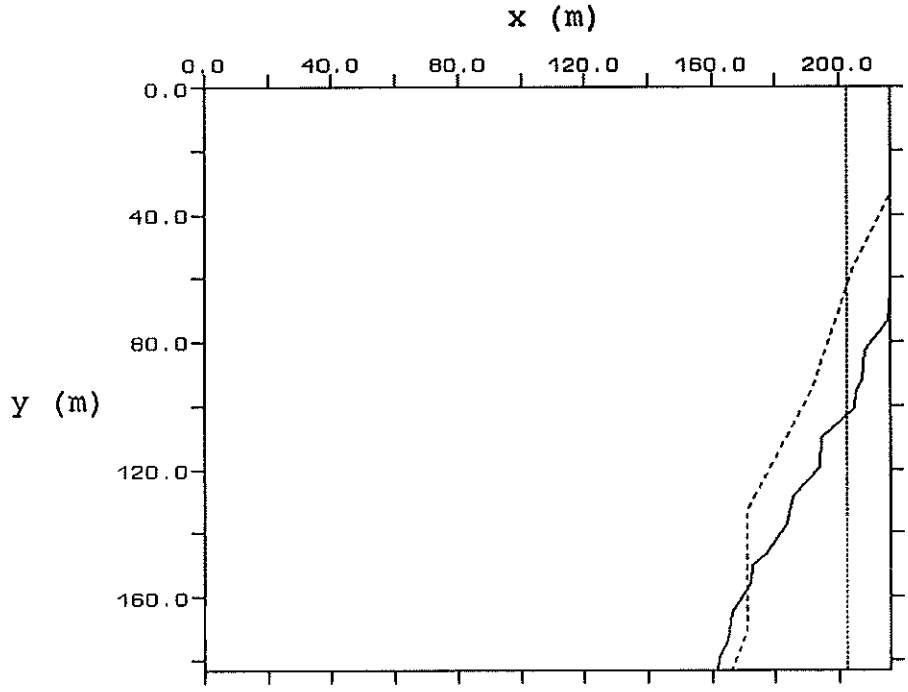

FIGURE 35. Advance Profile for Delta Field Experiment at 7 h. Field Data in Dashed Line, B2D in Continuous Line, and SIRMOD in Dotted Line.

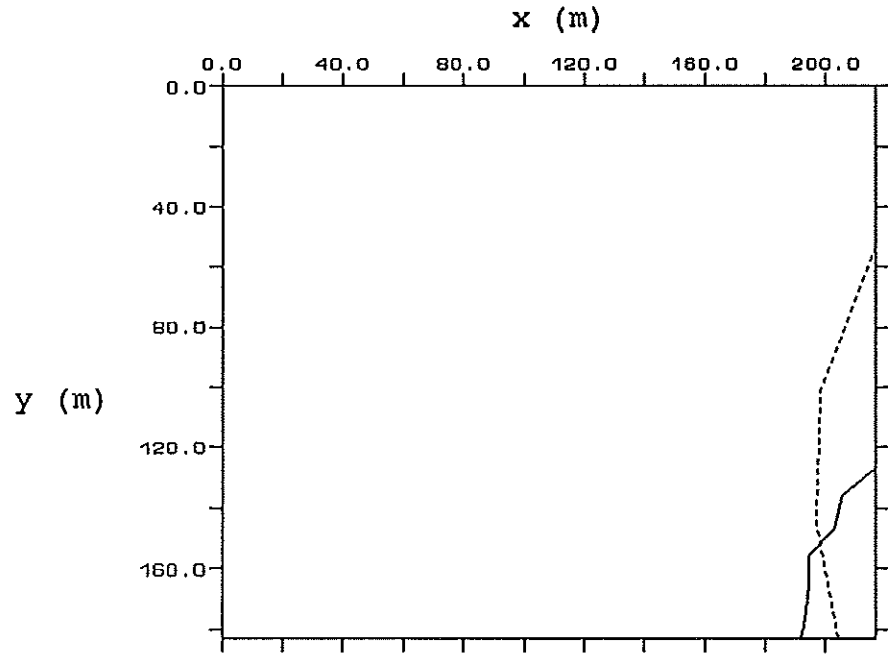

FIGURE 36. Advance Profile for Delta Field Experiment at 8 h. Field Data in Dashed Line, B2D in Continuous Line, and SIRMOD in Dotted Line (Advance Completed).

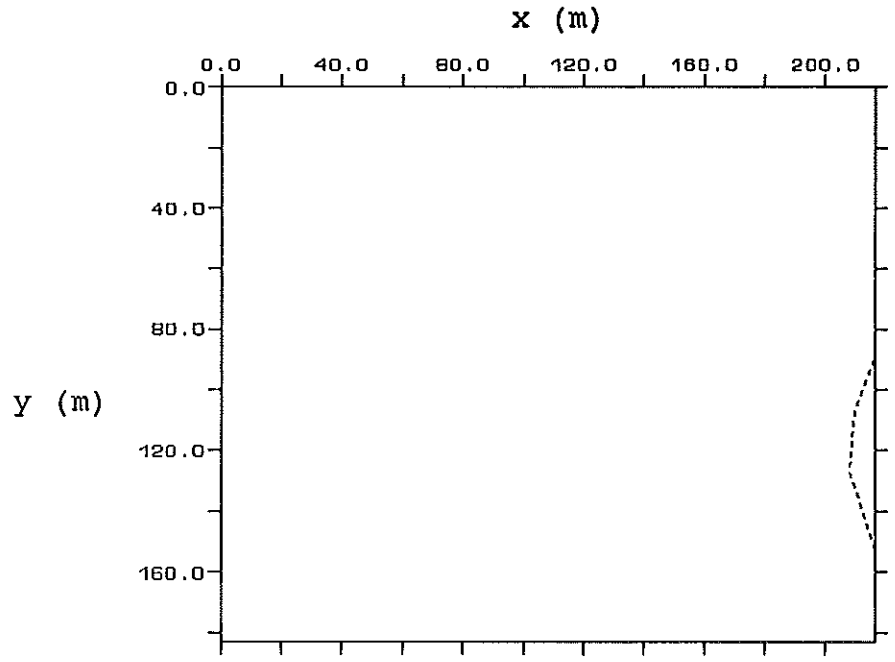

FIGURE 37. Advance Profile for Delta Field Experiment at 9 h. Field Data in Dashed Line, B2D in Continuous Line (Advance Completed), and SIRMOD in Dotted Line (Advance Completed).

Figures 27 to 29 present advance profiles for the field data and the B2D simulation. B2D profiles for the second and third hour are strongly symmetrical, while corresponding profiles for field data show faster advance in the southern direction due to the configuration of the inlet. After the third hourly profile, the advancing front reaches the domain's southwestern corner, and the advance profiles lose symmetry, but the effect of preferential flow towards the south is still noticeable in the field data.

Figures 30 to 37 compare hourly advance profiles for the field data, SIRMOD, and B2D. SIRMOD proves to be quite accurate for predicting the measured advance area, but it can only predict the advance profile as a straight line. Finally, Fig. 38 is a plot of application efficiency versus the required depth. Simulated data from SIRMOD and B2D produce very similar results, and both give good estimates of the field observations.

The field experiment demonstrates that B2D has good predictive capability, comparable to that of SIRMOD in terms of application efficiency, but B2D provides better estimates of advance trajectory and time of advance. It can also predict the shape of the advance profile with reasonable accuracy.

Table 14 in Appendix B displays the coordinates of some points at the advancing front at different times, as surveyed in the field experiment.

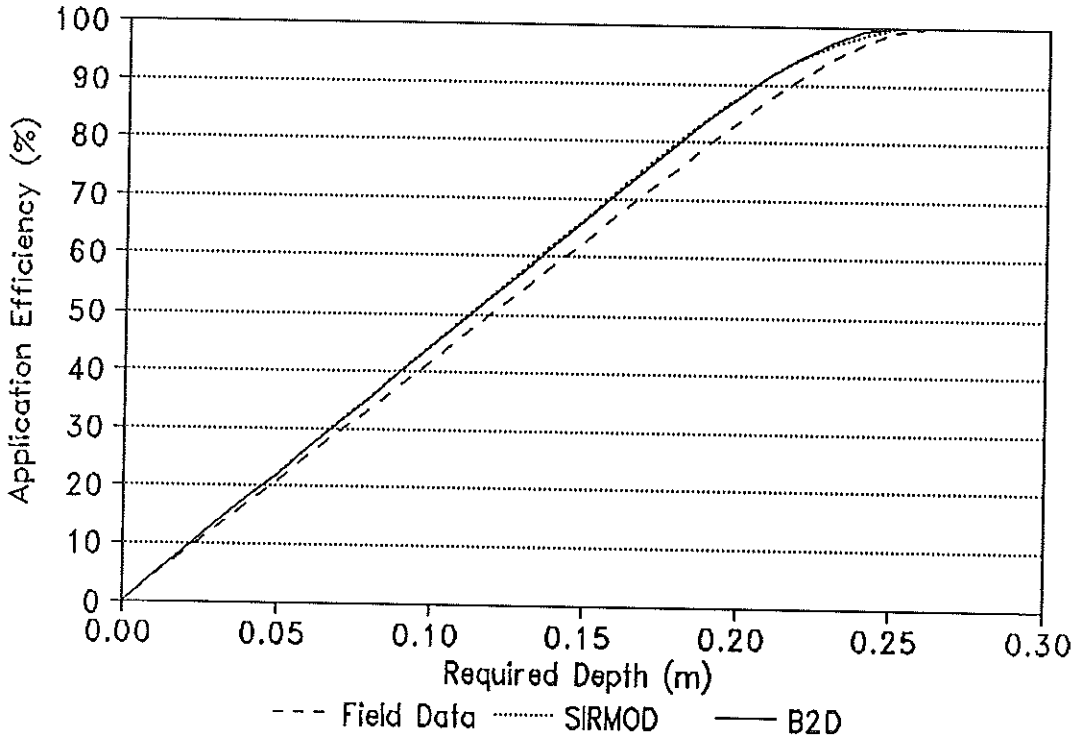

FIGURE 38. Application Efficiency (%) versus Required Depth (m) for Delta Field Data (Dashed Line) and Simulations by SIRMOD (Dotted Line), and B2D (Continuous Line).

Field Shape Effects on Irrigation Performance

The study of field shapes was restricted to rectangular areas. In particular, the case of a rectangular field of variable width with a corner inflow was analyzed. Two different grids were used in an attempt to establish the effect of grid fineness on the quality of the simulation for two-dimensional applications. Table 11 illustrates the different field shapes to be studied, the grid layout, and the corner discharge.

TABLE 11. Field Size, Shape, and Discharge for Case Study 7.

Shape Coeff	Length (m)	Width (m)	Coarse Grid # Nodes	Fine Grid # Nodes	Q m^3/s
1.0	100	100	11 x 11	21 x 21	0.20
0.9	100	90	11 x 10	21 x 19	0.18
0.8	100	80	11 x 9	21 x 17	0.16
0.7	100	70	11 x 8	21 x 15	0.14
0.6	100	60	11 x 7	21 x 13	0.12
0.5	100	50	11 x 6	21 x 11	0.10
0.4	100	40	11 x 5	21 x 9	0.08
0.3	100	30	11 x 4	21 x 7	0.06
0.2	100	20	11 x 3	21 x 5	0.04
0.1	100	10	11 x 3	21 x 3	0.02

The shape coefficient is defined as the ratio between the width and the length of the field. The value of the discharge for the different cases maintains a constant unit discharge over the width of the field so that the cases can be legitimately compared. Note that a minimum of three nodes must be maintained in the grids to ensure proper functioning of the finite difference procedure. The required dimensions of the grid are then obtained by adjusting the space between the nodes. In the case of a 0.10 shape coefficient, the inflow is defined as a line because this case is intended to represent a one-dimensional application.

Other characteristics of case study 7 are listed. The Manning's n was set to 0.04; no artificial viscosity was used; the Courant number was 0.8; discharge was cut off at time 60 min; and infiltration was characterized by families 0.10, 0.30, 0.60, 0.90, and 2.00 of the SCS infiltration classification system.

Table 12 displays the advance time obtained for the five considered infiltration families in different shape coefficients and grids. The table shows that the two-dimensional configuration slows the advance by about 20% (considering the fine grid in both cases). It should be noted that this effect is due only to the geometry of the field because all other parameters have been held constant. Thus, a significant error is observed when using a one-dimensional model to estimate the advance time in a square basin with corner inflow. Differences in recession times are

not significant, and irrigation efficiencies never differ by more than 1%, indicating the adequacy of one-dimensional models in the estimation of irrigation efficiency in two-dimensional problems.

Table 12 also points out the small differences in estimated advance times between both grids for the two-dimensional application, in contrast with Table 3 that showed a much larger dependence on grid fineness for one-dimensional applications of the same model.

TABLE 12. Advance Time (min) for Shape Coefficients 0.1 (Fine Grid) and 1.0 (Fine and Coarse Grid) for Case Study 7.

SCS Family and Soil Texture	Fine Grid Shape Coeff 0.1	Fine Grid Shape Coeff 1.0	Coarse Grid Shape Coeff 1.0
0.10 Clay	34.2	41.4 (-17.4)	40.5
0.30 Clay Loam	36.8	44.6 (-17.5)	43.9
0.60 Silty Loam	41.0	50.1 (-18.2)	49.4
0.90 Sandy Loam	46.6	57.4 (-18.8)	56.8
2.00 Sandy	86.1	109.8 (-21.6)	108.6

Note: Figures in Parenthesis Indicate Percentage Deviation between Shape Coefficients 0.1 and 1.0 for the Fine Grid.

Table 13 displays advance and recession times for different values of the shape coefficient for the 0.6 infiltration family. The table shows that advance times grow gradually as the field shape approaches a square. Figure 39 is a plot of advance time versus shape coefficient. The time of advance increases slowly at the beginning and steepens as the shape coefficient approaches a unit value, implying that one-dimensional models can accurately predict the time of advance in level basins whose shape coefficient is smaller than about 0.4.

TABLE 13. Advance and Recession Times (min) for Infiltration Family 0.6 and Different Shape Coefficients for Case Study 7.

Shape Coefficient	Advance Time (min)	Recession Time (min)
0.10	41.0	189.7
0.20	41.4	189.9
0.30	41.6	189.5
0.40	41.7	189.8
0.50	42.2	189.5
0.60	43.1	189.5
0.70	44.7	189.5
0.80	46.8	189.5
0.90	48.5	190.1
1.00	50.1	190.8

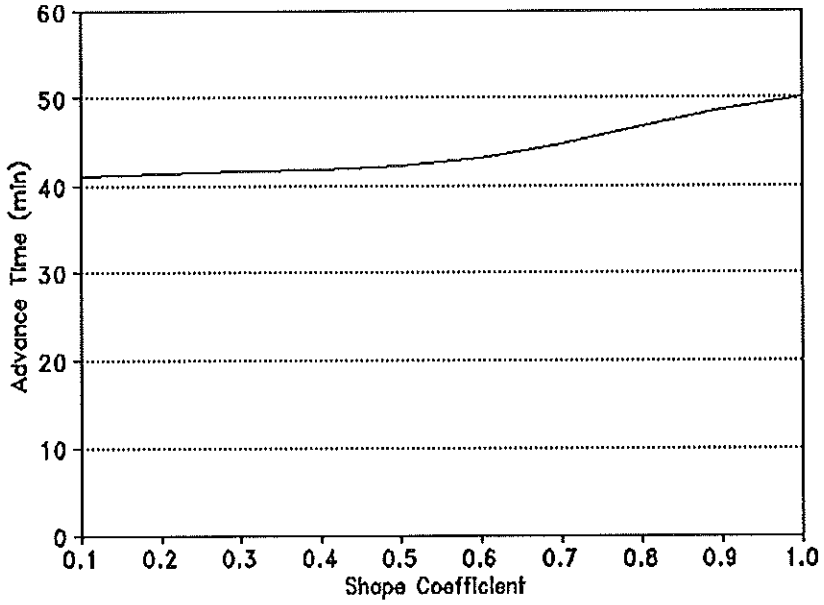

FIGURE 39. Advance Time (min) as a Function of the Shape Coefficient for Case Study 7 and Infiltration Family 0.6.

CHAPTER VI

SUMMARY AND CONCLUSIONS

Summary

A two-dimensional model for level basin irrigation was developed as a tool to simulate irrigation events that involve point inflows, irregular geometries, and internal high spots. The model has proven to be stable, accurate, and robust in the solution of a wide set of conditions.

Different numerical methods were considered as alternatives to solve the two-dimensional shallow water equations for the initial and boundary conditions that characterize level basin irrigation. Two models were developed based on the Petrov-Galerkin finite element scheme and the leapfrog finite difference scheme. After comparison of their performance, the leapfrog finite difference method was judged best due to its robustness, versatility, and computational speed.

The leapfrog numerical analysis scheme was implemented in a software application called B2D. This program can be run by computer operators who are not familiar with the underlying theory. The software also provides three-dimensional graphics that facilitate data analysis in addition to providing a variety of user-customized output files. The user interface is based on pull-down menus and dialogue boxes that make its operation fast and easy to learn.

The model was applied to the solution of one-dimensional problems and compared to the SIRMOD model. The agreement between the models was satisfactory, especially when fine grids were used in B2D.

B2D can deal with three types of inflow boundary conditions: line, corner, and fan. It can also simulate cases where the field is flooded simultaneously from several inflow sources. Due to the strictly nondissipative behavior of the leapfrog scheme, an artificial viscosity module was added to the model to eliminate high frequency parasitic waves. The results have shown that its use is not necessary in most applications, although it can improve the quality of the solution particularly in fan inflows and irregular areas. The use of artificial viscosity does not affect the time of advance or recession; it only has a smoothing effect on the overland flow profile.

The numerical procedure assumes that all nodes in the domain have a finite depth of water as an initial condition (10^{-10} m). Infiltration, however, does not start at a node until flow depth reaches a certain value. This threshold value is referred to as the minimum depth. Analyses of the results indicate that the value of the minimum depth does not modify the results of the simulation if it stays within the margins of 10^{-3} and 10^{-4} m.

A commonly used indicator of the quality of a surface irrigation simulation is the error in mass balance. This error is generated by violation of the mass continuity

equation, and it expresses the difference between the volume delivered by the inflows and the volume actually present as overland and infiltrated depth in each node. The mass balance error reaches values of up to 10% at the beginning of the simulation due to the approximation introduced by the initial condition, but it decreases exponentially and approaches zero after a few time steps.

The predictive capability of the model was evaluated by conducting a field experiment on a rectangular, laser-leveled basin irrigated from a corner. B2D accurately predicted the advance profiles and the advance and recession times of the irrigation event. In terms of comparison, SIRMOD also produced good estimates of the advance and recession times.

The model was used to study the effects of field shape on irrigation performance, and the results of the research indicate that one-dimensional models applied to simulation of square fields with one corner inflow can produce a serious underestimation of the time of advance, although still providing good estimates of the time of recession and efficiency terms.

Conclusions

The following conclusions can be drawn from the results of the research:

1. The presented two-dimensional model of basin irrigation constitutes a stable, accurate, and robust method for solving the two-dimensional shallow water equations, and

its speed of execution makes it a valuable tool to be used as an interactive model for design and management of surface irrigation systems.

2. The model complies with all the conditions established by Katopodes and Strelkoff (1977a) for accurate surface irrigation models: It is theoretically sound and free of empiricism; numerically consistent, stable, and accurate; physically complete; simple to program; and inexpensive to operate.

3. The accuracy of the model depends heavily on the fineness of the grid in one-dimensional applications, but this dependence is severely relaxed in two-dimensional applications, allowing for fast solutions that use a limited number of nodes. The change from an 11 x 5 grid to a 21 x 5 grid increased the advance time by an average 5% in a one-dimensional application. A change from an 11 x 11 grid to a 21 x 21 grid in a square corner inflow two-dimensional application increased the advance time by 1 to 2%.

4. One-dimensional models predict with reasonable accuracy the time of recession and the efficiency terms of rectangular two-dimensional applications, but they fail to give good estimates of the time of advance, incurring underestimations of up to 20%. This is particularly undesirable since most basin irrigation systems are designed and operated to cut off the inflow as soon as, or even before, the advance phase is completed. Underestimation of the time of advance at the design phase could lead to

irrigation events with incomplete advance and undersized irrigation structures. According to Fig. 37, the use of a two-dimensional model in rectangular fields irrigated from a corner is justified as soon as the shape coefficient reaches a value of 0.4, that is, when the width of the field is at least 40% of its length.

5. B2D successfully simulates irrigation events that cannot be handled by one-dimensional models without making serious approximations that endanger the representativity of the original data. Irregular field shapes, point inflows of the corner and fan type, and several simultaneous inflows had never been simulated before. B2D opens a new perspective of surface irrigation modeling that takes advantage of the new generations of personal computers and their high processing speed.

CHAPTER VII

RECOMMENDATIONS

B2D is the first two-dimensional surface irrigation model reported to date. The results presented in this dissertation are encouraging, and it is easy to envision new features and applications of the model. This chapter will discuss some of the possible areas of future research in this area of study.

1. Extension of the model to border irrigation. The model is ready to be extended by accommodating two new features: field slope and outflow boundary conditions. No major theoretical or programming developments are needed to implement these capabilities.

2. Regionalization of the infiltration parameters. A two-dimensional model could accurately simulate an irrigation event on a field with spatially varied infiltration characteristics. Several infiltration tests could be performed at key locations using a geostatistic routine to assign interpolated values of the infiltration parameters to all the nodes in the domain. The model would proceed as usual, but a different infiltration equation would be used at each node.

3. Microtopography. Implementation of microtopography would be similar to spatially varied infiltration. The field would be surveyed and an interpolated value of bed elevation would be assigned to each node. The field slopes would then

be computed locally, and the advance and recession trajectories would reflect the high and low spots of the field. A particularly interesting application of the model would consist of evaluating the economical consequences of laser-guided land leveling.

4. Farm level simulation. The use of two-dimensional models opens the way for a more integrated analysis of the irrigation problem. At the farm level, outflows from a field are often used as inflows for the next downstream field (usually as a corner inflow). This configuration calls for a two-dimensional analysis, particularly if the fields are approximately square. A farm level study would run a simulation on all the fields that are irrigated from a ditch and would provide improved estimates of the efficiency at farm level.

5. Surge irrigation. The benefits inherent to surge irrigation could be evaluated for two-dimensional conditions without any additional theoretical complication, since B2D can deal with several advancing fronts at a time. Provision should be made of the means to modify the infiltration parameters in time as required by the surge irrigation process.

6. Numerical procedure. The leapfrog scheme reveals some limitations that deserve further study. Its nondissipative character requires the implementation of artificial viscosity in selected cases; the performance of the model is not satisfactory in the presence of mild

gradients of the dependent variables; and smearing can be detected at the advancing front. These problems could be overcome by the implementation of an equally versatile explicit finite difference model with dissipative properties and a strong shock capturing capability.

7. Grid refinement. Several adaptative finite difference grid refinement procedures have been recently developed. These procedures could effectively decrease the number of elemental operations per time step by refining the grid where needed (where steep gradients of the dependent variables are present), while maintaining a coarse grid in the rest of the domain. As a result, the model would run faster, and accuracy and stability would be improved.

REFERENCES

Abarbanel, S.S. and E.M. Murman. 1982. Stability of two-dimensional hyperbolic initial boundary value problems for explicit and implicit schemes. *J. Comput. Physics* 48:160-167.

Akanbi, A.A. 1986. "Hydrodynamic modeling of two-dimensional overland flow," dissertation submitted in partial fulfillment of the requirements for the degree of Doctor of Philosophy in Civil Engineering, University of Michigan, Ann Arbor, Michigan.

Akanbi, A.A. and N.D. Katopodes. 1988. Model for flood propagation on initially dry land. *J. Hydr. Div.*, ASCE 114(7):689-706.

Arney, D.C. and J.E. Flaherty. 1986. A two-dimensional mesh moving technique for time-dependent partial differential equations. *J. Comput. Physics* 67:124-144.

Bassett, D.L. 1972. Mathematical model of water advance in border irrigation. *Transactions of the ASAE* 15(5):992-995.

Bassett, D.L. and D.W. Fritzsimmons. 1976. Simulating overland flow in border irrigation. *Transactions of the ASAE* 19(4):666-671.

Bellos, C.V. and J.G. Sakkas. 1987. 1-D dam break flood-wave propagation on dry bed. *J. Hydr. Div.*, ASCE 113(12):1510-1524.

Bellos, C.V., J.V. Soulis and J.G. Sakkas. 1988. "Computing 2-D unsteady open-channel flow by finite-volume method," *Proceedings of the VII Intl. Conf. on Computational Methods in Water Resources*: June, MIT, Boston.

Berger, M.J. and J. Oliger. 1984. Adaptative mesh refinement for hyperbolic partial differential equations. *J. Comput. Physics* 53:484-512.

Casulli, V. 1990. Semi-implicit finite difference methods for the two-dimensional shallow water equations. *J. Comput. Physics* 86:56-74.

Chow, V.T. 1959. Open channel hydraulics, McGraw-Hill Book Company, New York.

Clemmens, A.J. 1979. Verification of the zero-inertia model for border irrigation. *Transactions of the ASAE* 22(6):1306-1309.

Clemmens, A.J. and T. Strelkoff. 1979. Dimensionless advance for level-basin irrigation. *J. Irrig. Drain. Div.*, ASCE 105(3):259-273.

Clemmens, A.J., T. Strelkoff and A.R. Dedrick. 1981. Development of solutions for level-basin design. *J. Irrig. Drain. Div.*, ASCE 107(3):265-279.

Cunge, J.A., F.M. Holy, Jr. and A. Verwey. 1980. Practical aspects of computational river hydraulics, Pitman Publishers, Boston.

Elliott, R.L. 1981. "Zero-inertia furrow irrigation modeling applied to the derivation of infiltration parameters," Dissertation submitted in partial fulfillment of the requirements for the degree of Doctor of Philosophy in Agricultural and Chemical Engineering, Colorado State University, Fort Collins, Colorado.

Elliott, R.L., W.R. Walker, G.V. Skogerboe. 1983. Furrow irrigation advance rates: A dimensionless approach. *Transactions of the ASAE* 26(6):1722-1731.

Fennema, R.J. and M.H. Chaudry. 1986. Explicit numerical schemes for unsteady free-surface flows with shocks. *Water Resources Research* 22(13):1923-1930.

Foreman, M.G.G. 1984. A two-dimensional dispersion analysis of selected methods for solving the linearized shallow water equations. *J. Comput. Physics* 56:287-323.

Garcia, R. and R.A. Kahawita. 1986. Numerical solution of the St. Venant equations with the MacCormack finite-difference scheme. *International Journal for Numerical Methods in Fluids* 6:259-274.

Gelinas, R.J., S.K. Doss and K. Miller. 1981. The moving finite element method: Applications to general partial differential equations with multiple large gradients. *J. Comput. Physics* 40:202-249.

Gray, W.G. 1980. "Do finite element models simulate surface flow?" Finite Elements in Water Resources III, S. Y. Wang, ed., University of Mississippi Press, University, Lafayette Co., 1.122-1.136.

Irrigation Software Engineering Division. 1989. "SIRMOD, the surface irrigation simulation model. User's guide," Department of Agricultural and Irrigation Engineering, Utah State University. Logan, Utah.

Irrigation Software Engineering Division. 1992. "B2D, two dimensional Basin Irrigation simulation model. User's

guide," Department of Biological and Irrigation Engineering, Utah State University. Logan, Utah.

Katopodes, N.D. 1980. "Finite element model for open channel flow near critical conditions," Finite Elements in Water Resources III, S. Y. Wang, ed., University of Mississippi Press, University, Lafayette Co., 5.37-5.46.

Katopodes, N.D. 1984a. A dissipative galerkin scheme for open channel flow. *J. Hydr. Div.*, ASCE 110(4):450-466.

Katopodes, N.D. 1984b. Two dimensional surges and shocks in open channels. *J. Hydr. Div.*, ASCE 110(6):794-812.

Katopodes, N.D. and D.R. Schamber. 1983. Applicability of dam-break flood wave models. *J. Hydr. Div.*, ASCE 109(5):702-721.

Katopodes, N.D. and T. Strelkoff. 1977a. Hydrodynamics of border irrigation - complete model. *J. Irrig. Drain. Div.*, ASCE 103(3):309-323.

Katopodes, N.D. and T. Strelkoff. 1977b. Dimensionless solutions of border-irrigation advance. *J. Irrig. Drain. Div.*, ASCE 103(4):401-417.

Katopodes, N.D. and T. Strelkoff. 1978. Computing two-dimensional dam-break flood waves. *J. Hydr. Div.*, ASCE 104(9):1269-1288.

Katopodes, N.D. and C. Wu. 1986. Explicit computation of discontinuous channel flow. *J. Hydr. Div.*, ASCE 112(6):456-475.

Kincaid, D.C., D.F. Heermann and E.G. Kruse. 1972. Hydrodynamics of border irrigation advance. *Transactions of the ASAE* 15(4):674-680.

Kruger, W.E. and D.L. Bassett. 1965. Unsteady flow of water over a porous bed having constant infiltration. *Transactions of the ASAE* 8(1):60-62.

Lynch, D.R. and W.G. Gray. 1980. Finite element simulation of flow in deforming regions. *J. Comput. Physics* 36:135-153.

Luchini, P. 1987. An adaptative-mesh finite-difference solution method for the Navier-Stokes equations. *J. Comput. Physics* 68:283-306.

Mader, C.L. 1988. Numerical modeling of water waves, University of California Press, Berkley.

Reid, R.O. and B.R. Bodine. 1968. Numerical model for storm surges in Galveston Bay. *J. Waterways and Harbors Div.*, ASCE 94(1):33-57.

Sakkas, J.G. and T. Strelkoff. 1974. Hydrodynamics of surface irrigation-advance phase. *J. Irrig. Drain. Div.*, ASCE 100(1):31-48.

Schmitz, G.H. and G.S. Seus. 1989. Analytical model of level basin irrigation. *J. Irrig. Drain. Div.*, ASCE 115(1):78-95.

Schreiber, D.L. and D.L. Bassett. 1967. Hydraulic description of recession of shallow flow over a porous bed. *Transactions of the ASAE* 10(1):54-56.

Segerlind, L.J. 1984. Applied finite elements, John Wiley and Sons, New York.

Shatanawi, M.R. and T. Strelkoff. 1984. Management contours for border irrigation. *J. Irrig. Drain. Div.*, ASCE 110(4):393-399.

Souza, F. 1981. "Nonlinear hydrodynamic model of furrow irrigation," dissertation submitted in partial fulfillment of the requirements for the degree of Doctor of Philosophy in Engineering, University of California at Davis, Davis, California.

Steger, J.L. 1978. Implicit finite-difference simulation of flow about arbitrary two-dimensional geometries. *AIAA Journal* 16(7):679-686.

Strelkoff, T. 1969. One-dimensional equations of open-channel flow. *J. Hydr. Div.*, ASCE 95(3):861-876.

Strelkoff, T. 1970. Numerical solution of the Saint-Venant equations. *J. Hydr. Div.*, ASCE 96(1):223-252.

Strelkoff, T. 1977. Algebraic computation of flow in border irrigation. *J. Irrig. Drain. Div.*, ASCE 103(3):357-377.

Strelkoff, T. and N. Katopodes. 1977. Border irrigation hydraulics with zero inertia. *J. Irrig. Drain. Div.*, ASCE 103(3):325-342.

Thacker, W.C. 1977. Irregular finite difference techniques: Simulations of oscillations in shallow circular basins. *Journal of Physical Oceanography* 7:284-292.

Walker, W.R. and A.S. Humpherys. 1983. Kinematic-wave furrow irrigation model. *J. Irrig. Drain. Div.*, ASCE 109(4):377-392.

Walker, W.R. and G.V. Skogerboe. 1987. Surface irrigation, Theory and practice. Prentice-Hall, Inc., Englewood Cliffs, New Jersey.

Walters, R.A. and R.T. Cheng. 1979. A two-dimensional hydrodynamic model of a tidal estuary. *Advances in Water Resources* 1979(2):177-184.

Weare, T.J. 1976. Finite element or finite difference equations for the two-dimensional shallow water equations? *Computer Methods in Applied Mechanics and Engineering* 7:351-357.

Wu, C. 1985. "Prediction of wave motion in free surface flow," dissertation submitted in partial fulfillment of the requirements for the degree of Doctor of Philosophy in Civil Engineering, University of Michigan, Ann Arbor, Michigan.

Xanthopuolos, T. and C. Koutitas. 1976. Numerical simulation of a two-dimensional flood wave propagation due to dam failure. *Journal of Hydraulic Research* 14(4):321-331.

APPENDICES

Appendix A. B2D Input and Output Files

The following are contents of the input and output B2D files for case study 3. CASE_S_3.B2D is the input file. It is written by B2D once the user has finished creating the problem, and is intended to be a system file. This is why the file is not internally documented.

CASE_S_3.OUT is the customized comprehensive output of the model. It echoes the original data contained in CASE_S_3.B2D in a formatted and documented way, and then reports on the values of the dependent variables at user-defined time steps. At the end of the file, a final report summarizes the results and includes information about final infiltrated depths, opportunity times, and efficiency terms.

CASE_S_3.DAT is intended to be used by B2D itself to reproduce the run-time graphics and by other programs such as spreadsheets and three-dimensional plotting softwares. A header includes some specific information about the problem and then reports on different time steps follow. Each report is headed by the values of the time, discharge, and mass balance, and then the information is organized in six columns containing the values of x, y, h, z, p, and q at all the nodes in the domain.

CASE_S_3.OUT and CASE_S_3.DAT have been cut to save space. The sign "[DELETED]" denotes that part of the file has been cut at this point.

CASE_S_3.B2D

```
Case Study 3. Square Domain, Two corners delayed 10 min. Fam 0.8
      11        11
   10.000     10.000
     121  10000.000
       1
  6 2 2 2 2 2 2 2 2 2 7
  5 1 1 1 1 1 1 1 1 1 4
  5 1 1 1 1 1 1 1 1 1 4
  5 1 1 1 1 1 1 1 1 1 4
  5 1 1 1 1 1 1 1 1 1 4
  5 1 1 1 1 1 1 1 1 1 4
  5 1 1 1 1 1 1 1 1 1 4
  5 1 1 1 1 1 1 1 1 1 4
  5 1 1 1 1 1 1 1 1 1 4
  5 1 1 1 1 1 1 1 1 1 4
  8 3 3 3 3 3 3 3 3 3 9
       2
       1         1         0    0.1000    0.0000   30.0000
       2        11         0    0.1000   10.0000   40.0000
 0.5680000 0.0032400 0.0001740
    0.500 0.0010000     0.800     0.000 0.0400000
    1.000         1         1         0         0
CASB_S_3.OUT
    5.000         1         1         1         1         1
       1         1         1         0         1
CASB_S_3.DAT
    5.000         1
```

CASE_S_3.OUT

B2D, Two Dimensional Basin Irrigation Software, Version 1.00, Output File

Title: Case Study 3. Square Domain, Two corners delayed 10 min. Pam 0.8

Rows: 11
Columns: 11
Delta X (m): 10.000
Delta Y (m): 10.000
Number of nodes: 121
Area (m^2): 10000.000
Number of Inflows: 2

Code to Inflow Types

#	Type
1	Upper left corner
2	Upper right corner
3	Lower left corner
4	Lower right corner
5	Upper horizontal fan
6	Lower horizontal fan
7	Right vertical fan
8	Left vertical fan
9	Upper horizontal linear
10	Lower horizontal linear
11	Right vertical linear
12	Left vertical linear

Type	Initial node	Last node	Discharge (m^3/s)	Time in (min)	Time out (min)
1	1	0	0.1000	0.0000	30.0000
2	11	0	0.1000	10.0000	40.0000

Kostiakov-Lewis infiltration parameters:
a = 0.5680000
k = 0.0032400
fo = 0.0001740

Model Parameters:
Theta = 0.500
Minimum depth (m) = 0.0010000
Courant Number = 0.800
Viscosity (m^2/s) = 0.000
Manning's n = 0.0400000

OUT file: CASE_S_3.OUT
DAT file: CASE_S_3.DAT

Node Map

1	2	3	4	5	6	7	8	9	10	11
12	13	14	15	16	17	18	19	20	21	22
23	24	25	26	27	28	29	30	31	32	33
34	35	36	37	38	39	40	41	42	43	44
45	46	47	48	49	50	51	52	53	54	55
56	57	58	59	60	61	62	63	64	65	66
67	68	69	70	71	72	73	74	75	76	77
78	79	80	81	82	83	84	85	86	87	88
89	90	91	92	93	94	95	96	97	98	99
100	101	102	103	104	105	106	107	108	109	110
111	112	113	114	115	116	117	118	119	120	121

X coordinate (m)

0.00	10.00	20.00	30.00	40.00	50.00	60.00	70.00	80.00	90.00	100.00
0.00	10.00	20.00	30.00	40.00	50.00	60.00	70.00	80.00	90.00	100.00
0.00	10.00	20.00	30.00	40.00	50.00	60.00	70.00	80.00	90.00	100.00

0.00	10.00	20.00	30.00	40.00	50.00	60.00	70.00	80.00	90.00	100.00
0.00	10.00	20.00	30.00	40.00	50.00	60.00	70.00	80.00	90.00	100.00
0.00	10.00	20.00	30.00	40.00	50.00	60.00	70.00	80.00	90.00	100.00
0.00	10.00	20.00	30.00	40.00	50.00	60.00	70.00	80.00	90.00	100.00
0.00	10.00	20.00	30.00	40.00	50.00	60.00	70.00	80.00	90.00	100.00
0.00	10.00	20.00	30.00	40.00	50.00	60.00	70.00	80.00	90.00	100.00
0.00	10.00	20.00	30.00	40.00	50.00	60.00	70.00	80.00	90.00	100.00
0.00	10.00	20.00	30.00	40.00	50.00	60.00	70.00	80.00	90.00	100.00

Y coordinate (m)

100.00	100.00	100.00	100.00	100.00	100.00	100.00	100.00	100.00	100.00	100.00
90.00	90.00	90.00	90.00	90.00	90.00	90.00	90.00	90.00	90.00	90.00
80.00	80.00	80.00	80.00	80.00	80.00	80.00	80.00	80.00	80.00	80.00
70.00	70.00	70.00	70.00	70.00	70.00	70.00	70.00	70.00	70.00	70.00
60.00	60.00	60.00	60.00	60.00	60.00	60.00	60.00	60.00	60.00	60.00
50.00	50.00	50.00	50.00	50.00	50.00	50.00	50.00	50.00	50.00	50.00
40.00	40.00	40.00	40.00	40.00	40.00	40.00	40.00	40.00	40.00	40.00
30.00	30.00	30.00	30.00	30.00	30.00	30.00	30.00	30.00	30.00	30.00
20.00	20.00	20.00	20.00	20.00	20.00	20.00	20.00	20.00	20.00	20.00
10.00	10.00	10.00	10.00	10.00	10.00	10.00	10.00	10.00	10.00	10.00
0.00	0.00	0.00	0.00	0.00	0.00	0.00	0.00	0.00	0.00	0.00

Boundary Condition Map:

1 No boundary
2 Upper horizontal
3 Lower horizontal
4 Right vertical
5 Left vertical
6 Upper left corner
7 Upper right corner
8 Lower left corner
9 Lower right corner
10 Diagonal
11 Excluded

6	2	2	2	2	2	2	2	2	2	7
5	1	1	1	1	1	1	1	1	1	4
5	1	1	1	1	1	1	1	1	1	4
5	1	1	1	1	1	1	1	1	1	4
5	1	1	1	1	1	1	1	1	1	4
5	1	1	1	1	1	1	1	1	1	4
5	1	1	1	1	1	1	1	1	1	4
5	1	1	1	1	1	1	1	1	1	4
5	1	1	1	1	1	1	1	1	1	4
5	1	1	1	1	1	1	1	1	1	4
8	3	3	3	3	3	3	3	3	3	9

Time: 0.376 min.

Overland Flow Depth (m):

0.0181	0.0181	0.0000	0.0000	0.0000	0.0000	0.0000	0.0000	0.0000	0.0000	0.0000
0.0181	0.0000	0.0000	0.0000	0.0000	0.0000	0.0000	0.0000	0.0000	0.0000	0.0000
0.0000	0.0000	0.0000	0.0000	0.0000	0.0000	0.0000	0.0000	0.0000	0.0000	0.0000
0.0000	0.0000	0.0000	0.0000	0.0000	0.0000	0.0000	0.0000	0.0000	0.0000	0.0000
0.0000	0.0000	0.0000	0.0000	0.0000	0.0000	0.0000	0.0000	0.0000	0.0000	0.0000
0.0000	0.0000	0.0000	0.0000	0.0000	0.0000	0.0000	0.0000	0.0000	0.0000	0.0000
0.0000	0.0000	0.0000	0.0000	0.0000	0.0000	0.0000	0.0000	0.0000	0.0000	0.0000
0.0000	0.0000	0.0000	0.0000	0.0000	0.0000	0.0000	0.0000	0.0000	0.0000	0.0000
0.0000	0.0000	0.0000	0.0000	0.0000	0.0000	0.0000	0.0000	0.0000	0.0000	0.0000
0.0000	0.0000	0.0000	0.0000	0.0000	0.0000	0.0000	0.0000	0.0000	0.0000	0.0000
0.0000	0.0000	0.0000	0.0000	0.0000	0.0000	0.0000	0.0000	0.0000	0.0000	0.0000

Unit Discharge in the X direction (m^2/s):

0.0050	0.0025	0.0000	0.0000	0.0000	0.0000	0.0000	0.0000	0.0000	0.0000	0.0000
0.0025	0.0000	0.0000	0.0000	0.0000	0.0000	0.0000	0.0000	0.0000	0.0000	0.0000
0.0000	0.0000	0.0000	0.0000	0.0000	0.0000	0.0000	0.0000	0.0000	0.0000	0.0000

0.0000	0.0000	0.0000	0.0000	0.0000	0.0000	0.0000	0.0000	0.0000	0.0000	0.0000
0.0000	0.0000	0.0000	0.0000	0.0000	0.0000	0.0000	0.0000	0.0000	0.0000	0.0000
0.0000	0.0000	0.0000	0.0000	0.0000	0.0000	0.0000	0.0000	0.0000	0.0000	0.0000
0.0000	0.0000	0.0000	0.0000	0.0000	0.0000	0.0000	0.0000	0.0000	0.0000	0.0000
0.0000	0.0000	0.0000	0.0000	0.0000	0.0000	0.0000	0.0000	0.0000	0.0000	0.0000
0.0000	0.0000	0.0000	0.0000	0.0000	0.0000	0.0000	0.0000	0.0000	0.0000	0.0000
0.0000	0.0000	0.0000	0.0000	0.0000	0.0000	0.0000	0.0000	0.0000	0.0000	0.0000
0.0000	0.0000	0.0000	0.0000	0.0000	0.0000	0.0000	0.0000	0.0000	0.0000	0.0000

Unit Discharge in the Y direction (m^2/s)

-0.0050	-0.0025	0.0000	0.0000	0.0000	0.0000	0.0000	0.0000	0.0000	0.0000	0.0000
-0.0025	0.0000	0.0000	0.0000	0.0000	0.0000	0.0000	0.0000	0.0000	0.0000	0.0000
0.0000	0.0000	0.0000	0.0000	0.0000	0.0000	0.0000	0.0000	0.0000	0.0000	0.0000
0.0000	0.0000	0.0000	0.0000	0.0000	0.0000	0.0000	0.0000	0.0000	0.0000	0.0000
0.0000	0.0000	0.0000	0.0000	0.0000	0.0000	0.0000	0.0000	0.0000	0.0000	0.0000
0.0000	0.0000	0.0000	0.0000	0.0000	0.0000	0.0000	0.0000	0.0000	0.0000	0.0000
0.0000	0.0000	0.0000	0.0000	0.0000	0.0000	0.0000	0.0000	0.0000	0.0000	0.0000
0.0000	0.0000	0.0000	0.0000	0.0000	0.0000	0.0000	0.0000	0.0000	0.0000	0.0000
0.0000	0.0000	0.0000	0.0000	0.0000	0.0000	0.0000	0.0000	0.0000	0.0000	0.0000
0.0000	0.0000	0.0000	0.0000	0.0000	0.0000	0.0000	0.0000	0.0000	0.0000	0.0000
0.0000	0.0000	0.0000	0.0000	0.0000	0.0000	0.0000	0.0000	0.0000	0.0000	0.0000

Infiltrated Depth (m)

0.0000	0.0000	0.0000	0.0000	0.0000	0.0000	0.0000	0.0000	0.0000	0.0000	0.0000
0.0000	0.0000	0.0000	0.0000	0.0000	0.0000	0.0000	0.0000	0.0000	0.0000	0.0000
0.0000	0.0000	0.0000	0.0000	0.0000	0.0000	0.0000	0.0000	0.0000	0.0000	0.0000
0.0000	0.0000	0.0000	0.0000	0.0000	0.0000	0.0000	0.0000	0.0000	0.0000	0.0000
0.0000	0.0000	0.0000	0.0000	0.0000	0.0000	0.0000	0.0000	0.0000	0.0000	0.0000
0.0000	0.0000	0.0000	0.0000	0.0000	0.0000	0.0000	0.0000	0.0000	0.0000	0.0000
0.0000	0.0000	0.0000	0.0000	0.0000	0.0000	0.0000	0.0000	0.0000	0.0000	0.0000
0.0000	0.0000	0.0000	0.0000	0.0000	0.0000	0.0000	0.0000	0.0000	0.0000	0.0000
0.0000	0.0000	0.0000	0.0000	0.0000	0.0000	0.0000	0.0000	0.0000	0.0000	0.0000
0.0000	0.0000	0.0000	0.0000	0.0000	0.0000	0.0000	0.0000	0.0000	0.0000	0.0000
0.0000	0.0000	0.0000	0.0000	0.0000	0.0000	0.0000	0.0000	0.0000	0.0000	0.0000

Mass Balance

Surface Volume:	2.259 m^3
Infiltrated Volume:	0.000 m^3
Total Volume:	2.259 m^3
Inflow Volume:	2.259 m^3
Error:	0.000 %

Time: 5.159 min.

Overland Flow Depth (m):

0.0544	0.0467	0.0317	0.0253	0.0040	0.0001	0.0000	0.0000	0.0000	0.0000	0.0000
0.0467	0.0435	0.0302	0.0062	0.0002	0.0000	0.0000	0.0000	0.0000	0.0000	0.0000
0.0317	0.0302	0.0099	0.0007	0.0000	0.0000	0.0000	0.0000	0.0000	0.0000	0.0000
0.0253	0.0062	0.0007	0.0000	0.0000	0.0000	0.0000	0.0000	0.0000	0.0000	0.0000
0.0040	0.0002	0.0000	0.0000	0.0000	0.0000	0.0000	0.0000	0.0000	0.0000	0.0000
0.0001	0.0000	0.0000	0.0000	0.0000	0.0000	0.0000	0.0000	0.0000	0.0000	0.0000
0.0000	0.0000	0.0000	0.0000	0.0000	0.0000	0.0000	0.0000	0.0000	0.0000	0.0000
0.0000	0.0000	0.0000	0.0000	0.0000	0.0000	0.0000	0.0000	0.0000	0.0000	0.0000
0.0000	0.0000	0.0000	0.0000	0.0000	0.0000	0.0000	0.0000	0.0000	0.0000	0.0000
0.0000	0.0000	0.0000	0.0000	0.0000	0.0000	0.0000	0.0000	0.0000	0.0000	0.0000
0.0000	0.0000	0.0000	0.0000	0.0000	0.0000	0.0000	0.0000	0.0000	0.0000	0.0000

Unit Discharge in the X direction (m^2/s):

0.0050	0.0047	0.0027	0.0020	0.0001	0.0000	0.0000	0.0000	0.0000	0.0000	0.0000
0.0025	0.0034	0.0029	0.0002	0.0000	0.0000	0.0000	0.0000	0.0000	0.0000	0.0000
0.0000	0.0018	0.0003	0.0000	0.0000	0.0000	0.0000	0.0000	0.0000	0.0000	0.0000
0.0000	0.0001	-0.0000	0.0000	0.0000	0.0000	0.0000	0.0000	0.0000	0.0000	0.0000
0.0000	0.0000	0.0000	0.0000	0.0000	0.0000	0.0000	0.0000	0.0000	0.0000	0.0000
0.0000	0.0000	0.0000	0.0000	0.0000	0.0000	0.0000	0.0000	0.0000	0.0000	0.0000
0.0000	0.0000	0.0000	0.0000	0.0000	0.0000	0.0000	0.0000	0.0000	0.0000	0.0000
0.0000	0.0000	0.0000	0.0000	0.0000	0.0000	0.0000	0.0000	0.0000	0.0000	0.0000
0.0000	0.0000	0.0000	0.0000	0.0000	0.0000	0.0000	0.0000	0.0000	0.0000	0.0000
0.0000	0.0000	0.0000	0.0000	0.0000	0.0000	0.0000	0.0000	0.0000	0.0000	0.0000

0.0000	0.0000	0.0000	0.0000	0.0000	0.0000	0.0000	0.0000	0.0000	0.0000	0.0000

Unit Discharge in the Y direction (m^2/s)

-0.0050	-0.0025	0.0000	0.0000	0.0000	0.0000	0.0000	0.0000	0.0000	0.0000	0.0000
-0.0047	-0.0034	-0.0018	-0.0001	-0.0000	0.0000	0.0000	0.0000	0.0000	0.0000	0.0000
-0.0027	-0.0029	-0.0003	0.0000	0.0000	0.0000	0.0000	0.0000	0.0000	0.0000	0.0000
-0.0020	-0.0002	-0.0000	0.0000	0.0000	0.0000	0.0000	0.0000	0.0000	0.0000	0.0000
-0.0001	-0.0000	0.0000	0.0000	0.0000	0.0000	0.0000	0.0000	0.0000	0.0000	0.0000
-0.0000	0.0000	0.0000	0.0000	0.0000	0.0000	0.0000	0.0000	0.0000	0.0000	0.0000
0.0000	0.0000	0.0000	0.0000	0.0000	0.0000	0.0000	0.0000	0.0000	0.0000	0.0000
0.0000	0.0000	0.0000	0.0000	0.0000	0.0000	0.0000	0.0000	0.0000	0.0000	0.0000
0.0000	0.0000	0.0000	0.0000	0.0000	0.0000	0.0000	0.0000	0.0000	0.0000	0.0000
0.0000	0.0000	0.0000	0.0000	0.0000	0.0000	0.0000	0.0000	0.0000	0.0000	0.0000
0.0000	0.0000	0.0000	0.0000	0.0000	0.0000	0.0000	0.0000	0.0000	0.0000	0.0000

Infiltrated Depth (m)

0.0091	0.0091	0.0081	0.0068	0.0037	0.0000	0.0000	0.0000	0.0000	0.0000	0.0000
0.0091	0.0085	0.0070	0.0041	0.0000	0.0000	0.0000	0.0000	0.0000	0.0000	0.0000
0.0081	0.0070	0.0047	0.0000	0.0000	0.0000	0.0000	0.0000	0.0000	0.0000	0.0000
0.0068	0.0041	0.0000	0.0000	0.0000	0.0000	0.0000	0.0000	0.0000	0.0000	0.0000
0.0037	0.0000	0.0000	0.0000	0.0000	0.0000	0.0000	0.0000	0.0000	0.0000	0.0000
0.0000	0.0000	0.0000	0.0000	0.0000	0.0000	0.0000	0.0000	0.0000	0.0000	0.0000
0.0000	0.0000	0.0000	0.0000	0.0000	0.0000	0.0000	0.0000	0.0000	0.0000	0.0000
0.0000	0.0000	0.0000	0.0000	0.0000	0.0000	0.0000	0.0000	0.0000	0.0000	0.0000
0.0000	0.0000	0.0000	0.0000	0.0000	0.0000	0.0000	0.0000	0.0000	0.0000	0.0000
0.0000	0.0000	0.0000	0.0000	0.0000	0.0000	0.0000	0.0000	0.0000	0.0000	0.0000
0.0000	0.0000	0.0000	0.0000	0.0000	0.0000	0.0000	0.0000	0.0000	0.0000	0.0000

Mass Balance

Surface Volume:	24.962 m^3
Infiltrated Volume:	6.530 m^3
Total Volume:	31.492 m^3
Inflow Volume:	30.955 m^3
Error:	1.736 %

[DELETED]

==

FINAL REPORT

==

TIMES

=====

Advance Time : 0.00 minutes.
Depletion Time : 72.78 minutes.

INFILTRATED DEPTHS

=================

Table of Infiltrated depths (m):

0.0497	0.0497	0.0492	0.0487	0.0478	0.0464	0.0441	0.0442	0.0448	0.0449	0.0449
0.0497	0.0494	0.0488	0.0479	0.0467	0.0449	0.0426	0.0433	0.0444	0.0449	0.0449
0.0492	0.0488	0.0480	0.0470	0.0457	0.0438	0.0416	0.0424	0.0435	0.0444	0.0448
0.0487	0.0479	0.0470	0.0459	0.0444	0.0423	0.0403	0.0413	0.0424	0.0433	0.0442
0.0478	0.0467	0.0457	0.0444	0.0426	0.0403	0.0388	0.0397	0.0410	0.0421	0.0432
0.0464	0.0449	0.0438	0.0423	0.0402	0.0380	0.0370	0.0379	0.0392	0.0402	0.0417
0.0441	0.0423	0.0411	0.0394	0.0373	0.0357	0.0350	0.0356	0.0368	0.0374	0.0394
0.0406	0.0385	0.0376	0.0357	0.0343	0.0331	0.0326	0.0330	0.0338	0.0343	0.0363
0.0359	0.0337	0.0334	0.0317	0.0301	0.0291	0.0288	0.0295	0.0304	0.0307	0.0323
0.0246	0.0200	0.0199	0.0181	0.0174	0.0172	0.0174	0.0183	0.0200	0.0206	0.0245
0.0000	0.0000	0.0000	0.0000	0.0000	0.0000	0.0000	0.0000	0.0000	0.0000	0.0000

Average infiltrated depth (m): 0.0365

Standard Deviation of Infiltrated Depth (m): 0.0138
Maximum Infiltrated Depth (m): 0.0497
Minimum Infiltrated Depth (m): 0.0000

OPPORTUNITY TIMES
==========

Table of Opportunity Times (min):

72.8	72.8	71.8	70.8	68.8	65.8	61.1	61.2	62.6	62.7	62.7
72.8	72.2	71.0	69.0	66.5	62.7	57.9	59.4	61.6	62.7	62.7
71.8	71.0	69.3	67.1	64.4	60.4	56.0	57.6	59.8	61.6	62.6
70.8	69.0	67.1	64.8	61.6	57.5	53.3	55.3	57.6	59.4	61.2
68.8	66.5	64.4	61.6	57.9	53.3	50.4	52.2	54.8	57.0	59.3
65.8	62.7	60.4	57.5	53.2	48.9	47.0	48.6	51.2	53.2	56.1
61.1	57.3	55.0	51.5	47.5	44.5	43.2	44.4	46.5	47.8	51.5
54.0	49.9	48.1	44.5	41.8	39.7	38.7	39.5	41.0	41.8	45.5
44.9	40.8	40.2	37.1	34.3	32.5	32.1	33.2	34.8	35.3	38.2
25.2	18.2	18.0	15.6	14.6	14.4	14.6	15.8	18.2	19.0	25.0
0.0	0.0	0.0	0.0	0.0	0.0	0.0	0.0	0.0	0.0	0.0

Average Opportunity Time (min): 48.1903
Standard Deviation of Opportunity time (min): 20.9927
Maximum Opportunity time (min): 72.7836
Minimum Opportunity time (min): 0.0000

TIME EVOLUTION OF SELECTED VARIABLES
==========

			VOLUMES			Mass Balance	
Time (min)	Wetted Area (m^2)	(%)	Surface (m^3)	Infiltr. (m^3)	Total (m^3)	Inflow (m^3)	Error (%)
0.38	125.00	1.2	2.26	0.00	2.26	2.26	0.000
5.16	1025.00	10.2	24.96	6.53	31.49	30.95	1.736
10.06	2350.00	23.5	46.83	17.64	64.47	60.88	5.886
15.00	3800.00	38.0	85.70	38.58	124.28	120.14	3.445
20.10	5200.00	52.0	120.49	65.29	185.78	181.27	2.487
25.00	6150.00	61.5	152.27	92.65	244.93	240.15	1.989
30.04	6950.00	69.5	182.05	122.63	304.68	300.11	1.523
35.06	7800.00	78.0	181.28	153.71	334.99	330.23	1.440
40.08	8550.00	85.5	179.40	184.92	364.32	359.39	1.374
45.10	8650.00	86.5	148.75	215.70	364.45	359.39	1.408
50.13	9100.00	91.0	119.62	244.97	364.59	359.39	1.447
55.15	8900.00	89.0	92.32	272.27	364.59	359.39	1.448

EFFICIENCY REPORT
==========

Required Depth (m)	Deep Percolation Ratio (%)	Application Efficiency (%)	Water Requirement Efficiency (%)
0.000	100.000	0.000	100.000
0.005	86.972	13.028	95.000
0.010	73.943	26.057	95.000
0.015	60.915	39.085	95.000
0.020	48.207	51.793	94.417
0.025	36.409	63.591	92.740
0.030	24.825	75.175	91.361
0.035	14.411	85.589	89.157
0.040	6.097	93.903	85.590
0.045	0.933	99.067	80.264
0.050	0.000	100.000	73.211

0.055	0.000	100.000	66.555
0.060	0.000	100.000	61.009
0.065	0.000	100.000	56.316
0.070	0.000	100.000	52.293
0.075	0.000	100.000	48.807
0.080	0.000	100.000	45.757
0.085	0.000	100.000	43.065
0.090	0.000	100.000	40.673
0.095	0.000	100.000	38.532
0.100	0.000	100.000	36.605
0.105	0.000	100.000	34.862
0.110	0.000	100.000	33.278
0.115	0.000	100.000	31.831
0.120	0.000	100.000	30.505
0.125	0.000	100.000	29.284
0.130	0.000	100.000	28.158
0.135	0.000	100.000	27.115
0.140	0.000	100.000	26.147
0.145	0.000	100.000	25.245
0.150	0.000	100.000	24.404
0.155	0.000	100.000	23.616
0.160	0.000	100.000	22.878
0.165	0.000	100.000	22.185
0.170	0.000	100.000	21.533
0.175	0.000	100.000	20.917
0.180	0.000	100.000	20.336
0.185	0.000	100.000	19.787
0.190	0.000	100.000	19.266
0.195	0.000	100.000	18.772
0.200	0.000	100.000	18.303

CASE_S_3.DAT

Case Study 3. Square Domain, Two corners delayed 10 min. Fam 0.8

```
   121       11   10.0000   10.0000  0.001000
 6 2 2 2 2 2 2 2 2 2 7
 5 1 1 1 1 1 1 1 1 1 4
 5 1 1 1 1 1 1 1 1 1 4
 5 1 1 1 1 1 1 1 1 1 4
 5 1 1 1 1 1 1 1 1 1 4
 5 1 1 1 1 1 1 1 1 1 4
 5 1 1 1 1 1 1 1 1 1 4
 5 1 1 1 1 1 1 1 1 1 4
 5 1 1 1 1 1 1 1 1 1 4
 5 1 1 1 1 1 1 1 1 1 4
 8 3 3 3 3 3 3 3 3 3 9
```

[DELETED]

```
*   35.060    0.1000   181.28   153.71   334.99   330.23    1.44
    0.0000  100.0000   0.0257   0.0305   0.0000   0.0000
   10.0000  100.0000   0.0271   0.0305  -0.0002   0.0000
   20.0000  100.0000   0.0260   0.0300  -0.0003   0.0000
   30.0000  100.0000   0.0278   0.0294  -0.0005   0.0000
   40.0000  100.0000   0.0273   0.0282  -0.0007   0.0000
   50.0000  100.0000   0.0300   0.0264  -0.0010   0.0000
   60.0000  100.0000   0.0308   0.0235  -0.0014   0.0000
   70.0000  100.0000   0.0363   0.0236  -0.0021   0.0000
   80.0000  100.0000   0.0392   0.0244  -0.0033   0.0000
   90.0000  100.0000   0.0529   0.0245  -0.0049  -0.0025
  100.0000  100.0000   0.0545   0.0245  -0.0050  -0.0050
    0.0000   90.0000   0.0258   0.0305   0.0000  -0.0003
   10.0000   90.0000   0.0250   0.0302  -0.0001  -0.0002
   20.0000   90.0000   0.0261   0.0295  -0.0003  -0.0002
   30.0000   90.0000   0.0257   0.0283  -0.0004  -0.0002
   40.0000   90.0000   0.0274   0.0268  -0.0007  -0.0003
   50.0000   90.0000   0.0283   0.0245  -0.0009  -0.0004
   60.0000   90.0000   0.0312   0.0214  -0.0013  -0.0005
   70.0000   90.0000   0.0341   0.0224  -0.0016  -0.0009
   80.0000   90.0000   0.0387   0.0238  -0.0024  -0.0013
   90.0000   90.0000   0.0446   0.0245  -0.0032  -0.0033
  100.0000   90.0000   0.0534   0.0245  -0.0025  -0.0050
    0.0000   80.0000   0.0253   0.0300   0.0000  -0.0004
   10.0000   80.0000   0.0267   0.0295  -0.0001  -0.0004
   20.0000   80.0000   0.0255   0.0285  -0.0001  -0.0004
   30.0000   80.0000   0.0271   0.0272  -0.0003  -0.0004
   40.0000   80.0000   0.0263   0.0256  -0.0004  -0.0005
   50.0000   80.0000   0.0285   0.0230  -0.0006  -0.0005
   60.0000   80.0000   0.0286   0.0200  -0.0008  -0.0006
   70.0000   80.0000   0.0321   0.0212  -0.0011  -0.0009
   80.0000   80.0000   0.0333   0.0226  -0.0012  -0.0013
   90.0000   80.0000   0.0379   0.0238  -0.0013  -0.0024
  100.0000   80.0000   0.0392   0.0244   0.0000  -0.0034
    0.0000   70.0000   0.0248   0.0294   0.0000  -0.0005
   10.0000   70.0000   0.0239   0.0283  -0.0000  -0.0005
   20.0000   70.0000   0.0250   0.0272  -0.0002  -0.0006
   30.0000   70.0000   0.0246   0.0258  -0.0002  -0.0006
   40.0000   70.0000   0.0259   0.0238  -0.0004  -0.0006
   50.0000   70.0000   0.0264   0.0211  -0.0005  -0.0008
   60.0000   70.0000   0.0283   0.0182  -0.0007  -0.0009
   70.0000   70.0000   0.0299   0.0196  -0.0007  -0.0012
   80.0000   70.0000   0.0322   0.0212  -0.0008  -0.0014
   90.0000   70.0000   0.0338   0.0224  -0.0008  -0.0019
  100.0000   70.0000   0.0361   0.0236   0.0000  -0.0022
    0.0000   60.0000   0.0232   0.0282   0.0000  -0.0006
   10.0000   60.0000   0.0244   0.0268  -0.0000  -0.0007
   20.0000   60.0000   0.0233   0.0256   0.0000  -0.0006
   30.0000   60.0000   0.0244   0.0238  -0.0000  -0.0007
   40.0000   60.0000   0.0235   0.0214   0.0000  -0.0008
```

50.0000	60.0000	0.0244	0.0182	-0.0001	-0.0008
60.0000	60.0000	0.0241	0.0159	-0.0002	-0.0008
70.0000	60.0000	0.0259	0.0173	-0.0005	-0.0010
80.0000	60.0000	0.0271	0.0192	-0.0004	-0.0012
90.0000	60.0000	0.0286	0.0207	-0.0004	-0.0014
100.0000	60.0000	0.0296	0.0223	0.0000	-0.0017
0.0000	50.0000	0.0217	0.0264	0.0000	-0.0007
10.0000	50.0000	0.0206	0.0245	0.0000	-0.0006
20.0000	50.0000	0.0213	0.0230	-0.0000	-0.0006
30.0000	50.0000	0.0207	0.0211	0.0000	-0.0006
40.0000	50.0000	0.0211	0.0180	-0.0001	-0.0006
50.0000	50.0000	0.0216	0.0147	-0.0002	-0.0008
60.0000	50.0000	0.0227	0.0131	-0.0002	-0.0010
70.0000	50.0000	0.0234	0.0145	-0.0001	-0.0010
80.0000	50.0000	0.0239	0.0166	-0.0001	-0.0010
90.0000	50.0000	0.0246	0.0180	-0.0002	-0.0011
100.0000	50.0000	0.0253	0.0202	0.0000	-0.0011
0.0000	40.0000	0.0184	0.0235	0.0000	-0.0005
10.0000	40.0000	0.0194	0.0209	-0.0000	-0.0006
20.0000	40.0000	0.0184	0.0193	0.0000	-0.0006
30.0000	40.0000	0.0193	0.0168	0.0000	-0.0008
40.0000	40.0000	0.0185	0.0135	0.0001	-0.0009
50.0000	40.0000	0.0173	0.0108	0.0002	-0.0009
60.0000	40.0000	0.0155	0.0095	-0.0000	-0.0008
70.0000	40.0000	0.0177	0.0107	-0.0002	-0.0010
80.0000	40.0000	0.0197	0.0126	-0.0002	-0.0011
90.0000	40.0000	0.0205	0.0138	-0.0001	-0.0012
100.0000	40.0000	0.0213	0.0168	0.0000	-0.0011
0.0000	30.0000	0.0165	0.0186	0.0000	-0.0007
10.0000	30.0000	0.0142	0.0155	0.0001	-0.0006
20.0000	30.0000	0.0142	0.0140	0.0001	-0.0006
30.0000	30.0000	0.0104	0.0108	0.0002	-0.0003
40.0000	30.0000	0.0055	0.0079	0.0001	-0.0001
50.0000	30.0000	0.0020	0.0051	0.0000	-0.0000
60.0000	30.0000	0.0011	0.0034	0.0000	-0.0000
70.0000	30.0000	0.0020	0.0048	-0.0000	-0.0000
80.0000	30.0000	0.0045	0.0069	-0.0000	-0.0001
90.0000	30.0000	0.0058	0.0079	-0.0001	-0.0001
100.0000	30.0000	0.0120	0.0117	0.0000	-0.0005
0.0000	20.0000	0.0058	0.0111	0.0000	-0.0001
10.0000	20.0000	0.0015	0.0067	0.0000	-0.0000
20.0000	20.0000	0.0013	0.0058	0.0000	-0.0000
30.0000	20.0000	0.0007	0.0018	0.0000	-0.0000
40.0000	20.0000	0.0005	0.0000	-0.0000	-0.0000
50.0000	20.0000	0.0001	0.0000	0.0000	-0.0000
60.0000	20.0000	0.0000	0.0000	-0.0000	-0.0000
70.0000	20.0000	0.0001	0.0000	-0.0000	-0.0000
80.0000	20.0000	0.0003	0.0000	-0.0000	-0.0000
90.0000	20.0000	0.0005	0.0000	0.0000	-0.0000
100.0000	20.0000	0.0010	0.0026	0.0000	-0.0000
0.0000	10.0000	0.0009	0.0000	0.0000	-0.0000
10.0000	10.0000	0.0001	0.0000	0.0000	-0.0000
20.0000	10.0000	0.0001	0.0000	0.0000	-0.0000
30.0000	10.0000	0.0000	0.0000	0.0000	-0.0000
40.0000	10.0000	0.0000	0.0000	0.0000	0.0000
50.0000	10.0000	0.0000	0.0000	0.0000	0.0000
60.0000	10.0000	0.0000	0.0000	0.0000	0.0000
70.0000	10.0000	0.0000	0.0000	0.0000	0.0000
80.0000	10.0000	0.0000	0.0000	0.0000	0.0000
90.0000	10.0000	0.0000	0.0000	0.0000	0.0000
100.0000	10.0000	0.0000	0.0000	0.0000	-0.0000
0.0000	0.0000	0.0000	0.0000	0.0000	0.0000
10.0000	0.0000	0.0000	0.0000	0.0000	0.0000
20.0000	0.0000	0.0000	0.0000	0.0000	0.0000
30.0000	0.0000	0.0000	0.0000	0.0000	0.0000
40.0000	0.0000	0.0000	0.0000	0.0000	0.0000
50.0000	0.0000	0.0000	0.0000	0.0000	0.0000
60.0000	0.0000	0.0000	0.0000	0.0000	0.0000
70.0000	0.0000	0.0000	0.0000	0.0000	0.0000

80.0000	0.0000	0.0000	0.0000	0.0000	0.0000
90.0000	0.0000	0.0000	0.0000	0.0000	0.0000
100.0000	0.0000	0.0000	0.0000	0.0000	0.0000

[DELETED]

Appendix B. Delta Field Experiment Data

TABLE 14. Coordinates of the Advance Points Surveyed in the Delta Field Experiment at Different Times.

2 h		3 h		4 h		5 h	
x (m)	y (m)	x (m)	y (m)	x (m)	y (m)	x (m)	y (m)
0.0	34.7	0.0	9.9	45.8	0.0	87.7	0.0
23.5	39.4	50.9	18.7	74.2	9.3	115.1	10.9
69.6	63.7	71.6	32.1	98.5	24.4	125.4	41.9
93.9	96.8	118.7	81.8	112.0	50.2	141.5	54.4
121.3	164.6	138.4	135.1	136.8	70.9	157.0	77.1
118.2	183.2	145.1	183.2	148.7	95.3	169.4	99.4
				151.8	138.7	189.6	159.9
				169.9	169.3	185.9	183.2
				168.3	183.2		

6 h		7 h		8 h		9 h	
x (m)	y (m)	x (m)	y (m)	x (m)	y (m)	x (m)	y (m)
120.0	0.0	166.3	0.0	204.0	0.0	216.1	30.6
151.3	7.8	170.9	12.5	197.0	38.3	207.7	56.4
148.2	40.4	170.9	50.2	198.3	81.8	209.7	76.6
186.4	98.9	191.6	88.5	216.1	129.9	216.1	94.2
196.8	148.0	204.0	125.3				
205.6	169.8	216.1	150.1				
205.1	183.2						

VITA

Enrique Playán Jubillar

Candidate for the Degree of

Doctor of Philosophy

DISSERTATION: Two-Dimensional Hydrodynamic Simulation of Basin Irrigation: Analysis of Field Shape Effects on Irrigation Performance

MAJOR FIELD: Irrigation Engineering

BIOGRAPHICAL INFORMATION:

Personal Data: Born in Monzón (Huesca), Spain, December 12, 1964, son of Jose Playán Rios and Maria Jubillar Blanc.

Education: Graduated from Polytechnic University of Catalonia with an Ingeniero Técnico Agrícola (Agricultural Technical Engineer) degree in 1986, and with an Ingeniero Agrónomo (Agricultural Engineer) degree in 1988. Completed the requirements for the Doctor of Philosophy degree in Irrigation Engineering at Utah State University in September 1992.

Professional Experience: Doctoral student in the Soils and Irrigation Department of the Servicio de Investigación Agraria de la Diputación General de Aragón, Zaragoza, Spain, 1988-89.